ABSTRACT

MAHAJAN, HERAMB PRAKASH. Issues with Progressive Degradation Modeling of Reinforced Concrete members. (Under the direction of Dr. Tasnim Hassan.)

Reinforced concrete (RC) structures are common in earthquake prone regions and may sustain various degree of damages under any earthquake. Northridge (1994) and Kobe (1995) earthquakes are examples that RC structures may sustain significant damages during earthquakes. Subsequent to these earthquakes, seismic design methods have been improved primarily by the performance based design methodology, but RC structures still can sustain various degree of damages based on the limit states considered in the design. These limit states were primarily established based on the limited seismic experimental data and simplified analysis. However, experimental data also demonstrated that these limit states can be influenced by member geometry and loading type. Hence, precise estimation of limit states of a RC structural member will require a robust 3D finite element simulation model which has the capability to simulate progressive damage accumulation in RC members. With such a simulation model, in addition to improving design methodology, repair needs of damaged RC structures can be determined and thereby seismic resiliency of RC structures can be enhanced.

The fiber analysis technique, which is widely used for analysis of RC members, is dependent on empirical equations and uniaxial concrete constitutive models. The fiber analysis technique is unable to capture the multiaxial stress responses of concrete and rebar steel, and consequently fails to simulate the progressive accumulation of damages in concrete and steel, and consequently fails to simulate the failure mechanisms of RC members induced by the concrete strength degradation and crushing, and longitudinal rebar buckling and rupture. Hence, this study made efforts to perform 3D finite element analyses using the ANSYS,

ABAQUS and ATENA software packages and evaluated their multiaxial concrete constitutive models by comparing the simulated responses against the experimental responses.

The outcomes of this study demonstrates that the concrete constitutive models in ANSYS are not capable of simulating the RC member experimental responses. It is also pointed out that the concrete constitutive models in OPENSEES are primarily uniaxial, hence OPENSEES in its current state can't simulate multiaxial stress-strain responses. The concrete constitutive models in ABAQUS and ATENA are found to simulate reasonably the monotonic compressive responses of concrete cylinders, concrete filled steel tubes and RC columns. These two software packages can also simulate the RC column responses under lateral monotonic loading, but faced with divergence issues in simulating high ductility responses. The concrete smeared cracking model in ABAQUS cannot consider confining pressure, hence is not evaluated in this study. Concrete model in ATENA considers concrete cracking numerically but fails to converge under lateral loading early in the analysis. A modified smeared cracking model in literature has demonstrated better performance than the ATENA model, but simulations only up to intermediate ductility levels are demonstrated. In this study, physical concrete cracks are included in the analysis with ABAQUS to demonstrate the significance of concrete cracks in the simulation of RC member responses. These results demonstrate that the development of an advanced concrete constitutive model and numerical techniques to consider physical concrete cracking in RC member analysis is essential for enhancing seismic resilience of RC structures.

Issues with Progressive Degradation Modeling of Reinforced Concrete Members

by
Heramb Prakash Mahajan

A thesis submitted to the Graduate Faculty of
North Carolina State University
in partial fulfillment of the
requirements for the Degree of
Master of Arts

Civil Engineering

Raleigh, North Carolina

2016

APPROBED BY:

_____	_____
Dr. Gregory Lucier	Dr. Michael Borden

_____
Dr. Tasnim Hassan
Committee Chair

DEDICATION

To my parents, Prakash J. Mahajan and Pratibha P. Mahajan

and to my dear sisters Dr. Vilasini S. Choudhary & Dr. Vishakha A. Chaudhary

BIOGRAPHY

Heramb Mahajan was born in Mumbai, India on May 26, 1993. His interest in math, science and buildings inspired him to peruse degree in civil engineering. He received B. Tech. degree in Civil Engineering from Sardar Patel College of Engineering, Mumbai in 2014. While perusing this degree, he developed interest in structural engineering and decided to study this field in depth. He continued to explore structural engineering in North Carolina State University where he started working on concrete constitutive modeling under supervision of Dr. Tasnim Hassan.

TABLE OF CONTENTS

LIST OF TABLES

CHAPTER 2: Concrete modeling for axial loading

CHAPTER 3: Concrete modeling for lateral loading

LIST OF FIGURES

CHAPTER 1: Introduction

CHAPTER 2: Concrete modeling for axial loading

CHAPTER 3: Concrete modeling for lateral loading

1 Introduction

1.1 Background

Reinforced concrete (RC) structures are common in earthquake prone areas. These RC structures experiences various degrees of damages when subjected to earthquake. An extensive experimental study on RC columns under simulated seismic loading demonstrated such damages through crushing of concrete, rebar buckling and rebar rupture [1]. Earlier earthquakes, such as Northridge in 1994 of magnitude 6.7, Kobe in 1995 of magnitude 6.9, triggered significant damages to reinforced concrete structures including bridge columns and building frames, including collapse of many structures [2]. After these earthquakes, improvement in the design codes were made to sustain similar type of damages. Recent earthquake in Illapel, Chile 2015 of magnitude 8.3, structural damages were limited to cracking and spalling of concrete [3]. Even after significant improvement of design codes for earthquake resilience, damage is observed in RC structure [4].

Typical design procedure for designing of structures for earthquake loading is force based design. This design procedure assumes initial properties of structure, such as stiffness; to calculate forces. Once forces are known, structure is designed for calculated forces and displacements are checked for acceptance of design. When structure experiences damage due to earthquake, initial properties are no longer valid due to accumulated damages. Some recommendations are given in the code to consider this damage into account in determining more realistic properties of structural members, but the strength and stiffness are assumed to be independent [5], which is not realistic. In order to consider ductility of structure, force reduction factors are applied in force based design. These force reduction factors indirectly

indicates the available ductility capacity of structure. For standard buildings with equal floor height and spacing of columns, these force reduction factors estimates good response of structure but for irregular structures, behavior prediction is difficult [5]. Force based design technique doesn't consider cyclic behavior of structure [5] which is critical in determining damping of structure or absorbed hysteretic energy. This absorption of energy under cyclic loading gradually accumulate damage in structure [1]. Due to lack of consideration of hysteretic behavior, prediction of realist damages in structure is difficult. Due to problems associated with force based design, performance based design technique is introduced [1, 5, 6]. According to performance based design, damage evaluation of the structures are performed against specific limit states of the structure [1, 5, 6]. These limit states are defined either at global level such as story drift or at elemental level such as strains at cross sections of beams and columns. Once these limit states are specified for the structure which are determined by consideration of actual damage in structural members, seismic performance of a structure is determined by comparing against these limit states.

In performance based design, there are 5 limit states in RC structures, Cracking, Yielding, Service, Damage control and Collapse [5] as showed in Fig. 1 with respect to a monotonic lateral response of a column developed by Goodnight [1]. Cracking limit state indicates the cracking of concrete under tension, yielding indicates yielding of longitudinal rebars, service limit state indicates crushing of cover concrete and opening of concrete cracks for which service of the structures is not interrupted [5]. The service limit states indicates if this limit is exceeded repair of structure is needed but don't impose any safety concerns [6]. Exceeding damage control limit state indicates structure needs replacement. Exceeding the damage limit state generally indicates core concrete crushing, rebar buckling and rupture of

rebar [5]. Consequently, damage control limit state is considered as critical limit state [6], [4]. Collapse limit state can be reached by rupture of rebar(s) in many critical load carrying members, consequently significant strength loss and subsequent collapse of structure may occur.

In Fig. 1, it is observed that cracking and yielding limit states, the first two limit states, occurred at small displacements. The 3rd service limit state involving crushing of concrete cover needed small nonlinear deformation, usually around twice the yield deformation (μ_2) as shown in Fig. 1. At damage control limit (4th limit state), core concrete crushing occurs around ductility level of 16. As stated earlier, exceeding damage control limit state usually requires replacement of structures. Ultimately, the collapse limit state at very large ductility is defined by longitudinal rebar rupture causing failure of structure by collapse.

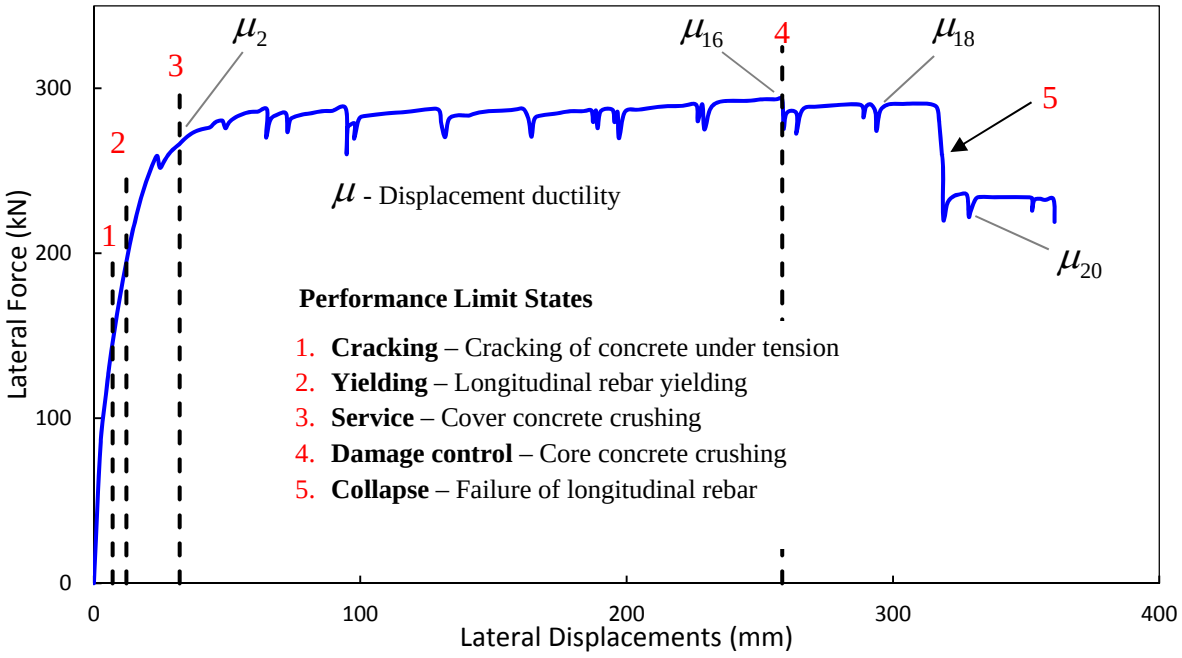

Fig. 1. Performance limit states of a reinforced concrete column under monotonic lateral loading (Data from Goodnight [1])

These five limit states of RC columns under simulated seismic loading are shown in Fig. 2, where it is observed that the cracking of concrete, yielding of longitudinal rebars and service limit states still occurs at small displacements or ductility levels similar to those under monotonic loading shown in Fig. 1. Damage control limit state under seismic loading is controlled by longitudinal rebar buckling and occurred around ductility level 8. Collapse limit state occurred, when pre-buckled longitudinal rebar suddenly rupture during ductility level 10 cycle. Damage control and collapse limit states under monotonic loading occurs at much larger ductility levels compared to those under seismic loading (compare Fig. 1 and 2). These differences indicate RC member may behave differently under different load history primarily because of the damage accumulation mechanism. Under cyclic loading, each cycle induce damage to the RC column in the form of concrete cracking, concrete crushing, rebar buckling, etc. Accumulation of these damages lead to progressive degradation of stiffness along with reduction in load carrying capacity and eventual failure or collapse of RC members.

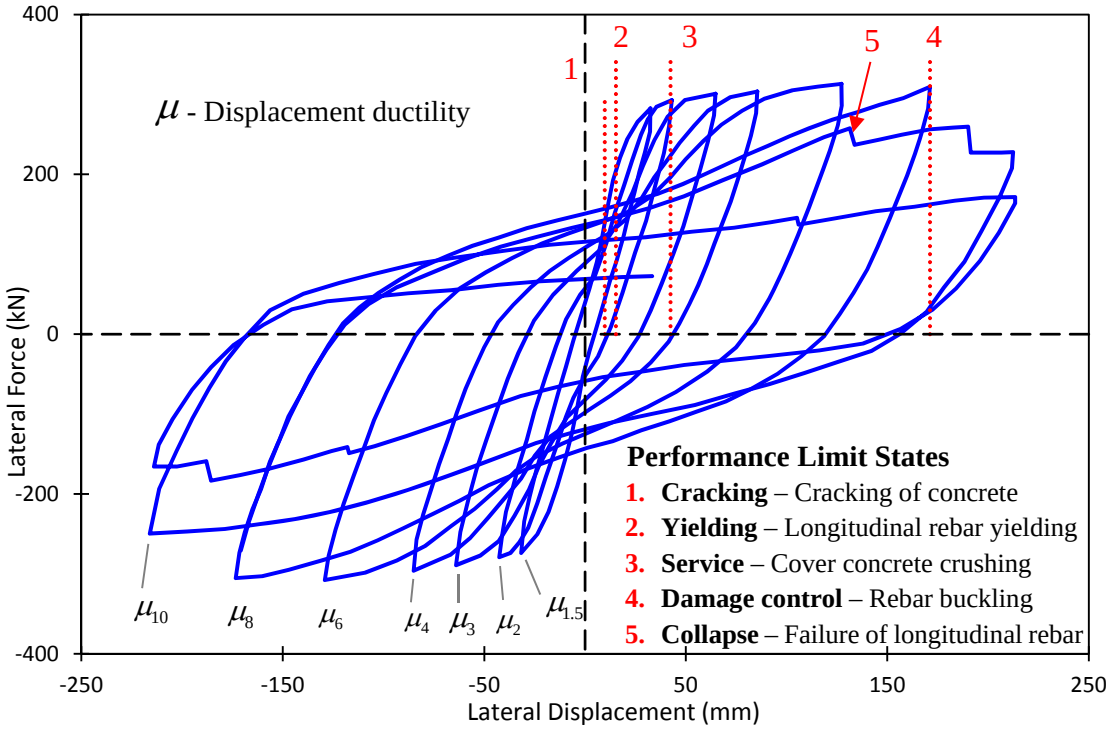

Fig. 2. Performance Limit states of reinforced concrete column under cyclic lateral loading (Data from Goodnight [1])

1.1.1 Failure mechanism of reinforced concrete members

Studies done by Atalay and Penzien [7], Scott et al. [8], Zahn et al. [9], Mander et al. [10], Lehman and Moehle [11] and Goodnight [1] experimentally demonstrated the progressive failure mechanism of RC columns. When reinforced concrete column was subjected to lateral cyclic loads, primary damage accumulation was observed in the form of spalling of cover concrete, widening of concrete cracks and yielding of transverse rebar in critical regions [7]. As per Scott et al. [8], transverse rebar fracture reduces buckling resistance of longitudinal rebars. Experiments performed by Lehman and Moehle [11] on well confined concrete columns subjected to lateral cyclic loading, demonstrated reduction in strength of columns due to extensive damage to core concrete. Analytical study conducted by Feng et al.

[12] showed that, bar buckling is dependent on history of the loading. Due to this load history dependence, prediction of the longitudinal bar buckling is a challenging task. Goodnight [1] demonstrated that after the longitudinal rebar buckled significantly under simulated seismic loading, the buckled rebars may rupture suddenly during load reversal. After bar rupture, significant loss in strength is observed [1], [11]. As earthquake loading is arbitrary in nature, analytical prediction of the progressive failure mechanisms of RC members are essential in order to determine their performances or limit states. Because of the complexity involved in developing RC member performance simulation tools, none of the widely used structural analysis packages are yet to be able to simulate the 3D seismic responses of RC members. There is no literature that demonstrated analytical analysis to simulate progressive damage accumulation towards simulation of the transverse rebar failure, core concrete crushing, longitudinal rebar buckling and longitudinal rebar rupture of RC members. Analytical capability to predict limit states of RC members can be helpful in improving design codes, determining repair needs and developing seismic performance enhancement techniques.

1.1.2 Analysis and modeling techniques

In order to predict limit states and progressive failure mechanisms of RC members, robust analysis tool is required [13] in order to predict the global response of RC members along with progressive damage accumulation in the plastic hinge region. For prediction of limit states of RC members, there are two common analysis techniques which are available in literature. First analysis technique is fiber section analysis, where structural member is discretized into several cross sections across the length of the member [13]. These cross sections are defined with linear fiber elements which connects the adjacent sections. This

method primarily considers axial stress-strain responses, hence uniaxial constitutive material models of concrete and steel are used for predicting structural responses. Fiber modeling method is computationally efficient and simple to use, and because of uniaxial stress-strain modeling, parameter determination is also simple. On the other hand, the second analysis technique available in literature is the finite element (FE) analysis technique which is significantly more complex and time consuming than the fiber modeling technique. Due to associated complexity in FE analysis, this method is criticized as nonviable option for the analysis and design verification of RC members [5]. Recent study [4], [14], [15], however, demonstrated the importance and potential of the FE analysis technique for prediction of seismic response along with the limit state estimation of RC members. FE analysis technique is mathematically robust, versatile and it is based on material responses and physical characteristics of the RC member. The concrete and rebar can be modeled without sacrificing their 3D geometric and physical characteristics. Actual loading conditions on the concrete core and rebars can be simulated in accurately predicting the damage accumulation and resulting failure mechanisms. That is why multiaxial material models of concrete and steel are considered in the FE analysis in order to account for accurate material responses and interactions between concrete and rebars [14].

Limitations of the fiber modeling technique for RC column response prediction especially for simulation of the plastic hinge region has been demonstrated by Feng et al. [12], Moharammi and Koutromanos [15], Priestley et al. [5]. One of limitations is assumption of cracked cross section considered to be plane in fiber analysis whereas in experiments conducted by Scott et al. [8], distortion of the cross section is demonstrated. Due to this assumption, interaction of shear and moment cannot be accounted which leads to inaccurate

response prediction in plastic hinge region. In addition, fiber analysis technique can't simulate shear deformations due to which special non-fiber elements has to be considered in analysis to predict shear deformations [5]. Interaction between transverse rebar and confined concrete cannot be considered. Consequently, unconfined strength and confined strength for concrete has to be manually defined in the analysis [5]. Due to lack of interaction of steel and concrete, simulation of local interaction behavior such as transverse rebar fracture, effect associated with dilation of concrete on longitudinal rebar buckling is not possible by using the fiber analysis technique [4], [12].

In finite element analysis, interaction between transverse rebar, longitudinal rebar and concrete can be modeled accurately, consequently simulation of actual reinforced concrete member responses and thereby limit states under seismic loading can be simulated. Due to this interaction, concrete confining stresses can be simulated considering the strengths of concrete and steel. This type of nonlinear analysis technique can be used for retrofitting of existing buildings and to evaluate performance of new design procedure especially when a design procedure doesn't comply with standard design code [13]. Study by Babazadeh et al. [14] have shown the successful prediction of intermediate damage limit states of RC members such as spalling and crushing of concrete by implementing the FE analysis technique. Moreover, in structural regions such as beam-column joints where multiaxial stresses in steel and concrete are prominent, finite element analysis is the only means to capture various essential responses, especially the hysteretic responses [15]. Consequently, FE analysis technique is a promising analysis technique for the prediction of the limit states and failure mechanisms of RC member. There are many challenges associated with this techniques. For example, complex geometry modeling, concrete and steel material model development, validation and calibration,

modeling interactions between steel and concrete, etc. To overcome challenges involved in 3D stress-strain analysis of RC members, clear goal and objectives are necessary for adoption of such nonlinear analysis technique [13]. Assumptions associated in this technique are at the constitutive material model level, but not at the member geometry and physical behavior level. Due to this reason constitutive material models are one of the important aspect in 3D FE analysis technique.

1.1.3 Constitutive models for concrete and steel

For concrete material, there are several uniaxial constitutive models available in literature such as Popovics [16], Mander et al. [17], Belarbi and Hsu [18], Chang and Mander [19]. Use of these models will require equations for determining confined stresses. These models consider the effect of transverse steel in to account by parametric adjustment of equations of uniaxial response of material [15]. Some of these models [17], [19] are implemented in fiber analysis technique. On the other hand, many multiaxial constitutive models to simulate the 3D behavior of concrete have been proposed. William and Warnke [20] and Hsieh et al. [21] models are two of the pioneering concrete constitutive models, which can represent the tri-axial failure surface of concrete. William and Warnke [20] model gives good agreement with experimental data in compression meridian and tension meridian [22]. Main objective for developing this model was to establish yield surface in multiaxial stress space primarily for failure analysis [15]. Lubliner et al. [23], Lee and Fenves [24], Nguyen and Korsunsky [25] proposed concrete damage model which considers degradation of strength and stiffness of concrete induced by cracking and crushing. Model proposed by Cervenka and Papanikolaou [26] consider coupling of plasticity and fracture mechanics to simulate the

cracking and post cracking behavior of reinforced concrete. All the multiaxial concrete models are mainly used to simulate the monotonic response [15]. Evaluation and validation of these models under cyclic loading are lacking in literature. Moharrami and Koutromanos [15] recently proposed smeared cracking model in order to simulate the influence of cracked concrete on RC member cyclic response.

For steel material, available uniaxial constitutive models are Ramberg and Osgood [27], Menegotto and Pinto [28], Filippou et al. [29], Dodd and Restrepo-Posada [30], Dhakal and Maekawa [31] which can only be used in fiber modeling. Other available models like Armstrong and Fedrick [32], Mroz [33], Chaboche [34] are multiaxial constitutive models which can simulate response of steel rebar under axial and shear loading more accurately. Multi-surface model can capture very good responses of materials in RC members under monotonic load, due to which this model was implemented for prediction of steel response in RC structure in the study by Babazadeh et al. [14]. Armstrong and Frederick [32] model is a nonlinear kinematic hardening model and can predict monotonic as well as cyclic response of the steel reasonably. One of the most advanced model for steel is Chaboche [34], which is basically an extension of Armstrong and Frederick model. The Chaboche model can represent multiaxial material response under both monotonic and cyclic loading quite well [35].

Some of the above constitutive models are available in FE analysis software packages, such as ANAYS, ABAQUS, ATENA etc. In ANSYS, available concrete model is William and Warnke model [20]. This model gives good estimation of confined strength of concrete but fails to predict the stress-strain response of concrete as elastic perfectly plastic stress-strain relationship is used in this model. Due to this reason, this model is not considered in this study. In ABAQUS, Lee and Fenves model [24] is used for prediction of concrete behavior. This

constitutive model have capability to simulate confined strength of concrete with stress-strain response along with degradation of stiffness of concrete under cyclic loading. Due to this reason, this model is considered for this study. Available smeared cracking model in ABAQUS fails to capture the multiaxial response of concrete, hence smeared cracking model is not considered in this study. In ATENA, model by Cervenka and Papanikolaou [26] is used for concrete model. This model gives good estimation of confined strength of concrete along with stress-strain response. Because of these reasons, this model is considered for this study. For material modeling simulation of steel in ABAQUS, multilinear model, model with advanced nonlinear hardening rule by Chaboche [34] are available. In ATENA, available constitutive models for steel materials are multilinear model for multiaxial modeling and Pinto model [28] for uniaxial modeling. This study made effort towards evaluating constitutive models for steel and concrete which are considered above in simulation of progressive degradation mechanism in RC member under seismic loading.

1.2 Scope and Organization

As discussed earlier, damage prediction or RC members is an important tool in performance based design. In order to predict the seismic response of RC members and progressive damage accumulation towards failure, robust analysis techniques involving advanced constitutive model along with physical and geometric characteristic of RC members are essential. Due to this fact, constitutive models has to be validated using 3D FE analysis of RC members subjected to simulated seismic loading. This study validate several multiaxial and robust constitutive models of concrete and steel which are available in widely used FE

software packages and are suitable for 3D stress-strain response analysis and damage accumulation studies.

Study is presented through four chapters. Chapter 1 is the current Introduction chapter. Chapter 2 presents existing constitutive models of concrete and steel, along with their validation against material level tests or RC member tests prescribing monotonic compressive loading. Detailed discussions are made on the application and limitation of the models. In verification of models, FE validation considered concrete material monotonic compressive responses under active and passive confinement.

In Chapter 3, constitutive models are then validated against RC members subjected to lateral cyclic loading in the presence of steady compressive loading. In this chapter, limitations of the existing models in predicting RC member seismic responses are presented.

Finally in Chapter 4, discussions and conclusion from this study are presented along with necessary future work in this field.

1.3 References

[1] Goodnight J., *The effects of Load History and Design Varialbes on Performance Limit States of Circular Bridge Columns,* PhD dissertation, North Carolina State Univeristy Raleigh, North Carolina, 2015.

[2] L. Decker, P. Ellis, K. Fleming, A. Giaconia, R. Hamburger, D. McCormick, M. Rojansky, S. Schleifer and J. Smallwood-Garcia, "The January 17, 1995 Kobe earthquake An EQE summary report," EQE International, April, 1995.

[3] Haro A.G. and Zuniga E. E., "Minor Structural damage - RC Buildings," EERI, Illapel, Chile earthquake clearinghouse, 15 October 2015. [Online]. Available: http://www.eqclearinghouse.org/2015-09-16-chile/2015/10/15/minor-structural-damage-rc-buildings/. [Accessed 15 June 2016].

[4] Feng Y., Kowalsky M. J. and Nau J. M., "Finite-Element Method to predict reinforcing bar buckling in RC structres," *ASCE,* 2014.

[5] Priestley M. N., Calvi G. M. and Kowalsky M. J., Displacement-Based Seismic Design of Structures, Pavia, ITALY.: IUSS PRESS, 2007.

[6] Goodnight J. C. , Kowalsky M. J. and Nau J. M., "Effect of load history on Performance Limit States of circular bridge columns," *J. of bridge Eng.,* vol. 18, no. 12, pp. 1383-1396, 2013.

[7] Atalay M. B. and Penzien J., "The seismic behavior of critical regions of Reinforced Concrete Components as influenced by moment, shear and axial force," Earthquake Engineering Research Center, Univeristy of California Berkeley, California, December, 1975.

[8] Scott B. D., Park R. and Priestley M. J. N., "Stress-strain behavior of concrete confined by overlapping hoops at low and high strain rates," *J. of the American Concrete Institute,* vol. 79, no. 2, pp. 13-27, 1982.

[9] Zahn F. A., Park R. and Priestley M. J. N., "Design of reinforced concrete bridge columns for strength and ductility," University of Canterbury, Christchurch, New Zealand, 1986.

[10] Mander J. B., Priestley J. N. and Park R., "Observed Stress-Strain Behavior of Confined Concrete," *J. Struct. Eng.,* pp. 1827-1849, 1988.

[11] Lehman D. E. and Moehle J. P., "Seismic performance of well-confined concrete bridge columns," Pacific Earthquake Engineering Research Center, University of California, Berkeley, December, 2000.

[12] Feng Y, Kowalsky M. J. and Nau J. M., "Fiber-Based modeling for investigation the effect of Load History on the behavior of RC Bridge Columns," in *15th World Conference on Earthquake Eng.2012,* Lisbon, Portugal, 2012.

[13] Deierlein, Gregory G., Reinhorn, Andrei M., and Willford, Michael R. (2010). “Nonlinear structural analysis for seismic design,” NEHRP Seismic Design Technical Brief No. 4, produced by the NEHRP Consultants Joint Venture, a partnership of the

Applied Technology Council and the Consortium of Universities for Research in Earthquake Engineering, for the National Institute of Standards and Technology, Gaithersburg, MD, NIST GCR 10-917-5.

[14] Babazadeh A., Burgueno R. and Silva P., "Use of 3D Finite-Element Models for Predicting Intermediate Damage Limit States in RC Bridge Columns," *J. Struct.Eng.*, pp. 04015012-1 to 04015012-11, 2015.

[15] Moharrami M. and Koutromanos I., "Triaxial Constitutive Model for Concrete under Cyclic Loading," *J. Struct. Eng.*, pp. 04016039-1 - 04016039-15, 2016.

[16] Popovics S., "A nuerical approach to the complete stress-strain curve of concrete," *Cement and concrete research, Volume 3,* pp. 583-599, 1973.

[17] Mander J. B., Priestley J. N. and Park R., "Theoretical Stress-Strain Model for Confined concrete," *J. Struct. Eng.*, pp. 1804-1826, 1989.

[18] Belarbi A. and Hsu T. T., "Constitutive laws of concrete in tension and reinforcing bars stiffened by concrete," *J. of American Concrete Institute,* vol. 91, pp. 465-474, 1994.

[19] Chang G. A. and Mander J. B., "Seismic energy based fatigue damage analysis of bridge columns: Part 1 - Evaulation of seismic capacity," NCEER-94-0006, University of Buffalo, New York, March, 1994.

[20] William K. J. and Warnke E. P., "Constitutive model for the triaxial behavior of concrete," *Int.Assiciation for Bridge and Struct. Eng.*, vol. 19, pp. 1-30, 1975.

[21] Hsieh S. S., Ting E. C. and Chen W. F., "A plstic-fracture model for concrete," *Int. J. Solids structures,* vol. 18, no. 3, pp. 181-197, 1982.

[22] W.-F. Chen, Constitutive Equations for Engineering Materials, Volume 1, 1994
.

[23] Lubliner J., Oliver J., Oller S. and Onate E., "A plastic-Damage Model for concrete," *J. of solids structures,* vol. 25, no. 3, pp. 299-326, 1989.

[24] Lee J. and Fenves G., "Plastic-Damage Model for cyclic Loading of Concrete structures," *J. Eng. Mech.*, pp. 892-900, 1998.

[25] Nguyen G. D. and Korsunsky A. M., "Development of an approach to constitutive modeling of concrete: Isotropic damage coupled with plasticity," *Int. J. of solids and Struct.* , vol. 45, no. 20, pp. 5483-5501, 2008.

[26] Cervenka J. and Papanikolaou V., "Three dimenxional combined fracture-plastic material model for concrete," *Int. J. of Plasticity*, pp. 2192-2220, December, 2008.

[27] Ramberg W. and Osgood W. R., "Description of stress-strain curves by three parameters," National advisory committee for aeronautics, 902, Washington, 1943.

[28] Menegotto M. and Pinto P. E., "Method of analysis for cyclically loaded R.C. Plane Frames including changes in geometry and non-Elasitc behavior of elements under combined normal force and bending," vol. 13, 1973.

[29] Filippou F. C. , Popov E. P. and Bertero V. V., "Effects of bond deterioration on hysteretic behavior of reinforced concrete joints," Earthquake Engineering Research Center, California, 1983.

[30] Dodd L. L. and Restrepo-Posada J. I., "Model for Predicting Cyclic Behavior of Reinforcing Steel," vol. 121, no. 3, 1995.

[31] Dhakal R. P. and Maekawa K., "Modeling for Postyield Buckling of Reinforcement," *Journal of Structural Engineering*, vol. 128, no. 9, pp. 1139-1147, 2002.

[32] Armstrong P. J. and Frederick C. O., "A mathematical representation of the multiaxial baushinger effect," CEGB, Report No. RD/B/N 731, 1966.

[33] Mroz Z., "On the description of anisotropic workhardening," *J. of Mech. and Physics of solids*, vol. 15, pp. 163-175, 1967.

[34] Chaboche J. L., "Time-Independent Constitutive Theories for Cyclic Plasticity," vol. 2, 1986.

[35] Bari S. and Hassan T., "Anatomy of coupled constitutive models for racheting simulation," *International Journal of Plasticity* , vol. 16, no. 3-4, pp. 381-409, 2000.

2 Concrete modeling for monotonic axial compressive loading

As discussed in early chapter, 3D finite element analysis can be used effectively for prediction of progressive damage accumulation in the structures under seismic loading. In order to identify suitable material models to be used in finite element analysis, available material models in the finite element software packages need to be validated against experimental responses.

Two types of concrete constitutive models are available in literature. The first type is the uniaxial material model which considers uniaxial loading only. The second type is the multiaxial material model developed for analysis of 3D stresses and strains.

The uniaxial constitutive models of concrete available in literature are Popovics [1], Mander et al. [2], Belarbi and Hsu [3], Chang and Mander [4], Legeron and Paultre [5], D'Amato et al. [6]. These models, except [1], considers the confinement effect on the compressive stress-strain response through empirical equations.

The multiaxial constitutive material models of concrete available in the literature are William and Wranke [7], Hsieh et al. [8], Lubliner et al. [9], Lee and Fenves [10], Nguyen and Korsunsky [11], Cervenka and Papanikolaou [12], Moharrami and Koutromanos [13]. Some of the early proposed models such as William and Wranke [7], Hsieh et al. [8] deals with determination of the failure surface for concrete under multiaxial loading. In these models, stress-strain relationship were idealized as elastic-perfectly plastic and consequently these models can't be used for predicting the strength degradation of concrete subsequent to ultimate strength. The William and Wranke model [7] is available in ANSYS [14] software package. The other types of model such as, extended Drucker-Prager and extended Drucker-Prager Cap

model [15] is available in ANSYS and are used for nonhomogeneous materials such as rock, soils. These model can be adjusted to predict the responses of concrete. In ABAQUS [16], Lee and Fenves model [10] is available for concrete plasticity response simulation. In ATENA [17], Cervenka and Papanikolaou [12] model is available for concrete of plasticity response simulation. Due to availability of these models in the commercial finite element software packages, these are investigation in this study in simulation concrete responses.

Three different types of experimental data are collected for this study. The first set includes concrete cylinder under active confinement, where concrete cylinder subjected to active hydraulic pressure and monotonic compressive loading. The second set of experiments includes the concrete filled steel tube under monotonic compression loading resulting in passive confinement of concrete. The third set of experiments considered are the reinforced concrete column subjected to monotonic compressive loading resulting in discrete passive confinement of concrete. All these experiments which are used for the validation of the constitutive models are briefly discussed in the following section.

2.1 Experimental data used for concrete constitutive model validation

2.1.1 Concrete cylinder experimental data

In the pioneering experimental study by Richart et al. [18], concrete cylinders were subjected to active (steady) hydraulic pressure 'p' and subsequently the monotonically increasing compressive force 'F' as showed in Fig. 1a. A set of experimented responses under several confinement pressure 'p' are plotted in the Fig. 1b. Compressive strength of the unconfined concrete was 25.23 MPa and under confinement pressure 3.79 to 28.19 MPa the compressive strength and ductility of concrete gradually increases as shown in Fig. 1b. Significant changes in the stress-strain response of concrete are observed with increase in confining pressure. Such stress-strain responses of concrete under various levels of confining pressure has to be simulated accurately by concrete constitutive model in order to simulate the limit states of RC members.

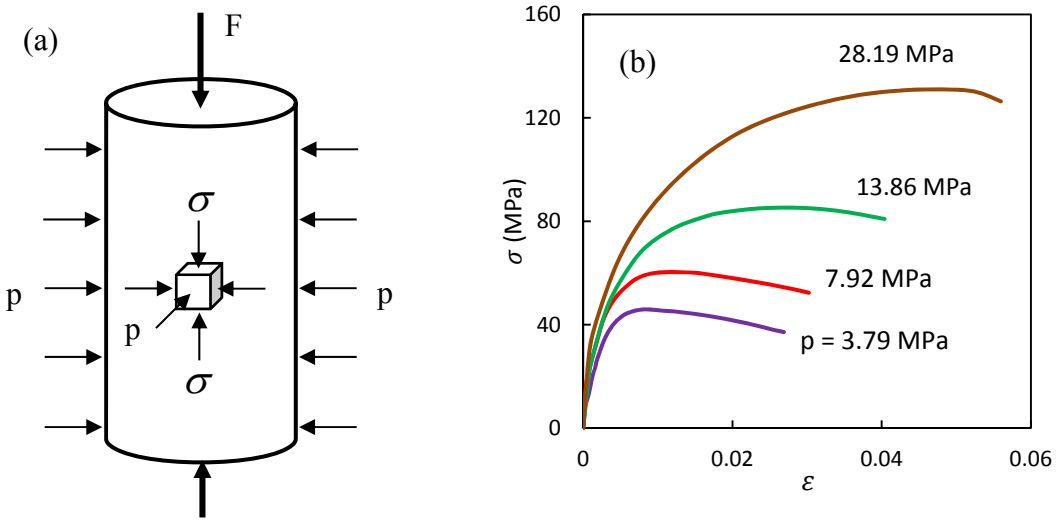

Fig. 1. Concrete cylinder experiments by Richart et al. [18] (a) Cylinder under active hydraulic pressure 'p' and monotonic increasing axial compressive force 'F' (b) Compressive stress-strain relationship under various level of active pressure

2.1.2 Concrete filled steel tube experimental data

Experiments were conducted on concrete filled steel tube (CFST) by Schneider [19] under monotonic compressive loading. Several specimens were tested with circular, rectangular and square cross sections. For concrete model validation study, two experiments with circular cross sections which are listed in Table 1 were considered.

Table 1. Experiments considered for simulation of concrete filled steel tubes

Experiment number	Unconfined Strength of concrete (MPa)	Yield point of steel (MPa)	Thickness of steel tube (mm)	Diameter of steel tube (mm)
C1	28.18	285	3	140.8
C2	23.8	313	6.5	141.4

Compressive force-displacement responses from these two experiments are plotted in Fig. 2, where it is observed that the increase in thickness of the steel tube increases the confining pressure, resulting in increase in the confined strength of the CFST column.

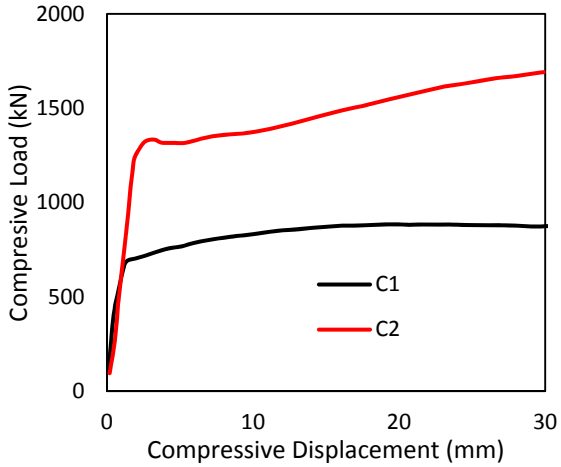

Fig. 2. Experimental Responses of concrete filled steel tubes (Data from Schneider [19])

2.1.3 Reinforced concrete column under monotonic compressive loading

Data from reinforce concrete column experiments conducted by Bing et al. [20] under monotonic compressive loading are considered for concrete material model validation. The specimens with transverse reinforcement steel having yield strength of 445 and 1318 MPa, and concrete strength varying from 52 to 82.5 MPa are considered. Longitudinal rebars used in the RC columns were same, six 12 mm diameter bars were used. The longitudinal rebar yield strength was 443 MPa. Diameter and length of the RC columns were 240 mm and 720 mm respectively. A total of 40 specimens have tested by Bing et al. [20] but for model verification purpose, 8 specimens were selected with 4 specimens have normal strength steel and other 4 specimens have ultra-high strength steel as transverse reinforcement as shown in Table 2. These columns were selected in such a way that they have different strengths of concrete and transverse rebar steel, and with two different spacing of the transverse rebar. This selection is made in order to validate concrete model against wider range of confining stress and different unconfined concrete strength.

Table 2. Details of experimental specimens

Specimen	f'_{cc} (MPa)	F_y of transverse rebar (MPa)	Spacing of transverse rebar (mm)	Dia. of transverse steel (mm)
6A	63.0	445	35	6.0
6B	72.3	445	35	6.0
9A	63.0	445	50	6.0
9B	72.3	445	50	6.0
4HB1	52.0	1318	35	6.4
4HC	82.5	1318	35	6.4
6HB	52.0	1318	50	6.4
6HC	82.5	1318	50	6.4

Through these experiments, Bing et al. [20] investigated the behavior and failure mechanism of RC column at higher ductility, including the influence of transverse rebar strength on RC column. Bing et al. [20] demonstrated that failure mechanism consist of longitudinal rebar buckling and transverse rebar fracture coupled with shear failure of RC column. Results of the experiments under consideration are shown in Fig. 3, where red color curves indicate experiments with higher strength concrete. Fig. 3 also demonstrates that the ultra-high strength steel increases the strength and ductility of RC column under monotonic compression.

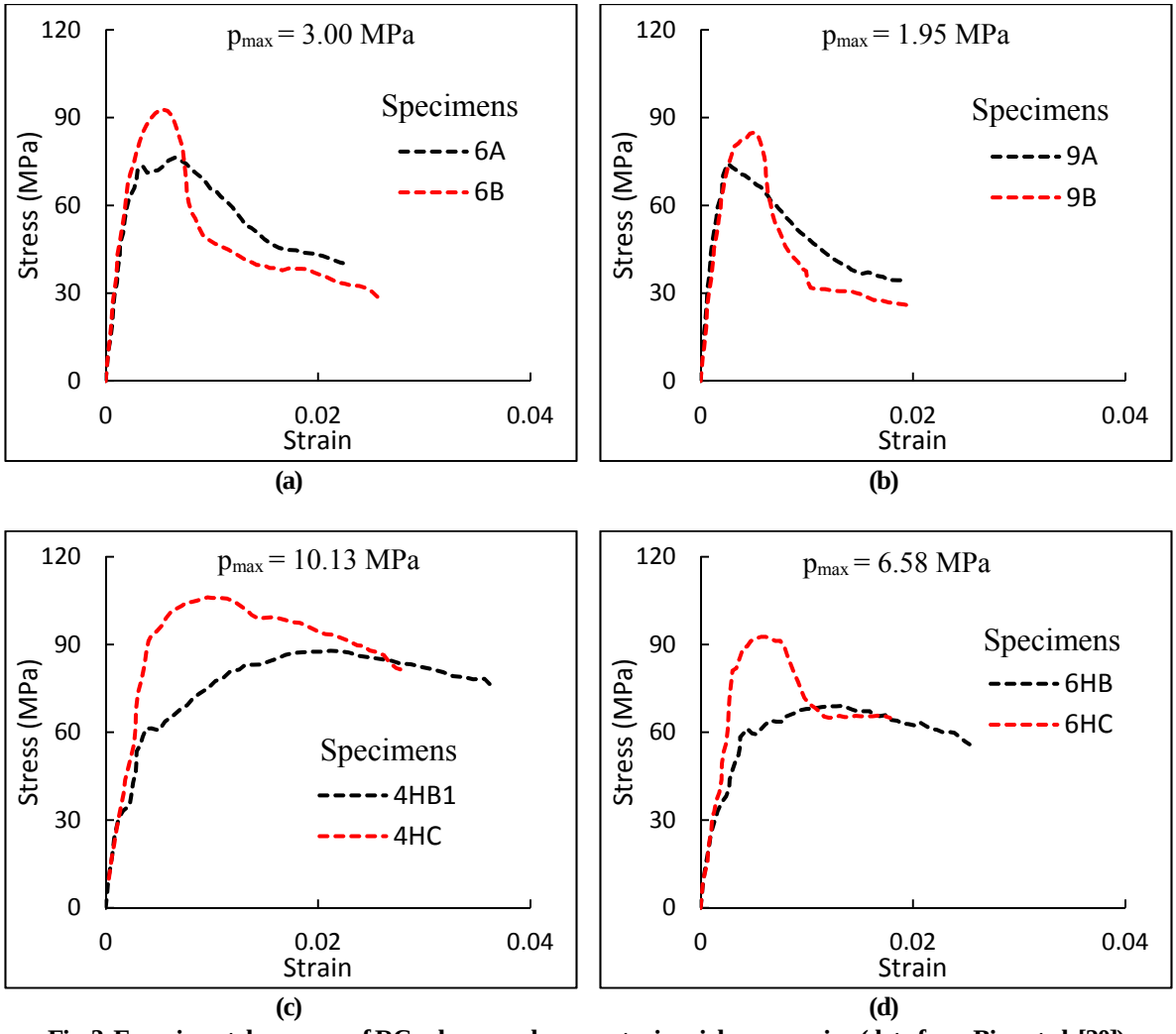

Fig. 3. Experimental response of RC column under monotonic axial compression (data from Bing et al. [20]) (a) Specimens 6A and 6B, (b) Specimens 9A and 9B, (c) Specimens 4HB1 and 4HC, (d) Specimens 6HB and 6HC, p_{max} is the confining pressure calculated by Mander model [2]

2.2 Concrete constitutive models

2.2.1 Uniaxial models

In uniaxial concrete models, Popovics [1], Mander et al. [2], Belarbi and Hsu [3], Chang and Mander [4], Legeron and Paultre [5], D'Amato et al. [6] are available in literature. Among these models, Mander model [2] is widely used hence, it is evaluated in this study.

Mander Model

Mander model [2] was developed to predict the compressive stress-strain response of RC columns. This model considers the geometric and material parameters of the RC column to determine the column strength. Geometric and material parameters included are,

1. Spacing of transverse rebar
2. Diameter of transverse rebar
3. Yield strength of transverse rebar
4. Unconfined strength of concrete
5. Diameter of core concrete column

First the passive confining stress in a column developed by transverse rebar is determined, followed by determination of the confined stress-strain response of the concrete column. In order to determine ultimate compressive strength, multiaxial Willam and Wranke [7] model was used. Mander model is developed on the basis of conservation of energy. Additional ductility of the confined concrete is assumed to be contributed by the energy stored in transverse reinforcement. In this model, the ultimate strength of confined concrete in a column is calculated by,

$$f'_{cc} = f'_{co}\left[-1.254 + 2.254\sqrt{1 - \frac{7.94f'_l}{f'_{co}}} - 2\frac{f'_l}{f'_{co}}\right] \quad (1)$$

Where, f'_{co} is unconfined strength of concrete and f'_l is confining stress in the concrete.

For circular columns, confining stress f'_l, is determined by,

$$f'_l = \frac{1}{2}k_e\rho_s f_{yh} \quad (2)$$

Where, k_e is effective confinement ratio, which is given by,

$$k_e = \frac{\left(1-\frac{s'}{2d_s}\right)^2}{1-\rho_{cc}} \quad \text{…for hoops} \quad (3)$$

$$k_e = \frac{1-\frac{s'}{2d_s}}{1-\rho_{cc}} \quad \text{…for spirals} \quad (4)$$

s' = clear spacing of transverse reinforcement as shown in Fig. 4a

d_s = diameter of column after subtracting the clear cover, i.e. diameter of core concrete as shown in Fig. 4a

f_{yh} = yield stress of transverse hoop steel considering elastic perfectly plastic model

ρ_{cc} = ratio of area of longitudinal steel area to confined core concrete

ρ_s = ratio of volume of transverse steel to confined core concrete

For rectangular columns, confinement in x and y direction are different which are given by,

$$f'_{lx} = \frac{1}{2}k_e\rho_x f_{yh} \quad \text{and} \quad f'_{ly} = \frac{1}{2}k_e\rho_y f_{yh} \quad (5)$$

From these two different confining pressure, either average confining pressure is utilized as f'_l in eq. (1) or interaction diagram suggested by Mander et al. [2] are used to calculate the total confining pressure f'_l. Effective confinement ratio k_e for rectangular columns is,

$$k_e = \frac{\left(1-\sum_{i=1}^{n}\frac{w'^{2}_{i}}{6b_c d_c}\right)\left(1-\frac{s'}{2b_c}\right)\left(1-\frac{s'}{2d_c}\right)}{1-\rho_{cc}} \qquad (6)$$

where, b_c = the breadth of the confined concrete core as shown in Fig. 4b

d_c = the depth of the confined concrete core as shown in Fig. 4b

s = spacing of the transverse rebar

s' = clear spacing of transverse reinforcement

w' = clear transverse spacing between adjacent longitudinal rebar

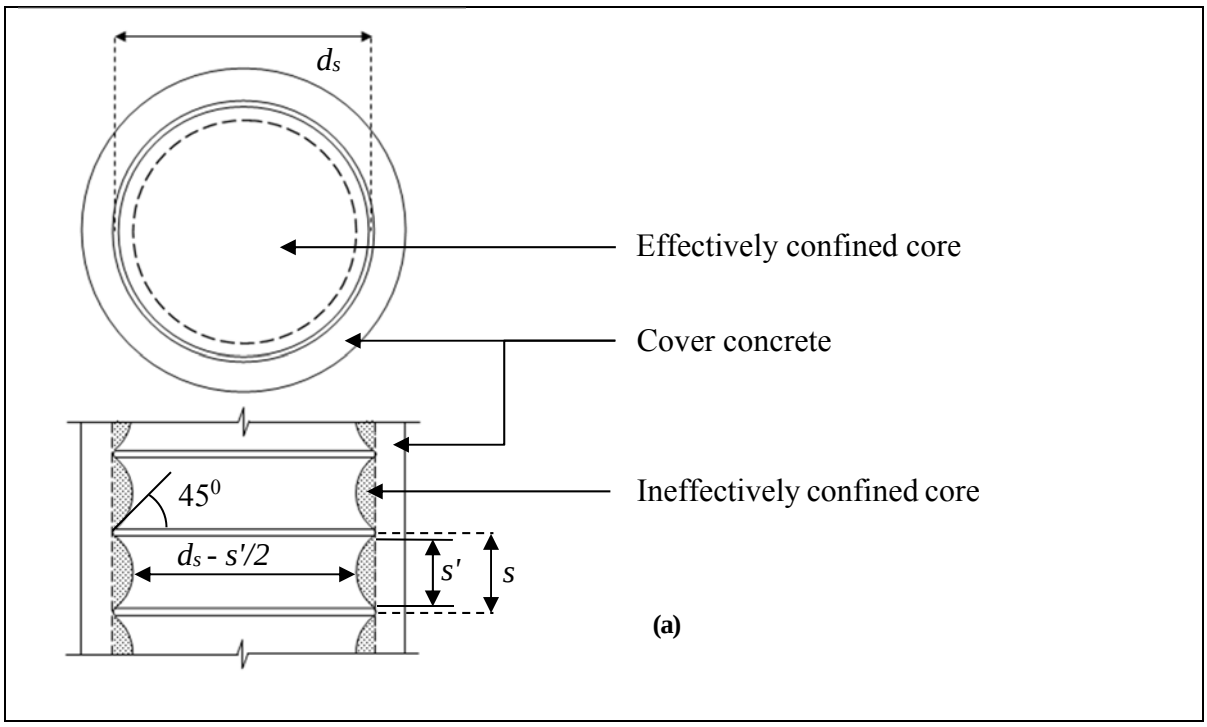

Fig. 4. Confined core of RC (a) Circular column, (b) Rectangular column

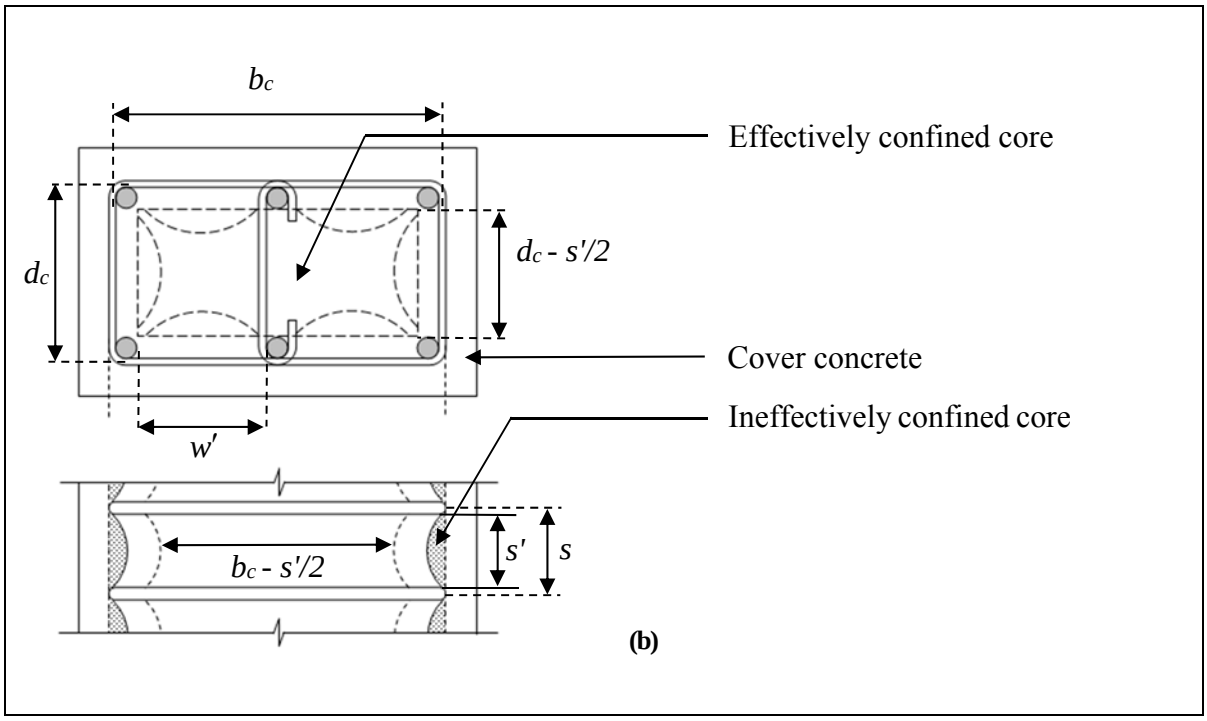

Fig. 4 Continued. Confined core of RC (a) Circular column, (b) Rectangular column

The relationship of the stress-strain in confined column is given by following equation,

$$f_c = \frac{f'_{cc}\, xr}{r - 1 + x^r} \qquad (7)$$

where,

$$r = \frac{E_c}{E_c - E_{\text{sec}}} \qquad (8)$$

$$x = \frac{\varepsilon_c}{\varepsilon_{cc}} \qquad (9)$$

where ε_{cc} is the strain at which confined concrete achieves its ultimate compressive strength which is given by,

$$\varepsilon_{cc} = \varepsilon_{co}\left[1 + 5\left(\frac{f'_{cc}}{f'_{co}} - 1\right)\right] \qquad (10)$$

ε_{co} is strain at unconfined concrete strength, f_c is stress at any given strain value ε_c , E_c is elastic modulus and E_{sec} is secant modulus at ultimate strength which is given by $E_{sec} = \frac{f'_{cc}}{\varepsilon_{cc}}$.

Mander et al. [21] performed a set of experiments to validate the Mander model [2]. In these experiments, reinforced concrete columns were subjected to monotonic compressive load till failure. Range of strength of concrete utilized in the experiments was 24 MPa to 32 MPa. Yield strength of the transverse steel was 340 MPa. The concrete confining pressure developed by the transverse rebar were in the range 0.85 to 4.18 MPa.

Work done by Legeron and Paultre [5] have shown that Mander model over predicts the ultimate strength of confined concrete when high-strength concrete is used with high-strength steel as transverse reinforcement. Study by Legeron and Paultre [5] didn't presented the stress-strain response of confined concrete, due to which experiments done by Bing et al. [20] is considered in this study for validation of the Mander model [2].

Comparison of the simulation by Mander model [2] against experimental responses of RC columns are presented in Fig. 5. In this comparison one experiment have transverse rebar with yield strength 445 MPa (Fig. 5a) and another with yield stress 1318 MPa (Fig. 5b). It is observed that the Mander model [2] well predicted the response of RC column with normal strength transverse rebar (Fig. 5a) where, as significantly over predicts the response of the RC column with ultra-high strength transverse rebar (Fig. 5b). Hence, Mander model gives good prediction of RC column under pure compression for low level of confining pressures, but at relatively higher level of confining pressure Mander model over predicts the response.

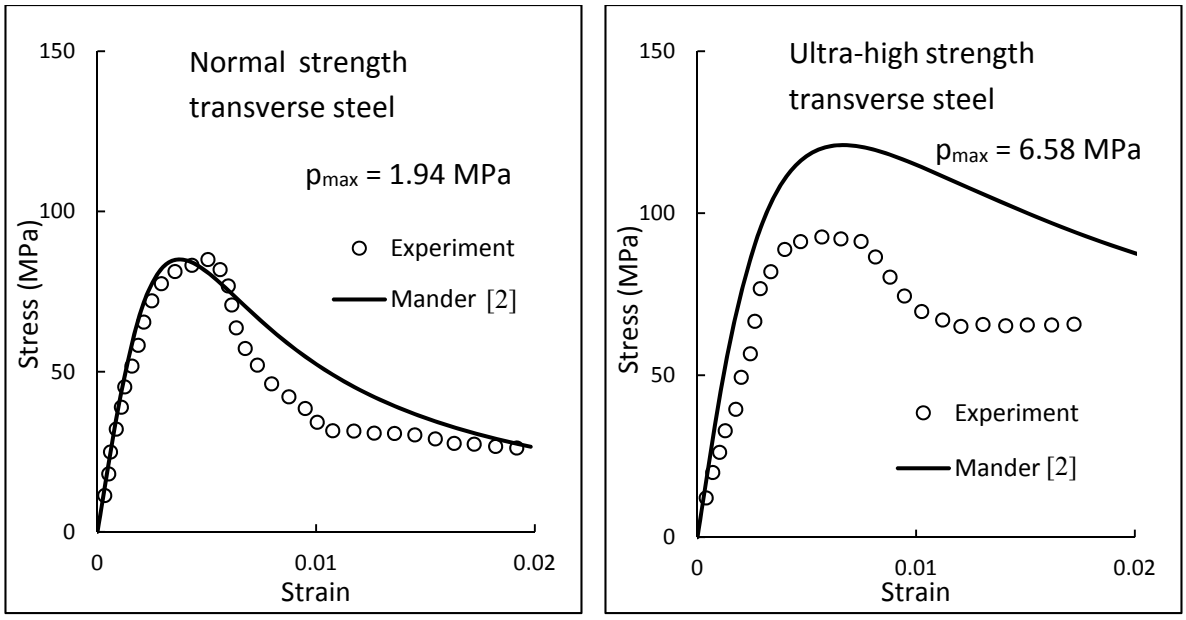

Fig. 5. Performance of Mander model [2] against experimental RC column reference with transverse steel of yield stress (a) 445 MPa (normal strength steel) to yield maximum confining pressure of 1.94 MPa and (b) 1318 MPa (ultra-high strength steel) to yield maximum confining pressure of 6.58 MPa

The Mander model [2] is easy to implement, numerically efficient but because of its uniaxial nature, lacks the capability to describe the multiaxial stress state in RC columns. Hence, Mander model can't be used for prediction of the limit states and failure mechanism under seismic loading, especially the longitudinal rebar buckling.

OPENSEES models

In OPENSEES, there are several uniaxial concrete constitutive models are available such as Popovics model [1], Mander model [2], Chang and Mander [4], Belarbi and Hsu [3], etc. One of the advanced model by Chang and Mander [4] is widely used which can simulate cyclic uniaxial stress-strain response of concrete. This model considers the Mander model [2] to determine the confined strength of concrete from geometry of the RC column. Then this confined strength is used for determination of cyclic response of RC column. Simulation of this model are promising when compared against experimental cyclic stress-strain response of

plane concrete cylinders as well as RC columns [4]. But this model lacks the ability to predict the multiaxial effect of concrete which is essential in damage accumulation in RC members. Along with this fact, simulation of failure mechanism caused due to accumulation of damage such as core concrete crushing, transverse rebar failure and longitudinal rebar buckling is not possible with uniaxial models. When this model is implemented in OPENSEES, shear forces and shear deformations are neglected which causes incorrect predictions of response of RC column. Hence, uniaxial models such as Mander model [2], Chang and Mander [4] can be used to determine the force-displacement response or stress-strain response of RC members but these models fails to simulate the detailed failure mechanism occurring in RC members. As this study is focused on the prediction of accumulation of damage and failure mechanism occurring in RC members, OPENSEES software is not used for the simulation of cyclic responses of RC members.

2.2.2 Multiaxial models based on plasticity

Multiaxial constitutive modeling of concrete and relevant basic concepts are discussed in this section. Consider the Fig. 6a, where stress point P is shown in Haigh-Westergaard stress space such that stress axes indicate the principal stress directions. Axis having direction cosines as $\left(\frac{1}{\sqrt{3}},\frac{1}{\sqrt{3}},\frac{1}{\sqrt{3}}\right)$ is considered as hydrostatic axis which is I_1 axis (Fig. 6a) and plane perpendicular to this axis is known as π-plane. Yield surface is defined as the surface in stress space outside of which stresses induce irreversible plastic strains. For metals, cross section of the von-Mises yield surface in π-plane is circular on shape but concrete material have complex shape on π-plane as shown in Fig. 6b.

Fig. 6b indicates the view from π-plane where arrows indicate the compression stress and red dotted line indicates the tensile meridian. In this case, the meridians are separated by 60^0 angle. Experiments done by Kupfer et al. [22], shown that failure limit for concrete on tension meridian is different from compressive meridian. Due to this reason, some of the early study on concrete constitutive modeling was performed to capture the failure surfaces in multiaxial stress space [7], [8]. Following discussion presents failure surfaces proposed by different studies.

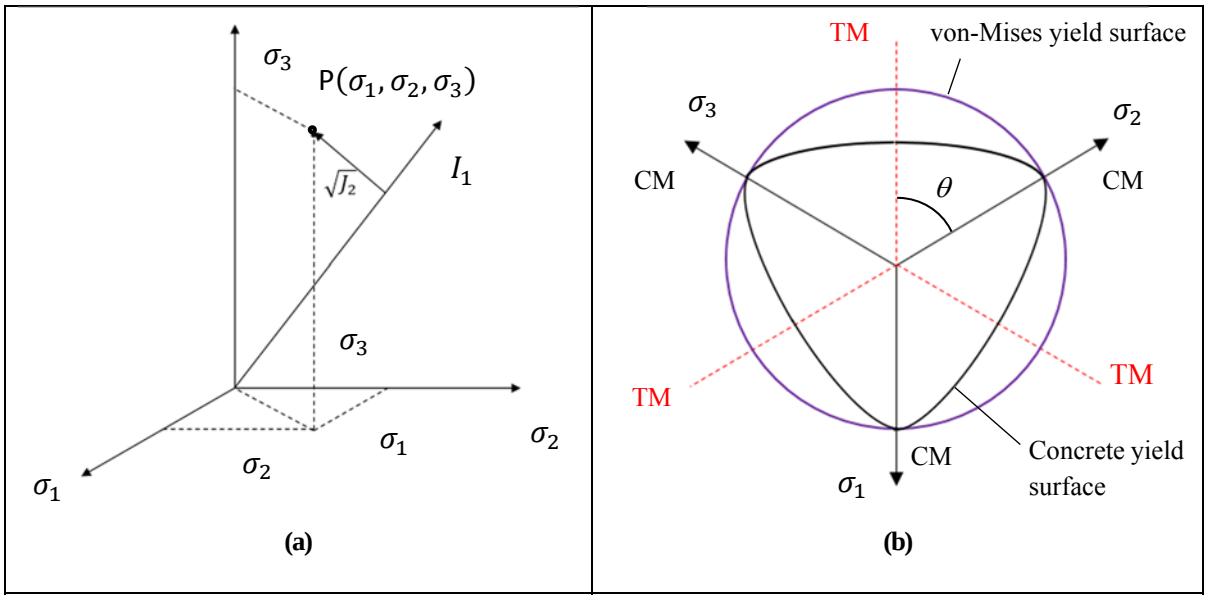

Fig. 6. Basics definitions (a) Stress Invariants (b) Tension and compression meridians in π-plane

One parameter Model – Rankine

This model considers the most basic failure criterion [23]. In this model, failure of concrete is considered as brittle failure in tension which is maximum tensile stress criterion. The equation of the fracture surface in terms of principal stress terms is given by,

$$\sigma_1 = f_t', \ \sigma_2 = f_t', \ \sigma_3 = f_t' \qquad (11)$$

These failure surfaces are referred as failure cutoff surface or tension cutoff. These equations suggest whenever stress along a principal direction satisfy the failure condition, brittle failure of the material occurs. Same equation in deviator stress space can be given by [23],

$$f\left(I_1, \mathrm{J}_2, \theta\right) = 2\sqrt{3}\sqrt{\mathrm{J}_2}\cos\theta + I_1 - 3f'_t = 0 \qquad (12)$$

In this equation, the only parameter required is f'_t, which is fracture stress of concrete in tension. This criterion is often combined with other models to represent the brittle nature of concrete in tension. As discussed earlier, this model just considers the failure surface of concrete by cracking, hence this model can't be used for simulation of RC member responses.

Two Parameter models

As one parameter model is not enough to represent the multiaxial responses, two parameter models, such as, Mohr-Coulomb, Drucker-Prager model were introduced. These models can capture the failure surface of the pressure sensitive materials such as soils, rocks, concrete but don't have the capacity to predict the concrete stress-strain response. Following discussion give a brief introduction of these multiaxial failure surface models.

1. Mohr-Coulomb model

The two parameters needed for this model are cohesion 'c' and internal frictional angle 'ϕ'. Once these parameters are known following equations can be used to determine the concrete failure surface.

$$\sigma_1 \frac{\left(1+\sin\phi\right)}{2c\cos\phi} - \sigma_3 \frac{\left(1-\sin\phi\right)}{2c\cos\phi} = 1 \qquad (13)$$

Though, this model is essentially used for soils and rocks, it can be calibrated for concrete rupture simulation. There are some limitations of this model such as over prediction of the response in tension, constant failure surface in tension and compression meridian, linear dependency of strength over hydrostatic pressure.

2. Drucker-Prager model

In the Drucker-Prager model [24], two parameters under consideration are α and k. Yield surface equation is given by,

$$f\left(I_1, J_2\right) = \alpha I_1 + \sqrt{J_2} - k = 0 \qquad (14)$$

This model is the extension of the von-Mises criterion for pressure dependent materials to pressure (hydrostatic stress) dependent material such as concrete, rock and soil. The dependency of the hydrostatic pressure is considered into account through the model parameters α and k. This model have some similar limitation as Mohr-Coulomb's model such as over prediction of tensile strength and similar failure in tension and compression meridian. Due to this reason, some modifications were proposed such as Extended Drucker-Prager Model and Extended Drucker-Prager Cap model.

1. In Extended Drucker-Prager model available in ANSYS [14], yielding of the material in tension is governed by either hyperbolic function or power law. One function has to be selected which gives best fit for experimental data. These function are given as,

   $F = \sqrt{b^2 + J_2} + \alpha I_1 - k = 0$ Hyperbolic *(15)*

   $F = \left(\sqrt{J_2}\right)^b + \alpha I_1 - k = 0$ Power law *(16)*

Where, b is the parameter characterizing the shape of the yield function. This parameter gives control over the yielding in tensile region so as to reduce the effective tensile strength.

2. In Extended Drucker-Prager Cap model [15], failure equation is controlled by the value of I_1. If I_1 is positive then failure is in tension region. Failure in this region is governed by failure cap called as tension cap. This tension cap is defined as,

$$Y_t\left(I_1,\sigma_0\right)=1-H\left(I_1\right)\left(\frac{I_1}{R_t^Y Y_s\left(0,\sigma_0\right)}\right)^2 \qquad (17)$$

When I_1 is lesser than K_0, then failure is governed by compaction cap which is given as,

$$Y_t\left(I_1,K_0,\sigma_0\right)=1-H\left(K_0-I_1\right)\left(\frac{I_1-K_0}{R_t^Y Y_s\left(K_0,\sigma_0\right)}\right)^2 \qquad (18)$$

The region between $K_0 < I_1 < 0$ is governed by shear function where failure is governed by shear failure and its equation is,

$$Y_S\left(I_1,\sigma_0\right)=\sigma_0-Ae^{\beta^Y I_1}-\alpha^Y I_1 \qquad (19)$$

where, A, α^Y, β^Y are material parameters which controls the shape of failure surface, σ_0 is cohesion related material constant and H is step function.

Failure plane in π-plane is controlled by,

$$\Gamma\left(\beta,\psi\right)=\frac{1}{2}\left(1+\sin 3\beta+\frac{1}{\psi}\left(1-\sin 3\beta\right)\right) \qquad (20)$$

where, $\beta(J_2, J_3) = -\frac{1}{3}\sin^{-1}\left(\frac{3\sqrt{3}J_3}{2J_2^{3/2}}\right)$ and Ψ is ratio of tri-axial extension strength to compression strength. This value ranges from 1 to 0.778. At Ψ = 1, failure surface resembles von-Mises criterion.

As stated earlier, the extended Drucker-Prager Cap model can be used for concrete response simulations, for which the unconfined concrete was fitted by multilinear model.

Stress-strain responses simulated by the Extended Drucker-Prager Cap model [15] is compared to the Mander model [2] simulations in Fig. 7. It is observed from Fig. 7 that strength degradation after reaching the ultimate strength is not simulated by the Extended Drucker-Prager Cap model (EDPC). In addition, this model can't simulate degradation of stiffness due to which this model was not considered in this study.

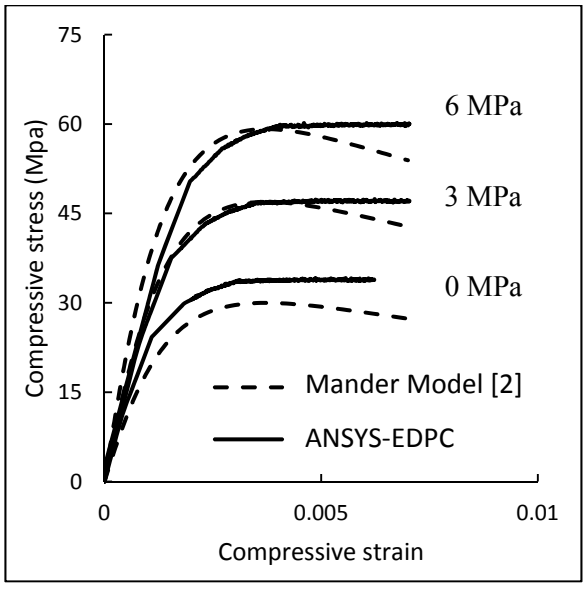

Fig. 7.Comparison of Stress-strain response for different confining stress from Extended Drucker-Prager Cap model (EDPC) [15] and Standalone Mander [2] model response.

William and Warnke [7]

This is a 5 parameter model. These parameters are the uniaxial compressive strength f'_c, uniaxial tensile strengthf'_t, biaxial compressive strength, confined biaxial compression strength on compression meridian, confined biaxial compression strength such that stress point lies on tension meridian. The William and Warnke [7] surface can be given by:

$$\sigma_m = a_0 + a_1 r_1 + a_2 r_1^2 \qquad (21)$$

$$\sigma_m = b_0 + b_1 r_2 + b_2 r_2^2 \qquad (22)$$

where, $\sigma_m = I_1/3$, r_i is stress components normal to the hydrostatic axis along the tension and compression meridian, a_i and b_i are the material constants. As both meridians intersect hydrostatic axis at the same point, $a_0 = b_0$, hence total parameters became 5 which can be determined by strengths mentioned above.

Equation of the stress point normal to the hydrostatic axis is given by,

$$r(\theta) = \frac{2r_2\left(r_2^2 - r_1^2\right)\cos\theta + r_2\left(2r_1 - r_2\right)\left[4\left(r_2^2 - r_1^2\right)\cos^2\theta + 5r_1^2 - 4r_1 r_2\right]^{1/2}}{4\left(r_2^2 - r_1^2\right)\cos^2\theta + \left(r_2 - 2r_1\right)^2} \qquad (23)$$

where, $\cos\theta = \dfrac{\sigma_1 + \sigma_2 - 2\sigma_3}{\sqrt{2}\left[\left(\sigma_1 - \sigma_2\right)^2 + \left(\sigma_2 - \sigma_3\right)^2 + \left(\sigma_3 - \sigma_1\right)^2\right]^{1/2}}$

Failure surface is given by,

$$f(\sigma) = \frac{1}{2}\frac{\sigma_a}{f_{cu}} + \frac{1}{r(\theta)}\frac{\tau_a}{f_{cu}} - 1 \qquad (24)$$

where, f_{cu} is ultimate uniaxial compressive strength of concrete and

$\sigma_a = \dfrac{1}{3}\left(\sigma_1 + \sigma_2 + \sigma_3\right)$ and $\tau_a = \dfrac{1}{\sqrt{15}}\left[\left(\sigma_1 - \sigma_2\right)^2 + \left(\sigma_2 - \sigma_3\right)^2 + \left(\sigma_3 - \sigma_1\right)^2\right]^{1/2}$

In Fig. 8a, failure surfaces are plotted at compressive and tensile meridian for comparison. In this figure, compressive stresses are considered as negative. As stress intensity decreases (compressive loading), hydrostatic pressure I_1 decreases and failure stress increases. This increase in strength at higher I_1 captures the 'confining effect' of the concrete. In order to control the shape of the failure surface, parameters has to be adjusted such that, $0.5 < \frac{r_1}{r_2} \leq 1$. If this ratio is half, then failure surface is triangular and for value of one, it resembles the von-Mises surface in π-plane (Fig. 8b). Five parameter model is good to capture the failure surface closely. This model is available in ANSYS software for concrete material.

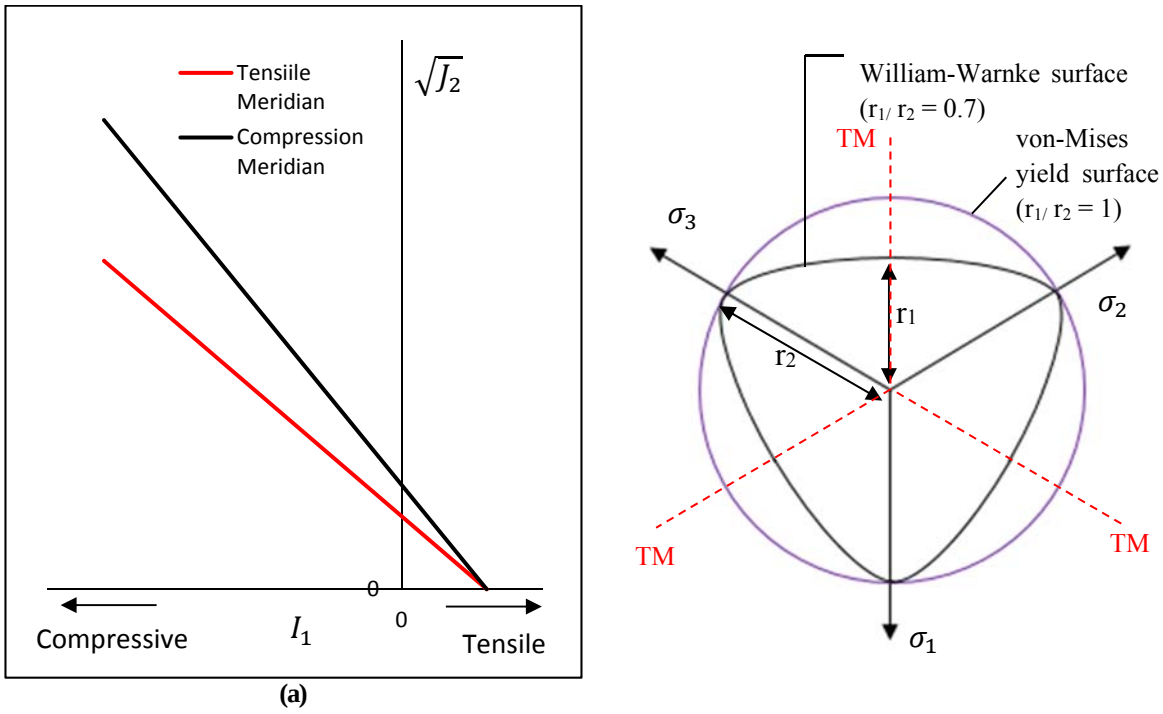

Fig. 8. William and Warnke failure surface (a) Comparison of tension meridian and compressive meridian over I_1 v/s $\sqrt{J_2}$ (b) Shape of failure surface in π plane

The main drawback of this model is assumption of elastic-perfectly plastic stress-strain relationship due to which this model can't be used to simulate the hardening and softening response of concrete. Hence, this model is not used in this study.

Lubliner model [9]

This model considers concrete as frictional material with cohesion such that isotropic hardening of the concrete is considered in form of evolution of cohesion which depends on plastic damage variable. Damage accumulated in the material leads to vanishing of cohesion which indicates the softening of concrete.

Total strains are decomposed in elastic and plastic strains which is given by,

$$\varepsilon = \varepsilon^e + \varepsilon^p = D^{-1}\sigma + \varepsilon^p \qquad (25)$$

Yield surface:

Yield surface is a function of second invariant of stress deviator (J_2) and first invariant (I_1) of total stress as shown in Eq. (26). Due to this reason, surface in total stress space is a complex shape in π-plane, at $I_1 \to -\infty$ the yield surface shape is circular and at $I_1 \to 0$, the shape tends to get triangular [9].

$$F(\sigma) = \frac{1}{1-\alpha}\left[\sqrt{3J_2} + \alpha I_1 + \beta\langle\sigma_{\max}\rangle - \gamma\langle-\sigma_{\max}\rangle\right] \qquad (26)$$

Where, α, β, γ are the parameters which are determined as follows,

$$\alpha = \frac{(f_{bo}/f_{co})-1}{2(f_{bo}/f_{co})-1} \qquad (27)$$

f_{bo}, f_{co} is biaxial and uniaxial strength of the concrete.

$$\beta = (1-\alpha)\left(\frac{f_{bo}}{f_{co}}\right) - (1+\alpha) \qquad (28)$$

$$\gamma = \frac{3(1-\rho)}{2\rho - 1} \qquad (29)$$

$$\rho = \frac{\left(\sqrt{J_2}\right)_{TM}}{\left(\sqrt{J_2}\right)_{CM}} \qquad (30)$$

$$\sigma_{\max} = \tfrac{1}{3}\left(I_1 + 2\sqrt{3J_2}\right) \qquad \text{TM} \qquad (31)$$

$$\sigma_{\max} = \tfrac{1}{3}\left(I_1 + \sqrt{3J_2}\right) \qquad \text{CM} \qquad (32)$$

TM and CM indicates tension meridian and compression meridian.

Definition of plastic damage variable

Consider the uniaxial stress-strain curve for concrete under compression. From this stress-strain curve, stress-plastic strain curve is determined and area under the curve is considered as g_c. Damage parameter of concrete in compression zone is given as,

$$\kappa = \frac{1}{g_c}\int_0^{\varepsilon^p} \sigma d\varepsilon^p \qquad (33)$$

In a similar way, by considering concrete uniaxial stress-strain curve for tension loading, damage parameter in tension is defined as,

$$\kappa = \frac{1}{g_t}\int_0^{\varepsilon^p} \sigma d\varepsilon^p \qquad (34)$$

g_t is areas under uniaxial tensile stress-plastic strain curve. These equations can be applied to any stress-strain curve and damage parameter can be determined for that specific curve.

Eq. (33) in rate form is given as,

$$\dot{\kappa} = -\frac{1}{g_c} f_c(\kappa) \dot{\varepsilon}_t^p \qquad (35)$$

In this model, uniaxial stress-strain curve was considered which is given by,

$$\sigma = f_0 \left[(1+a) \exp\left(-b\varepsilon^p\right) - a \exp\left(-2b\varepsilon^p\right) \right] \qquad (36)$$

where, f_0 is stress at which no damage is observed in concrete. This function is defined to capture experimental observation, where level of zero stress is achieved asymptotically. In this equation, 'a' and 'b' are the model parameters. Parameter 'a' is determined by using following equation.

$$a = 2\left(f_m / f_o\right) - 1 + 2\sqrt{\left(f_m / f_o\right)^2 - \left(f_m / f_o\right)} \qquad (37)$$

where, f_m is the maximum stress achieved and f_0 is the initial stress at zero plastic strain as shown in Fig. 9. If a > 1 then it represents ascending branch of the curve which is initial hardening else is it softening. Because of this parameter, same set of equations can be used for compressive and tensile stress-strain input. Fig. 9 represents the uniaxial compressive stress-strain equation used in this model.

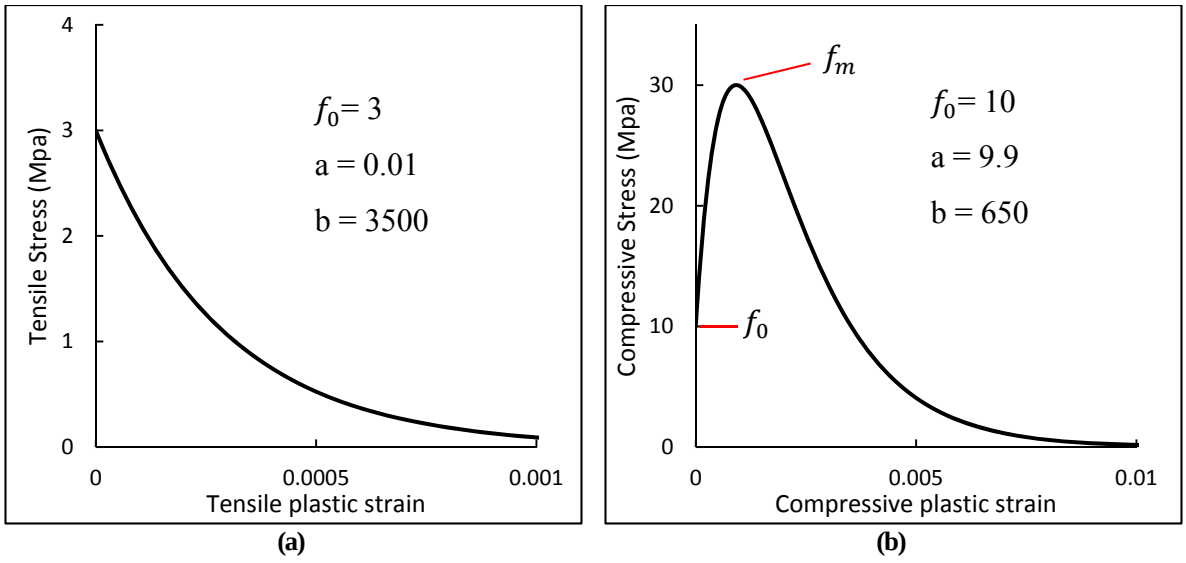

Fig. 9. Stress-strain equation used by Lubliner et al. (a) Parameter a < 1 (uniaxial tensile stress-strain response), (b) Parameter a > 1 (uniaxial compressive stress-strain response)

Relation of damage parameter and cohesion

Rate equations for damage parameters and cohesion are assumed to be in form as follows,

$$\dot{\kappa} = h(\sigma, c, \kappa)\dot{\varepsilon}^p \qquad (38)$$

$$\dot{c} = k(\sigma, c, \kappa)\dot{\kappa} \qquad (39)$$

Cohesion in concrete and damage parameter is related in such a way that $c \to 0$ as $\kappa \to 1$. For general compression and tension stress-strain dependency, cohesion and damage parameter dependency is given as follows,

$$k(\sigma, \kappa, \mathrm{c}) = \mathrm{c}\left[\frac{r(\sigma)}{f_t(\kappa)} f_t'(\kappa) + \frac{1 - r(\sigma)}{f_c(\kappa)} f_c'(\kappa)\right] \qquad (40)$$

where $r(\sigma) = \dfrac{\sum_{i=1}^{3} \langle \sigma_i \rangle}{\sum_{i=1}^{3} |\sigma_i|}$ which termed as weight factor.

From eq. (39) and (40), after rearranging terms, cohesion is determined as follows.

$$c = f_{co}\left(f_t / f_{to}\right)\left(f_c / f_{co}\right)^{1-r} \exp\left[\int \ln\left(f_c / f_t\right) dr\right] \qquad (41)$$

where, f_{co} is uniaxial compressive strength of concrete and f_{to} is uniaxial tensile strength.

Flow rule:

$$\dot{\varepsilon}^p = \dot{\lambda}\frac{\partial G}{\partial \sigma} \qquad (42)$$

Where, $\dot{\lambda}$ is plastic loading factor and $\frac{\partial G}{\partial \sigma}$ is normal to the plastic potential surface G. Plastic potential surface is given by,

$$G = \frac{I_1}{3}\sin\Psi + \sqrt{J_2}\left(\cos\theta - \frac{\sin\theta\sin\Psi}{\sqrt{3}}\right) \qquad (43)$$

where, Ψ is angle of dilatancy

Tangent elastic-plastic stiffness operator with H as plastic modulus is given as,

$$D^{ep} = D - \frac{\left(D\frac{\partial G}{\partial \sigma}\right)\left(D\frac{\partial F}{\partial \sigma}\right)^T}{H + \left(\frac{\partial F}{\partial \sigma}\right)^T D\frac{\partial G}{\partial \sigma}} \qquad (44)$$

Degradation of modulus

In this model, it is assumed that D depends on the degradation variables. Simplest form of elastic degradation in initial stiffness D_0 based on single variable d is given by,

$$D = (1-d)D_0 \qquad (45)$$

This equation gives the dependency of the undamaged property to that of damaged property of material. Due to single damage variable, the stiffness D can be replaced by $(1-d)D_0$ to consider induced damage. So, damaged state of any stress can be given as $\sigma = (1-d)\sigma_0$. This is applicable for both, tension and compression stress. But due to lack of dependency between

the tension and compression stress, two different damage parameters has to be considered for tension and compression.

From here on in all equations, D depends on the degradation variables. For stress and strain dependency, following equation is considered.

$$\dot{\sigma} = C_e \dot{\varepsilon} - C_p \dot{\varepsilon}^p \qquad (46)$$

where, C_e, C_p are linear and nonlinear operator respectively which is given as,

$$C_e \dot{\varepsilon} = D\dot{\varepsilon} - \frac{\phi_1}{1-d_1}\sigma_0 I\left\langle \mathrm{k}_1^T \dot{\varepsilon} \right\rangle - \frac{\phi_2}{1-d_2}\sigma_0 s\left\langle \mathrm{k}_2^T \dot{\varepsilon} \right\rangle \qquad (47)$$

$$C_p = D - \sum_i \partial D / \partial \delta_i \, D^{-1}\sigma I_j \qquad (48)$$

where, s is stress deviator, σ_0 is mean normal stress, $k_1 = \sigma_0 I,\ k_2 = s$. From monotonic radial loading, ϕ_1 and ϕ_2 can be calculated for any function which represents dependency of moduli with corresponding strain.

Consistency condition is given as,

$$\left(\frac{\partial F}{\partial \sigma}\right)^T \dot{\sigma} = \dot{c} \qquad (49)$$

From Eq. (38), (39), (35) and (46),

$$\left(\frac{\partial F}{\partial \sigma}\right)^T C_e \dot{\varepsilon} = \left(H + \left(\frac{\partial F}{\partial \sigma}\right)^T C_p \frac{\partial G}{\partial \sigma}\right)\dot{\lambda} \qquad (50)$$

where H is plastic modulus which is given as,

$$H = kh\frac{\partial G}{\partial \sigma} \qquad (51)$$

and $\dot{\lambda} = \dfrac{\left\langle \dfrac{\partial F}{\partial \sigma} C_e \dot{\varepsilon} \right\rangle}{H + \dfrac{\partial F}{\partial \sigma} C_p \dfrac{\partial G}{\partial \sigma}}$ *(52)*

Elastic-plastic tangent stiffness is defined as,

$$\dot{\sigma} = C_e \dot{\varepsilon} - C_p \frac{\partial G}{\partial \sigma} \dot{\lambda} \qquad (53)$$

One major drawback of this model is the definition of damage ratio in tension and damage ratio is compression and that means there is no dependency between tension and compression damage ratios. It indicates that damage occurred in tension have no influence on damage in compression. This leads to inconsistency in uniaxial response. In the experiments, at higher level of strains, higher strength in concrete is observed when concrete is subjected to confining pressures. This model fails to model the higher stresses at higher level of strains in multiaxial stress condition. Due to these reasons, this model is not used for the simulation of cyclic response of RC column.

Lee-Fenves Model [10]

Lee-Fenves proposed modification of Lubliner model to capture the degradation in concrete under cyclic load. Total strain is decomposed in elastic and plastic strains, same as Lubliner model (eq. (25)). Effective stress $\bar{\sigma}$ in undamaged material is givens as follows.

$$\bar{\sigma} = E_0 : (\varepsilon - \varepsilon^p) \qquad (54)$$

where, E_0 is undamaged elastic stiffness. When damage parameter D is considered for determination of stress intensity in damaged material, damage stress can be rewritten as,

$$\sigma = (1 - D) E_0 : (\varepsilon - \varepsilon^p) \qquad (55)$$

Where, dependency of stresses in damaged material and damage parameters is given by $\sigma = (1-D)\bar{\sigma}$.

In this model, evolution of the damage parameter is defined such that it accounts coupling of tension and compression damage parameter. This model is available in ABAQUS. According to Lubliner model, consideration of damage ratios is as follows,

$$f_t = \left[1 - D_t(\kappa_t)\right]\overline{f_t}(\kappa_t) \quad \text{and} \quad f_c = \left[1 - D_c(\kappa_c)\right]\overline{f_c}(\kappa_c) \qquad (56)$$

Subscript t and c indicates tension and compression, respectively.

Lee and Fenves model proposed total degradation *D* as,

$$D = D(\kappa) = 1 - (1 - D_t)(1 - D_c) \qquad (57)$$

and uniaxial responses are given by,

$$f_t = [1 - D]\overline{f_t} \qquad (58)$$

$$f_c = [1 - D]\overline{f_c} \qquad (59)$$

For the plasticity part of the model, this model is extension of the Lubliner model where isotropic hardening is changed to cohesion based kinematic hardening and damage parameters is introduced in the yield criterion.

$$F(\sigma, \kappa) = \frac{1}{1-\alpha}\left[\sqrt{3J_2} + \alpha I_1 + \beta(\kappa)\langle \sigma_{\max} \rangle\right] - C_c(\kappa) \qquad (60)$$

C_c is the compression cohesion, C_t is tensile cohesion and α parameter is defined in the same way as in Lubliner's model [9] eq. (27). But the parameter β is defined in different way, which is given by,

$$\beta = \frac{C_c(\kappa)}{C_t(\kappa)}(1-\alpha) - (1+\alpha) \qquad (61)$$

Flow rule is given by $\dot{\varepsilon}^p = \dot{\lambda}\frac{\partial G}{\partial \bar{\sigma}}$ where G is plastic potential function which is given by,

$$G = \sqrt{2J_2} + \alpha_p I_1 \qquad (62)$$

where, α_p is parameter considered to provide proper dilatancy in material. Other calculations involved in determination of damage in compression and damage in tension are similar to Lubliner et al. model [9].

When concrete material subjected to cyclic loading, there is opening and closing of cracks in the material. Once cracks are closed, recovery of stiffness of cracked concrete is observed. In order to capture this effect, stiffness recovery term is defined. This term considers elastic stiffness recovery when loading is from tensile to compressive state. Degradation parameter is defined as,

$$D\left(\kappa, \bar{\sigma}\right) = 1 - \left(1 - D_c(\kappa)\right)\left(1 - s(\bar{\sigma})D_t(\kappa)\right) \qquad (63)$$

Calculation of damage ratios in compression and tension is calculated by following equation, where $\aleph$ indicates either compression (c) or tension (t).

$$1 - D_{\aleph} = \exp(-\mathrm{d}_{\aleph}\,\varepsilon^p) \qquad (64)$$

$s(\bar{\sigma})$ is the parameters which controls stiffness recovery, which is given as follows.

$$s(\bar{\sigma}) = s_0 + \left(1 - s_0\right) r(\hat{\sigma}) \qquad (65)$$

Total stress including stiffness recovering term is given by,

$$\sigma = \left(1 - D_c(\kappa)\right)\left(1 - s(\bar{\sigma})D_t(\kappa)\right) E_0 : \left(\varepsilon - \varepsilon^p\right) \qquad (66)$$

One of the major drawback of this model is lack of consideration of effects of ductility in concrete. Concrete cylinder subjected to confining pressure shows higher strength at higher strain level [18]. This model can predict ultimate strength of confined concrete correctly but early degradation of strength is observed, hence this model fails to capture the higher strength of concrete at higher strain level. Another drawback of this model is lack of consideration of cracking of concrete. Although, crack opening and closing is captured by stiffness recovery terms, it works only for very small tensile strain. For larger strain range, this model fails to capture the response of experiment. Hence, simulation of cracked concrete in tension is not possible with this model.

Cervenka and Papanikolaou Model [12]

This model considers the fracture mechanics approach which is coupled with plasticity formulations [12]. In this approach cracking of the concrete is considered numerically (smeared cracking) to account its influence on the response of concrete. This model is available in the software ATENA.

The strain decomposition in this model considers, strain due to cracking as follows,

$$\varepsilon_{ij} = \varepsilon_{ij}^{e} + \varepsilon_{ij}^{p} + \varepsilon_{ij}^{f} \qquad (67)$$

where, ε_{ij}^{f} is the strain considered for modeling cracking of concrete.

New stress state in computed by,

$$\sigma_{ij}^{n} = \sigma_{ij}^{n-1} + E_{ijkl}\left(\Delta\varepsilon_{kl} - \Delta\varepsilon_{kl}^{p} - \Delta\varepsilon_{kl}^{f}\right) \qquad (68)$$

To simulate behavior of concrete cracking, Rankine failure criterion is used.

$$F_{i}^{f} = \sigma'^{t}{}_{ij} - f'_{ti} \leq 0 \qquad (69)$$

where, σ'^{t}_{ij} is trial stress and f'_{ti} is tensile strength of concrete in direction 'i'. If this equation is satisfied at any point, then concrete is cracked and for calculation of cracking strain, it is assumed that stress state satisfy the following equation.

$$F_i^f = \sigma'^{t}_{ii} - f'_{ti} = \sigma'^{t}_{ii} - E_{iikl}\Delta\varepsilon'^{f}_{kl} - f'_{ti} = 0 \qquad (70)$$

For fracturing strain increment is determined by,

$$\Delta\varepsilon'^{f}_{ij} = \Delta\lambda \frac{\partial F_k^f}{\partial \sigma_{ij}} = \Delta\lambda\delta_{ik} \qquad (71)$$

From substitution of $\Delta\varepsilon'^{f}_{ij}$ value in Eq. (65) we get,

$$\Delta\lambda = \frac{\sigma'^{t}_{kk} - f'_{tk}}{E_{kkkk}} = \frac{\sigma'^{t}_{kk} - f'_{t}\left(W_k^{\max}\right)}{E_{kkkk}} \qquad (72)$$

Where, $W_k^{\max} = L_t\left(\hat{\varepsilon}'^{f}_{kk} + \Delta\lambda\right)$

$\hat{\varepsilon}'^{f}_{kk}$ is total cracking strain which indicates the maximal fracturing strain reached during loading and ε'^{f}_{kl} is current cracking strain. Current cracking strain is computed from following equation,

$$\varepsilon'^{f}_{kl} = \left(E_{ijkl} + E'^{cr}_{ijkl}\right)^{-1} E_{klmn}\varepsilon'_{mn} \qquad (73)$$

Where E'^{cr}_{ijkl} , is determined by $\sigma'_{ij} = E'^{cr}_{ijkl}\varepsilon'^{f}_{kl}$.

For first mode of cracking, crack stiffness is given by

$$E'^{cr}_{iiii} = \frac{f'_{t}\left(W_k^{\max}\right)}{\hat{\varepsilon}'^{f}_{ii}} \quad \text{(where repeated indices do not indicate summation.)} \qquad (74)$$

and for second and third mode of cracking,

$$E'^{cr}_{ijij} = s_F \min\left(E^{cr}_{iiii}, E^{cr}_{jjjj}\right) \text{ (where repeated indices do not indicate summation.)} \qquad (75)$$

S_F is shear factor coefficient which defines the relationship between shear and normal crack stiffness. In order to calculate shear strength of cracked concrete, Modified Compression Field Theory is used.

$$\sigma_{ij} \le \frac{0.18\sqrt{f'_c}}{0.31+\frac{24w}{a_g+16}} \ , \ \mathrm{i} \neq \mathrm{j} \qquad (76)$$

a_g in above equation is maximum aggregate size and w is maximum crack width.

For determination of plastic strains in Eq. (63), following equation is used.

$$\Delta\varepsilon_{ij}^{p} = \Delta\lambda \frac{\partial G^{p}\left(\sigma_{ij}^{t}\right)}{\partial\sigma_{ij}} \qquad (77)$$

where, G is plastic potential function which is given by,

$$G^{p}\left(\sigma_{ij}\right) = \beta\frac{1}{\sqrt{3}} I_1 + \sqrt{2J_2} \qquad (78)$$

If $\beta < 0$, material is under compaction, if $\beta > 0$ then material is dilating. If $\beta = 0$, then it indicts the volume of material under consideration is constant.

For concrete crushing simulation, following failure surface is used.

$$F_{3P}^{p} = \left[\sqrt{1.5}\frac{\rho}{f'_c}\right]^2 + m\left[\frac{\rho}{\sqrt{6}f'_c} r(\theta,e) + \frac{\xi}{\sqrt{3}f'_c}\right] - c = 0 \qquad (79)$$

Where, $m = 3\dfrac{f'^{\,2}_c - f'^{\,2}_t}{f'_c\, f'_t}\dfrac{e}{e+1}$,

$$r(\theta,e) = \frac{4\left(1-e^2\right)\cos^2\theta + \left(2e-1\right)^2}{2\left(1-e^2\right)\cos\theta + \left(2e-1\right)\left[4\left(1-e^2\right)\cos^2\theta + 5e^2 - 4e\right]^{\frac{1}{2}}}$$

This failure surface is defined in Heigh-Westergaard coordinates (ξ, ρ, θ), f'_c and f'_t are strength of concrete in compression and tension. Parameter e governs the roundness of the failure surface such that 0.5 > e > 1. For e = 1, failure surface resembles to von-Mises surface with complete circular surface and for e = 0.5, failure surface have sharp corners. This parameters resembles the ratio of $\frac{r_1}{r_2}$ in William Wranke model [7].

Hardening and softening is controlled by parameter C which is evolving parameter.

$$C = \left(\frac{f'_c\left(\varepsilon_{eq}^{p}\right)}{f'_c} \right)^2 \qquad (80)$$

ε_{eq}^{p} is equivalent plastic strain and $f'_c\left(\varepsilon_{eq}^{p}\right)$ is hardening law which is given by,

$$\sigma = f_{co} + \left(f_c - f_{co} \right) \sqrt{1 - \left(\frac{\varepsilon_c - \varepsilon_{eq}^{p}}{\varepsilon_c} \right)^2} \qquad (81)$$

This law is based on uniaxial compressive test. Hardening behavior is dependent on strains while softening behavior is dependent on displacement.

Due to consideration of crack in the form of cracking strain, there is no residual plastic tensile strain in concrete. As concrete is cracked, strains in the material after cracking is considered numerically. Due to these reasons, this model prediction up to ultimate strength of concrete is good along with stress-strain response predictions [12]. This model is validated for columns under axial compression and under flexural load [12]. But in the validation study done by Cervenka and Papanikolaou [12], applied displacement on the beam was small as compared to the displacement considered in the earthquakes. Hence, this model needs further verification for large displacements. In addition, this model needs to be extended beyond

ultimate strength of the cracked concrete, where compressive strength of concrete is dependent on cracks in all other direction.

Various attributes of the concrete constitutive models available in the finite element software ANSYS, ABAQUS, ATENA and OPENSEES are presented in Table 3. As stated earlier, present constitutive models in ANSYS are Willam and Wranke model [7] and Extended Drucker-Prager Cap (EDPC) model [15] which fails to simulate softening of concrete. For bond model of steel and concrete, cohesion and friction bond models are available. ANSYS software was not considered in this study because of weakness of the concrete constitutive model. In ABAQUS, Lee and Fenves model [10] and smeared cracking model are available for concrete response simulation. Smeared cracking model prediction for confinement effect is not in agreement with experimental data due to which this model was not considered for simulation of RC member. Available steel-concrete bond model in ABAQUS is elastic perfectly plastic friction model. ATENA incorporated Cervenka and Papanikolaou [12] concrete constitutive plasticity model coupled with fracture mechanics which considers the tri-axial behavior of concrete as well as cracking of concrete into account. But this constitutive model is not numerically stable under large lateral deformation which is demonstrated in next chapter. However, this model works nicely for simulating response of RC column under monotonic axial compressive loading. OPENSEES software have concrete constitutive model by Chang and Mander [4], which can simulate confinement effect with consideration of crack opening and closing mechanism. This model also includes the degradation of stiffness of RC member. But as discussed earlier, these models lacks the ability to simulate the local interaction behavior of RC member such as lateral pressure on longitudinal rebar which is required for the simulation of longitudinal rebar buckling. Hence, this model is not considered in this study.

Table 3. Available concrete constitutive models in various software

SOFTWARE	ANSYS		ABAQUS		ATENA	OPENSEES
Concrete-steel bond relationship	Cohesion, Friction (Multilinear)		Friction (Elastic-plastic)		Bond model	Bond model [25]
Concrete constitutive Models	Willam-Wranke [7] Elastic-perfectly plastic	EDPC model [15] Multilinear	Lee and Fenves [10] Multilinear	Smeared cracking [16] Multilinear	Cervenka-Papanikolaou [12] Exponential hardening	Chang and Mander [4] Non-linear
Softening	NO	NO	YES	YES	YES	YES
Confinement effect	YES	YES	YES	NO	YES	YES
Cyclic stiffness degradation	NO	NO	YES	NO	NO	YES
Crack opening-closing mechanism	NO	NO	NO	YES	YES	YES
Numerical stability under large lateral loading	---	---	YES	---	NO	---
Ability to predict the multiaxial behavior of material	YES	YES	YES	YES	YES	NO

2.3 Steel constitutive models

RC member analysis with ABAQUS, ANSYS, ATENA and OPENSEES can consider different types of steel constitutive models. In a study performed by Babazadeh et al. [26] with ABAQYS software, steel constitutive model used was multilinear isotropic hardening. They simulated monotonic lateral response of the RC bridge column. As monotonic response was simulated, isotropic hardening behavior assumption of steel material was a good assumption, however the same analysis model may not be applicable to seismic analysis because of different material of response evolution. A recent study on RC column simulation by Moharammi and Koutromanos [13] considered uniaxial steel model originally developed by Dodd and Restrepo-Posada [27]. This model considers only one dimensional stress-strain relationship. Consequently, combined action of shear and axial stresses in the steel rebar, under earthquake loading can be simulated.

Multilinear stress-strain fit of steel rebar is most widely used because of its simplicity of parameter determination. However, this model parameters are determined using monotonic responses, response under cyclic loading can't be simulated correctly.

Yield criterion in this model is given by von-Mises,

$$f\left(\underset{\sim}{\sigma}-\underset{\sim}{\alpha}\right)=\left[\frac{3}{2}\left(\underset{\sim}{s}-\underset{\sim}{a}\right)\bullet\left(\underset{\sim}{s}-\underset{\sim}{a}\right)\right]^{\frac{1}{2}}-\sigma_0=0 \qquad (82)$$

Kinematic hardening is given as,

$$\alpha = 2G\varepsilon^{sh} \qquad (83)$$

where, G is shear modulus.

$$d\varepsilon^{sh} = \frac{C}{2G}d\varepsilon^{pl} \qquad (84)$$

and $C = \frac{2}{3}\frac{EE_T}{E - E_T}$ is the plastic modulus of the current linear segment.

E is Young's Modulus and E_T is tangent modulus of the current linear segment.

For multilinear model, determined by series of (ε_k, σ_k), k = 1, 2 … N, back stress evolution is defined in such a way that, effective stress-effective plastic strain curve is multilinear as per give stress-strain input. Behavior of the material is weighted for each linear segment where each weight is given by following equation.

Plastic strain for each linear segment is calculated by,

$$d\varepsilon^{pl} = \sum_{i=1}^{N} w_i d\varepsilon_i^{pl} \qquad (85)$$

where, N is total number of linear segment and w_i is given by,

$$w_k = \frac{E - E_t}{E - \frac{1-2\upsilon}{3}E_t} - \sum_{i=1}^{k-1} w_i \qquad (86)$$

Chaboche model [28] and Armstrong-Fedrick model [29] are available in ANSYS and ABAQUS. In Armstrong-Fedrick model, one nonlinear back stress term is considered whereas in Chaboche model, back stress is decomposed into 2 to 4 back stress terms. The reason behind consideration of multiple back stresses is to capture the nonlinear behavior of steel. Apart from the back stress formulation, rest of the equations are same for these two models. von-Mises yield function is used in these models which is given in eq.(80) Other equations used are,

Flow rule (rate independent):

$$d\underset{\sim}{\varepsilon}^{p} = \frac{1}{H}\left\langle \frac{\partial f}{\partial \underset{\sim}{\sigma}} \bullet d\underset{\sim}{\sigma} \right\rangle \frac{\partial f}{\partial \underset{\sim}{\sigma}} \qquad (87)$$

Back stress

$$d\underset{\sim}{a} = \frac{2}{3} C d\underset{\sim}{\varepsilon}^{p} - \gamma \underset{\sim}{a} dp \qquad \textbf{Armstrong Fedrick Model} \qquad (88)$$

$$d\underset{\sim}{a} = \sum_{i=1}^{m} d\underset{\sim}{a}_i = \sum_{i=1}^{m} \left[\frac{2}{3} C_i d\underset{\sim}{\varepsilon}^{p} - \gamma_i \underset{\sim}{a}_i dp \right] \qquad \textbf{Chaboche Model (m = 2 to 4)} \qquad (89)$$

where, $dp = \left| d\varepsilon^{p} \right|$ (90)

In Fig. 10, simulation by Chaboche model and Armstrong-Fedrick models are compared against a hysteretic loop experimental response of grade 60 steel.

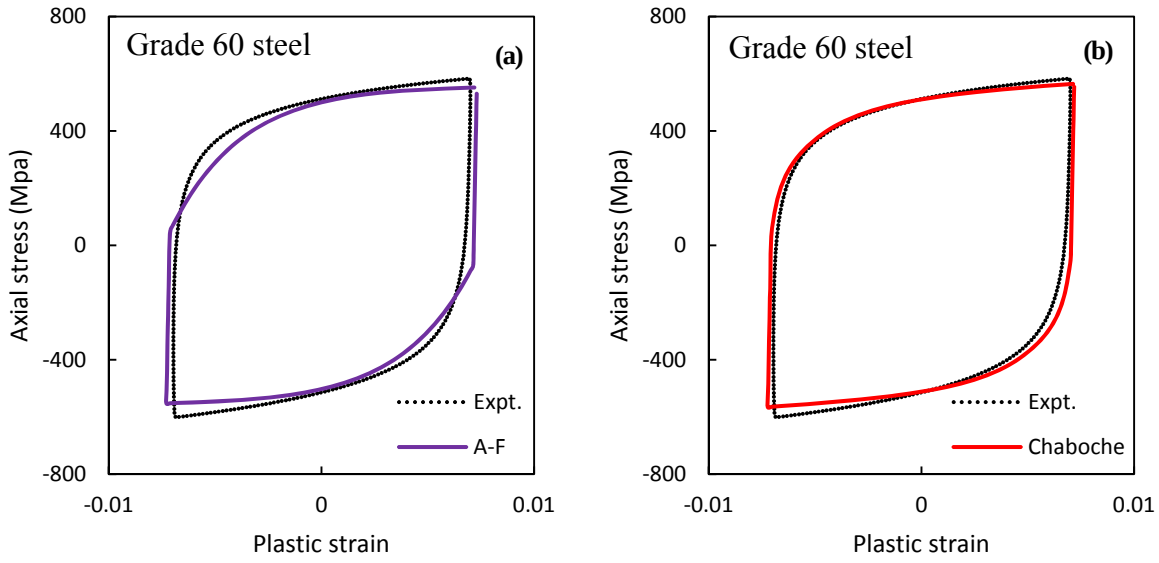

Fig. 10. Comparison of the experimental response and model simulations, (a) Armstrong-Frederick (A-F) [29], (b) Chaboche [28]

In ABAQUS, Chaboche model can be used for 2D and 3D elements. But Chaboche model can't be used for beam element. Beam elements are supported by the uniaxial Johnson-Cook [30] plasticity model, bilinear and multilinear model. From these models, multilinear and Johnson-Cook [30] are isotropic hardening model and bilinear model is kinematic hardening.

Hence, bilinear kinematic hardening model is used as rebar in the lateral cyclic loading RC column simulations. RC columns were modeled using the beam element for evaluation of constitutive models. .

It is noted that once the concrete constitutive models are established for RC column seismic analysis, improved constitutive models, like Chaboche [28], will improve RC column degradation analysis.

Steel models available in OPENSEES

In OPENSEES, some of the available steel models are Ramberg-Osgood [31] Menegotto and Pinto [32], Dodd and Restrepo-Posada [27], Dhakal and Maekawa [33], etc. Ramberg-Osgood [31] and Menegotto and Pinto model [32] uses nonlinear equation with isotropic hardening to determine the uniaxial stress-strain response of steel. Dodd and Restrepo-Posada model [27] is coupled with Dhakal and Maekawa model [33] to predict the uniaxial stress-strain response of buckled rebars. Buckling under consideration is dependent on the aspect ratio of rebar, hence Dhakal and Maekawa model [33] has to be calibrated for specific case of longitudinal rebar buckling. This model fails to consider the interaction of concrete and steel rebar such as lateral pressure excreted by the concrete on longitudinal rebar which is one of the important aspects in buckling. Hence, constitutive models for steel material has to be calibrated separately. When RC column is subjected to earthquakes, rebars experiences axial as well as shear stresses. Due to lack of consideration of multiaxial behavior in model, shear stresses are neglected in the simulation. Because of all the limitations associated with these models, uniaxial models are excluded from the study.

2.4 Validation of the constitutive models

For the validation of the Lee and Fenves model [10] available in ABAQUS, input of unconfined stress-strain curve of concrete is needed to be defined. Stress-strain relationship considered by Lee and Fenves model is as given in eq. (36) which is known as Barcelona model [34]. Stress-strain curve of this model is presented in Fig. 11. In Barcelona model, parameter 'a' and 'b' are constant values. Parameter 'a' can be calculated by using eq. (37) which controls the ultimate strength of unconfined concrete and parameter 'b' controls the shape of stress-strain curve. As parameter 'b' is not an evolving parameter, once this parameter is fixed for given unconfined stress-strain curve, eq.(36) fails to capture the ductility of confined concrete. For unconfined concrete, Barcelona model is representative of the experimental response but for confined concrete, this model suggest early degradation of strength because of lack of evolution of parameter 'b'. Experiment conducted by Richart [18] on concrete cylinders subjected to active confining pressures suggest slower degradation of strength at higher strains. Due to this limitation associated with Barcelona model, Popovics model [1] is utilized where control over negative stiffness is possible as presented in Fig. 11. Hence, in order to control negative stiffness of concrete in the softening range, Popovics model [1] was utilized to obtained unconfined stress-strain curve for concrete. The stress-strain relation in Popovics model is given by,

$$f = f_0 \frac{\varepsilon}{\varepsilon_0} \frac{n}{n-1+\left(\varepsilon / \varepsilon_0\right)^n} \qquad (91)$$

where, f_0 is unconfined strength of concrete and corresponding strain ε_0 with 'n' as material parameter.

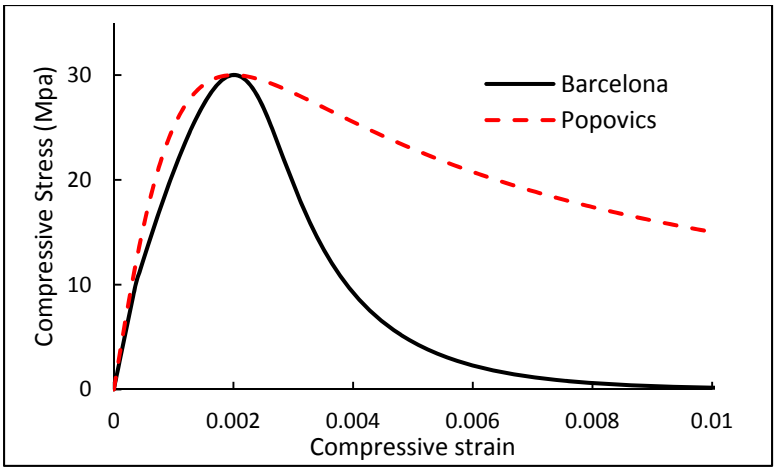

Fig. 11. Comparison of Lee and Fenves and Popovics model for uniaxial monotonic stress-strain relationship

Value for parameter 'n' used as 1.75, instead of the suggested value by Popovics [1] to control the negative stiffness of the concrete in softening. By using this model, stress-strain curve of unconfined concrete is obtained (Fig. 11) and then this curve is used as input stress-strain for Lee and Fenves model [10] in ABAQUS. The three linear segment tensile stress-strain curve is assumed as shown in Fig. 12. Elastic modulus of concrete in all simulations are calculated using,

$$E_c = 5000\sqrt{f'_c} \qquad (92)$$

where, f'_c is unconfined strength of concrete,

Poisson's ratio is considered as 0.2. For parameters of Lee and Fenves model, dilation angle were considered as 35. Biaxial to uniaxial compression ratio as 1.18 and invariant stress ratio as 0.69, flow potential eccentricity as 0.1 and viscosity parameter as 0. Lee and Fenves [10], gave recommendation for the stiffness damage parameters, but these stiffness degradation parameters don't alter the behavior of monotonic response. Due to this reason stiffness recovery factor for tension and compression are considered as 1 in monotonic simulations.

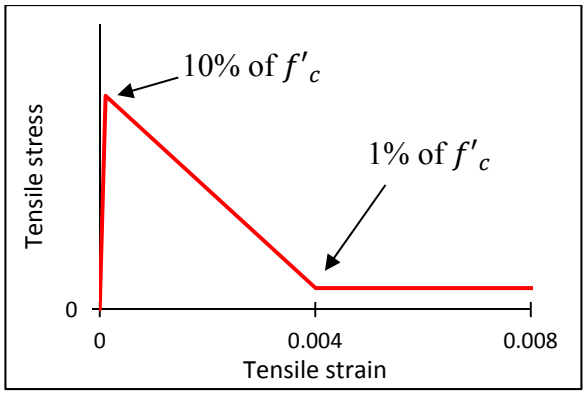

Fig. 12. Assumed tensile stress-strain relationship

2.4.1 Simulation of concrete cylinder under monotonic compressive loading with active confinement

The concrete constitutive models are first validated against the experimental data of Richart [18]. As stated earlier, Richart [18] conducted a set of experiments on concrete cylinder subjected to active confinement pressure and monotonic compressive loading. In order to simulate the responses of concrete under active confinement using the finite element analysis, cube element is modeled as showed in Fig. 13 where active confinement pressure (p) was applied on the sides of the cube and it is axially loaded by stress σ.

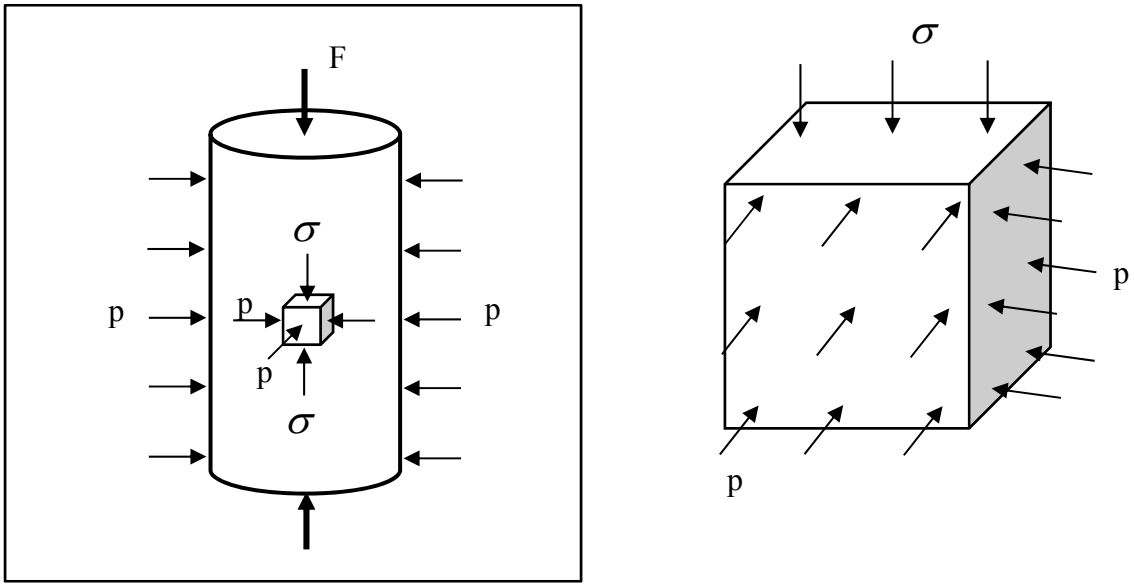

Fig. 13. Modling consideration of concrete for material level

Results obtained by using Lee and Fenves model [10] with stress-strain input from Popovics Model [1] are presented in Fig. 14a, where dotted line indicates the experimental responses and solid line indicates the simulated responses. Lee and Fenves [10] with Popovics model [1] prediction for ultimate strength is close to the experimental observation, but

prediction of the stress-strain curve is not in agreement with experimental stress-strain curve. Strengths at higher strains are under predicted by this model for most confining pressures except at p = 28.19 MPa which is very large compared to most practical confining pressure in RC columns. Results obtained from the smeared cracking model in ABAQUS is plotted Fig. 14b. Stress-strain curves and ultimate strength predictions by this model is significantly under predicted. Due to this reasons, smeared cracking model in ABAQUS was not considered for RC column response simulations in this study. One point should be noted that available smeared cracking models in literature such as model from Moharammi and Koutromanos [13] improved the model so as to capture the confining effect along with other behavioral aspects of RC column such as stiffness degradation. These models are not implemented in any of the existing FE software and goal of this study to evaluate constitutive models available in the software under consideration. Cervenka and Papanikolaou model [12] considers smeared cracking of concrete by using fracturing strain. Although at material level, simulation by this model are not representative of experimental data but this model shows good simulation when used to simulation structural responses [12]. Hence, this model is considered for verification purposes and utilized to simulate RC column responses.

Mander model [2] is compared against the experimental results which are presented in Fig. 14c. For low level of confining pressures, ultimate strength predictions and stress-strain responses simulations by Mander model are in well agreement with an experimental data. But for higher level of confining pressures, ultimate strength and stress values are significantly under predicted by Mander model.

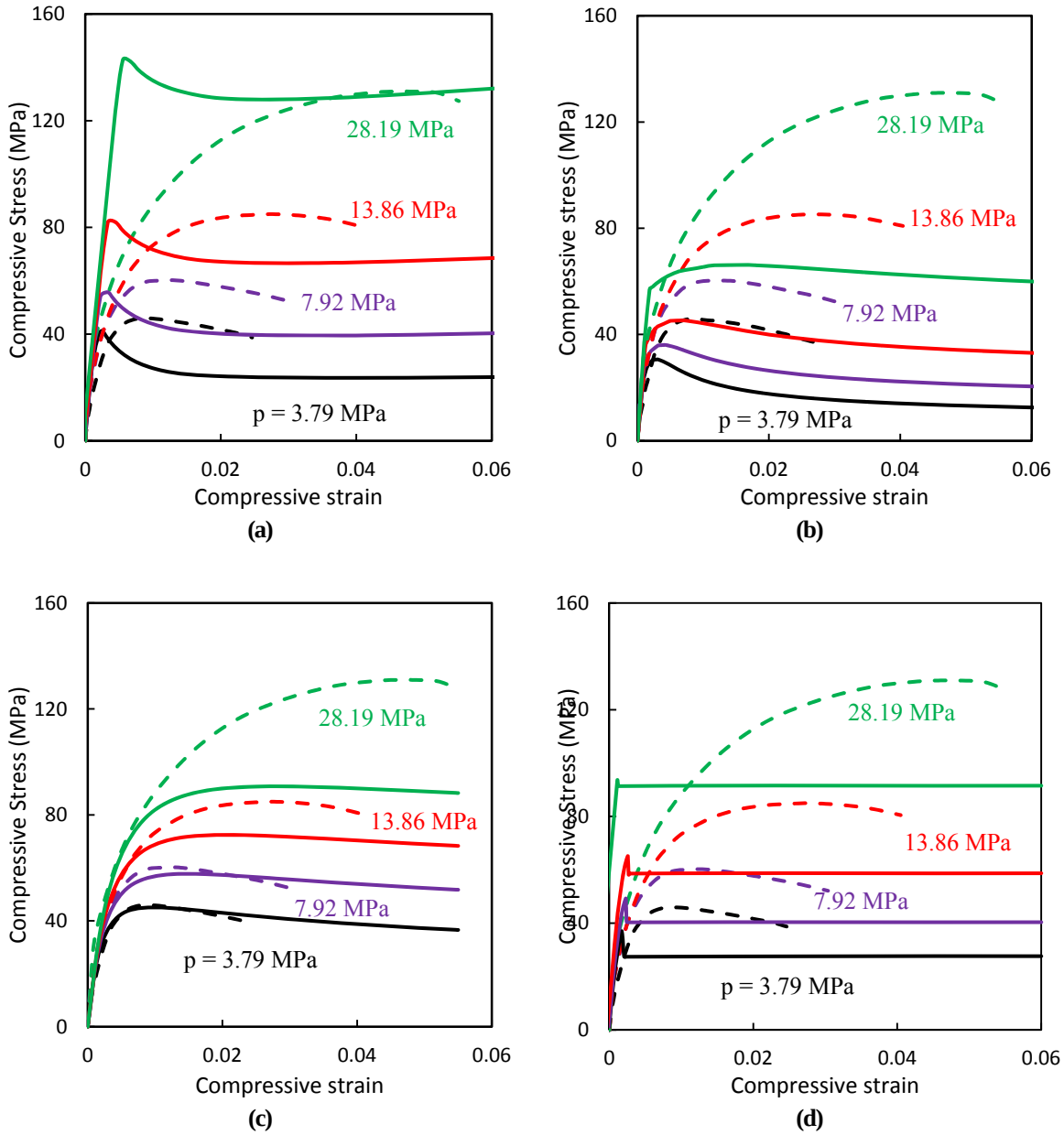

Fig. 14 Continued. Comparison of experimental and simulated responses (a) Lee and Fenves model [10] (b) Smeared cracking model (c) Mander model [2] (d) Cervenka and Papanikolaou model [12], p indicates applied active pressure on concrete

In order to address the issue of under prediction of strength of confined concrete at larger strains, new method is introduced. This method uses Mander model [2] to determine the confined stress-strain curves. Then, the response is normalized with confined strength of the concrete. Once normalized stress-strain curve is determined, this stress values are multiplied

by unconfined strength of concrete which is needed to be simulated in given experiment. This response is used as input for ABAQUS for unconfined stress-strain curve.

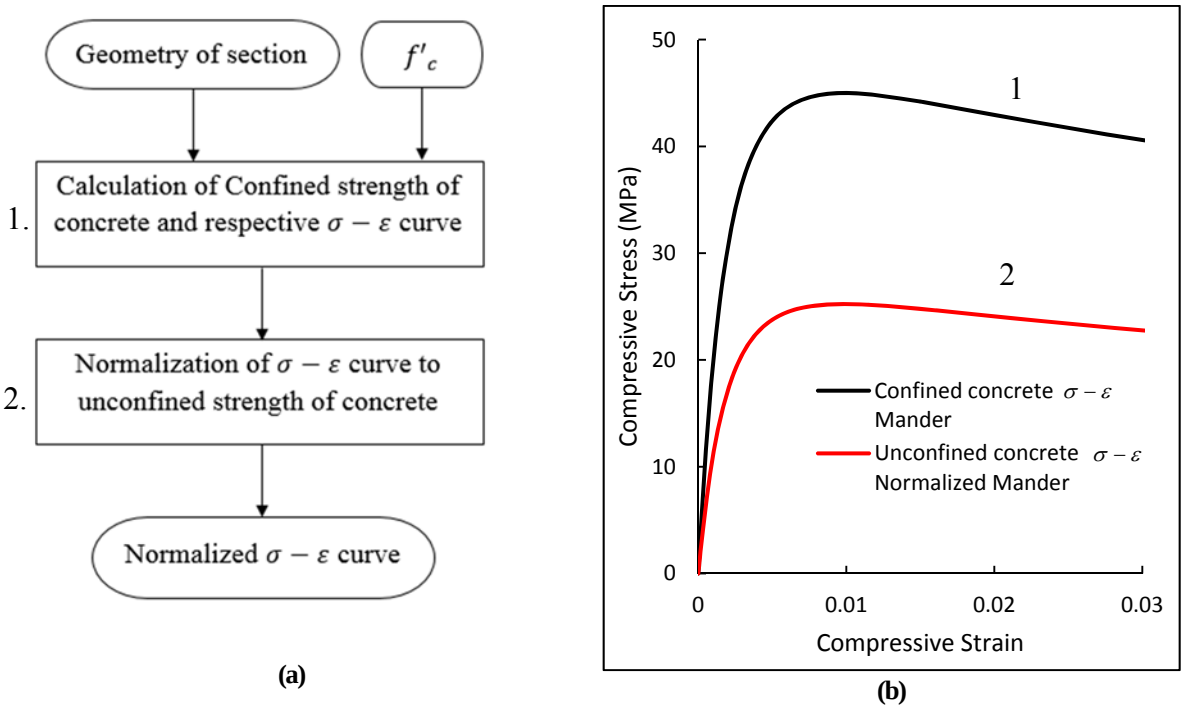

Fig. 15. Normalized Mander (a) Flow chart for normalized mander technique (b) Representation of the steps in the preocesse normalized mander

For example, consider case with unconfined strength (f'_c) as 25.23 MPa and with active confinement pressure (f'_l) as 3.79 MPa. Then from Mander model [2], confined stress-strain response of the concrete can be determined which is given in Fig. 15b–curve 1. Computed confined strength of concrete by using Mander model [2] is 45 MPa. This curve is normalized to the unconfined stress-strain curve of concrete by dividing all the stress values by 45 and then multiply by 25.23 to get normalized unconfined stress-strain curve which is showed in Fig. 15b–curve 2. By using this technique, normalized stress-strain curve is obtained and it is used as input in finite element software along with Lee and Fenves model [10] to

capture the high strength at higher level of ductility. So for validation purpose, normalized Mander model was utilized with Lee and Fenves model and results are showed in Fig. 16.

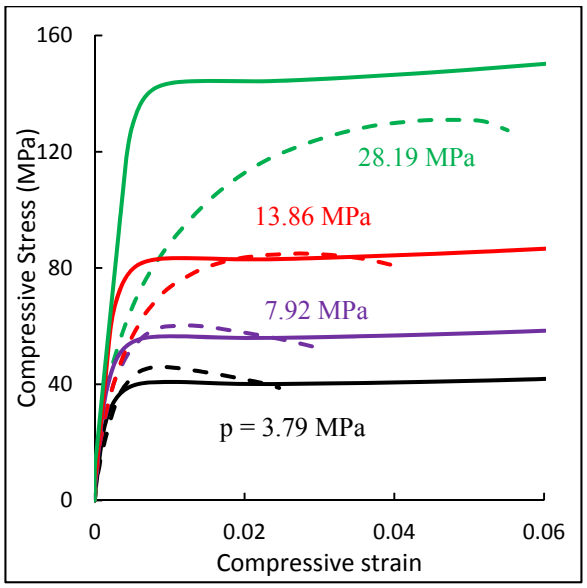

Fig. 16. Normalized Mander model comparison against experimental response, p indicates applied active pressure on concrete

Simulation by using normalized Mander model is presented in Fig. 16, where one can observe that prediction of ultimate strength is acceptable when compared against experimental data. Issue of early degradation of strength at higher level of ductility in Lee and Fenves with Popovics model was prevented by this model. However, stress-strain response prediction at higher confining pressure and lower range of strains is consistently over predicted by this model. Stress-strain response of the confined concrete at high confining range is over predicted.

As shown earlier, smeared cracking model significantly under predict the confined strength of concrete hence, this model is not used for simulation of RC column. Simulation of ultimate strength by Lee and Fenves model [10] with Popovics model [1] and Lee and Fenves

model [10] with normalized Mander model is in well agreement with experimental strengths hence these models are used for the RC column simulation.

2.4.2 Simulation of concrete filled steel tubes

In this section, Mander, LFP (Lee and Fenves with Popovics) and LFNM (Lee and Fenves with normalized Mander) will be validated against the experimental responses by Schneider [19]. In this experiment, the passive pressure is uniformly distributed throughout the specimen. For the material modeling of concrete, Lee and Fenves model [10] was used along with Popovics model [1] and Normalized Mander model. As discussed in earlier discussion, Popovics model [1] and Normalized Mander model was used to define stress-strain curve of unconfined concrete which is given as input for Lee and Fenves model [10] in FE software, ABAQUS. For steel material, bilinear model with isotropic hardening was utilized. In this case, multilinear model or Chaboche model [28] can be used but these models need additional experimental data for calibration.

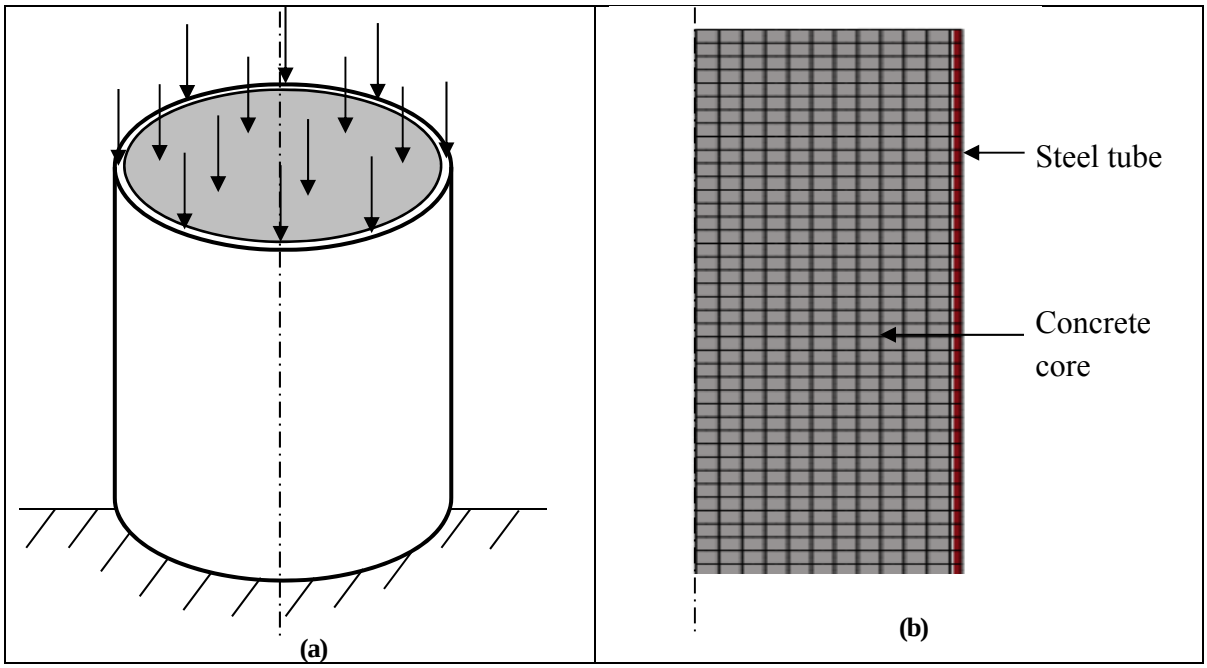

Fig. 17. Concrete filled steel tubes simulation (a) Schematic representation (b) Geometry for simulation with meshing in finite element software

In modeling of concrete filled steel tubes, axisymmetric case was considered where steel and concrete are modeled with axisymmetric explicit elements (CAX8R). In order to simulate contact between steel tube and concrete core, surface contact with hard normal contact along with penalty friction with coefficient of friction as 0.3 is defined. To prevent overclosure error, meshing of steel and concrete is done in such a way that steel and concrete are connected by node to node [16].

Results obtained from the simulations were compared to the experimental responses in Fig. 18. This figure shows that for concrete filled steel tubes, Mander model over predicts the responses. Simulation with Lee-Fenves [10] with Popovics model [1] gives good estimation of the response as compared to standalone Mander model. As Mander model do not consider energy dissipation due to cracking in to account, predictions from this model are not representative to the experimental response beyond initial response. Lee and Fenves model

[10] with normalized Mander over predicts the response but this over prediction is acceptable as compared to Mander model [2] over prediction of response.

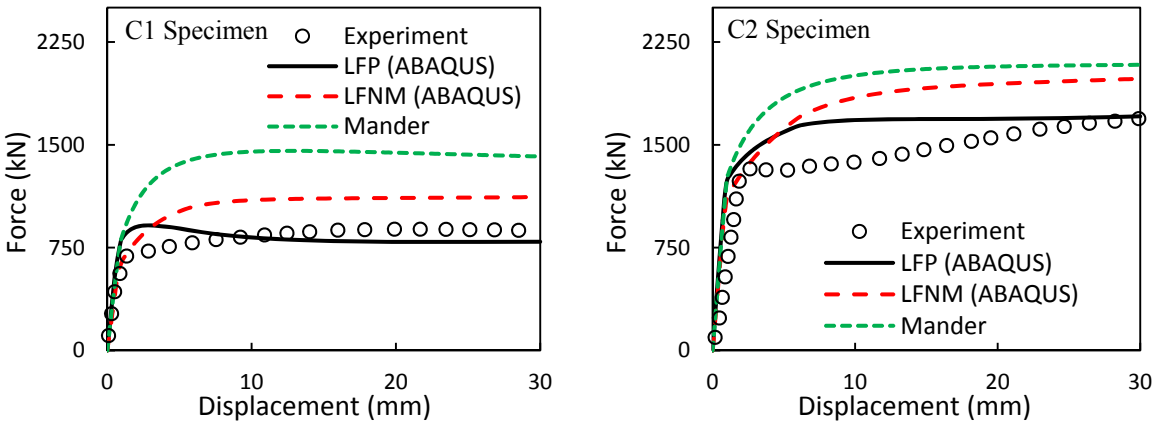

(a) **(b)**

Fig. 18. Concrete filled steel tubes simulation, (a) and (b) for experimental specimen C1, (c) and (d) for experimental specimen C2 where LFP: Lee and Fenves model with Popovics model LFNM: Lee and Fenves model with normalized Mander

2.4.3 Simulation of reinforced concrete column under monotonic compressive loading

Reinforced concrete column subjected to monotonic compressive loading is simulated for validation of the constitutive models. In this case, concrete is subjected to discrete passive confinement, where individual transverse steel reinforcement impose discrete confining pressure [21].

For modeling convenience, transverse rebar is considered as rectangular having equal cross section area as circular rebar and same projected depth of the circular rebar diameter as showed in Fig. 19a.

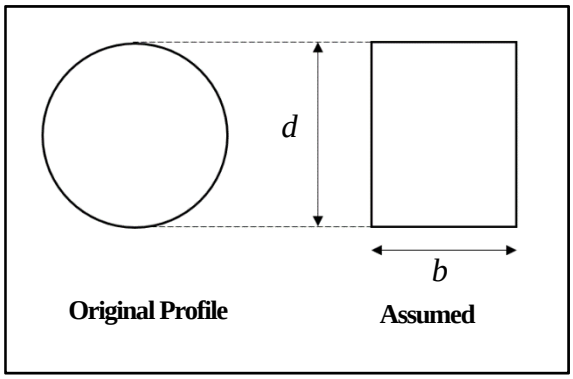

(a) Transverse bar profile for modeling

Area of rebar, $A_{rebar} = \frac{\pi}{4} d^2$

Area of rectangle $A_{rect} = bd$

Hence, $b = \frac{\pi}{4} d$

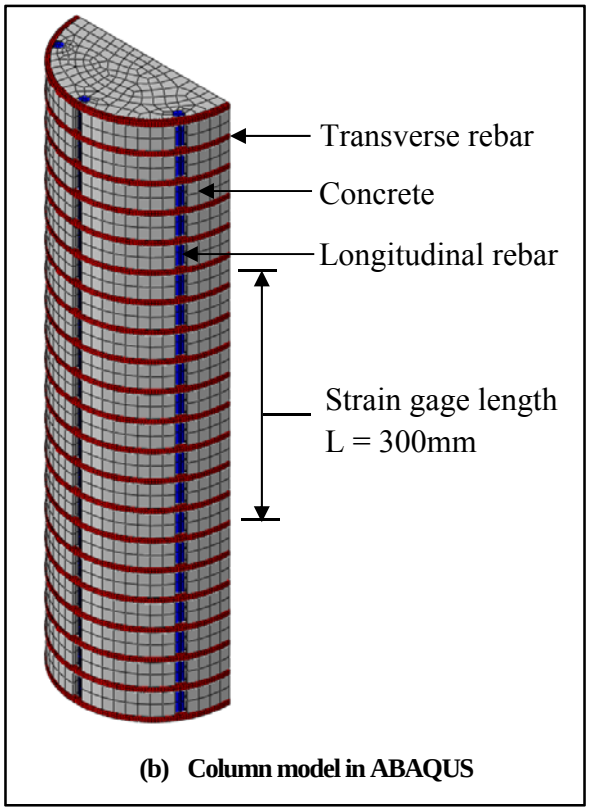

(b) Column model in ABAQUS

Fig. 19. Modeling aspects for reinforced concrete column

Same depth of the rebar was considered to maintain the equivalent confining stress, as confining pressure depends on the spacing of the transverse rebar as well as the projected

height of the rebar on concrete core. This rectangular rebar does not sacrifice any physical characteristics because governing parameters for transverse rebar which influences confining stress are cross sectional area and the projected depth of the transverse steel. This assumption is made, to get larger contact area between longitudinal steel and transverse steel. With this assumption, modeling and numerical issues with single point contact between longitudinal rebar and transverse rebar can be eliminated. In order to prevent complex meshing in the concrete, cover concrete was not modeled.

Modeling of contact area between transverse steel and longitudinal steel can be obtained by two different ways. In case A (Fig. 20b), small portion from transverse rebar was removed so as to get larger contact area instead of single contact point between transverse steel and longitudinal steel. In case B (Fig. 20c), small portion of the longitudinal steel is removed such that large surface area is in contact between transverse steel and longitudinal steel.

For case A, cross section area of the transverse rebar is rectangular and the distance of insertion of longitudinal rebar is 0.2 mm (d_c). Due to which area of the modified transverse rebar A_f , can be calculated as,

$$A_f = (b - 0.2)d = 4.52 \times 6 = 27.12 mm^2$$

$$A_{original} = 4.72 \times 6 = 28.32 mm^2$$

From this calculation, % reduction in area of transverse rebar was 4.2%.

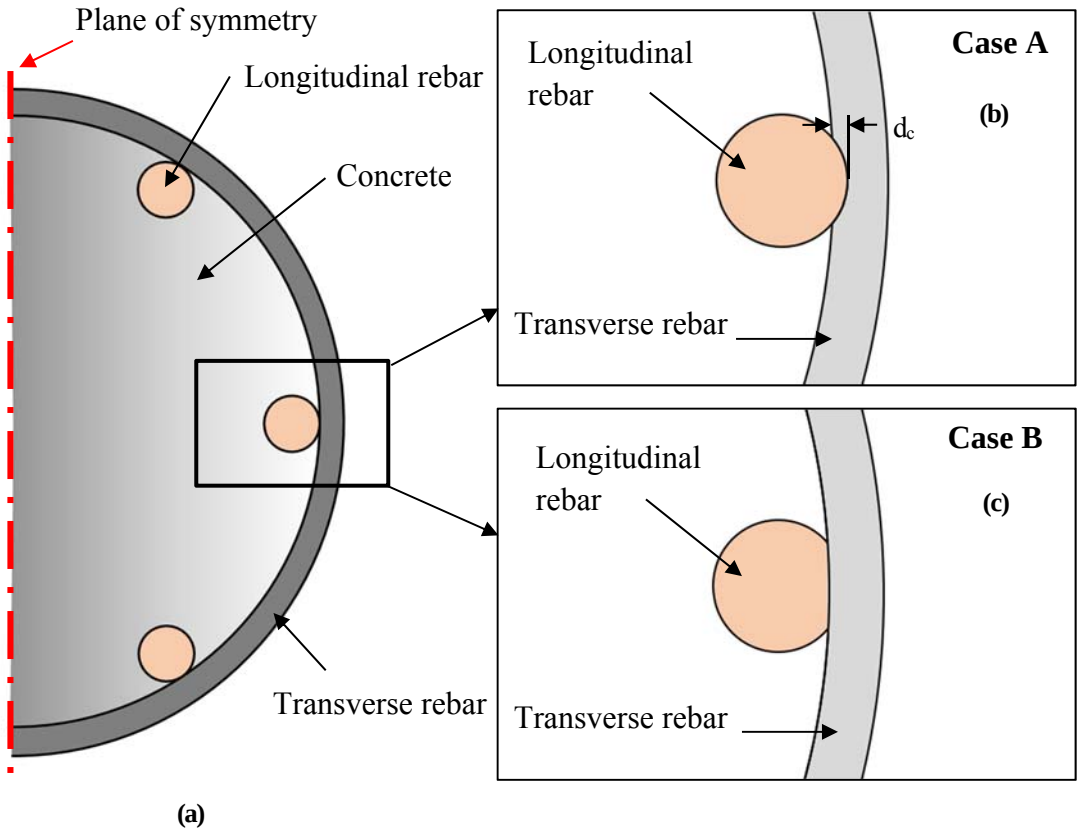

Fig. 20. (a) Representative figure of reinforced concrete with plane of symmetry (b) Case A: modification of transverse rebar, (c) Case B: modification of longitudinal rebar, schematic representation of contact development in transverse rebar and longitudinal rebar

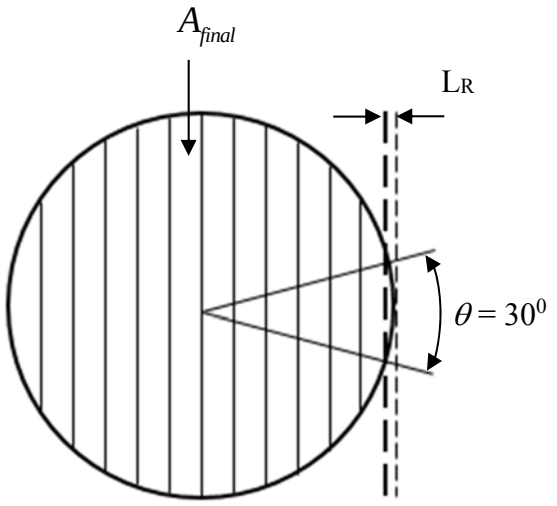

Fig. 21. Schematic representation of longitudinal rebar for modeling purpose

For case B, to determine the % removal of area from longitudinal rebar, following calculations were done.

Length of the removal = L_R =0.2mm

$$A_{final} = A_{rebar} - A_r$$

$$A_r = \frac{\theta}{360}\pi r^2 - A_{triangle}$$

Where, $\theta = 30^0$, r = 6mm

$$A_{triangle} = 2\left[\frac{1}{2}(r - L_R)(r - L_R)\tan\left(\frac{\theta}{2}\right)\right] = 9.0138 \text{ mm}^2$$

$$A_r = \frac{30}{360}\pi(6)^2 - 9.0138 = 0.41097 \text{ mm}^2$$

From calculation we get,

Total area = 113.0973 mm^2

Final area = A_{final} = 113.0973-0.411=112.6863 mm^2

% Area reduction = 0.3%

This longitudinal rebar modeling assumption is justified as original cross section of the rebar is not exactly circular so area variation of 0.3% does not changes any physical characteristics of the column. Also, this small reduction of the area acts as initial imperfection in simulation of buckling. In case A, % of reduction of area is higher than that of case B. Hence, case B was considered for simulations.

For the simulation purposes, half symmetry of the column is utilized. In this case, actual angle of symmetry is 30^0. But buckling of longitudinal rebar may not be along the plane of symmetry, hence least angle of symmetry is 60^0. But for ease of modeling and meshing

purposes, half symmetry is utilized as shown in Fig. 20a. As stated earlier, cover concrete was neglected as this concrete gets crushed in early stages of loading as shown by Mander et al. [21], which indicates the cover concrete doesn't play a major role in RC column response. Concrete outside of longitudinal rebar was neglected (Fig. 22b) due to complex geometry, meshing and numerical divergence issues associated with extreme distortion of elements. Elements used for concrete and steel are C3D8R, which are 3D-8 nodded explicit linear elements. Contact elements with area to area contact were defined between steel to concrete and steel to steel, such that hard contact for normal direction and frictional contact with coefficient of friction of 0.5 is considered. Convergence studies are done to determine mesh density required for analysis. To prevent overclosure error, meshing is done such that elements of concrete and longitudinal steel share same location for nodes in cross section of the RC member [16]. Along the longitudinal direction of RC specimen, different mesh sizes were utilized for longitudinal rebar and concrete core. Finer mesh is used in longitudinal and transverse rebar to account for buckling and necking respectively.

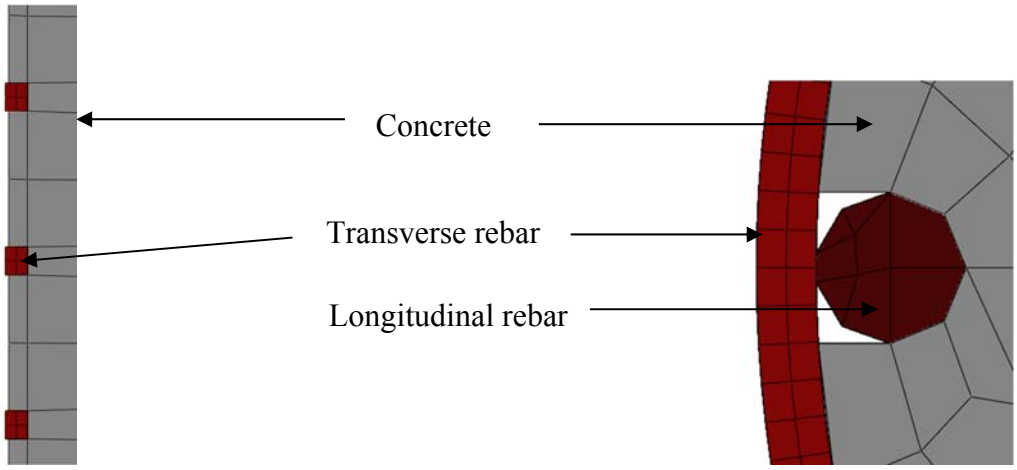

(a) Cross sectional side view **(b) Top view**

Fig. 22. Detailing of the geometric shapes (a) cross section side view of the RC column for detailing of the concrete in between transverse rebar (b) Top view showing removal of concrete outside of longitudinal rebar

Displacement is prescribed at top of the specimen and rigid boundary condition was defined for the support condition. As shown in Fig. 19b, strains are determined within gauge length of 300 mm at mid-height of specimen as per experimental setup.

Simulations of the concrete stress-strain responses for normal strength transverse steel rebar are shown in Fig. 23. Confining pressure calculated by using Mander model [2] are 3 and 1.95 MPa for (6A, 6B) and (9A, 9B) respectively. When Lee and Fenves model [10] was used along with Popovics model [1], prediction are good for normal strength transverse steel which is shown in Fig. 23a, c, e, g. Lee and Fenves model with normalized Mander predictions are similar as compared to the Lee and Fenves model with Popovics model for normal strength transverse steel case. Mander model predictions for ultimate strength and stress-strain curve are in well agreement with experimental data. Cervenka and Papanikolaou model [12] prediction (Fig. 23b, d, f, h) are comparatively better even for 6B and 9B cases as well, where early softening is predicted as per experimental results.

Comparison of the model prediction against experimental response for ultra-high strength steel transverse reinforcement is shown Fig. 24. Confining pressure calculated by using Mander model [2] are 10.13 and 8.58 MPa for (4HB1, 4HC) and (6HB, 6HC) respectively. Mander model consistently over predict the ultimate strength of the section as well as the complete stress-strain response of column at these higher level of confining pressures (Fig. 24b, d, f, h). Reason behind this over prediction is assumption of yielding of the steel at the point where confined strength is highest [2]. This assumption is result of the consideration of strain energy stored in transverse steel is equivalent to strain energy caused dilation in concrete. This assumption holds good for the steel with relatively lower yield stress

but for high strength steel, core concrete of the column achieve ultimate strength before yielding of steel occurs as observed in experiments [20]. This is due to the fact that, strain energy required to cause yielding in high strength steel is higher than energy required to cause crushing of the core concrete. Due to this reason, Mander model consistently over predict the strength. Same as Mander model [2], Lee and Fenves model [10] coupled with normalized Mander consistently over predict the ultimate strength and response of column (Fig. 24a, c, e, g) but earlier elastic predictions in all the cases are better as compared to all other models. Lee and Fenves [10] coupled with Popovics model [1] gives good estimation till ultimate strength of the specimen (Fig. 24a, c, e, g). Stress prediction by this model in softening region in under predicted when compared to experimental data. Cervenka and Papanikolaou model [12] predictions of strength and stress-strain response are relatively better as compared to other models (Fig. 24b, d, f, h) but degradation of strength after reaching ultimate strength in descending branch of stress-strain curve is not simulated well.

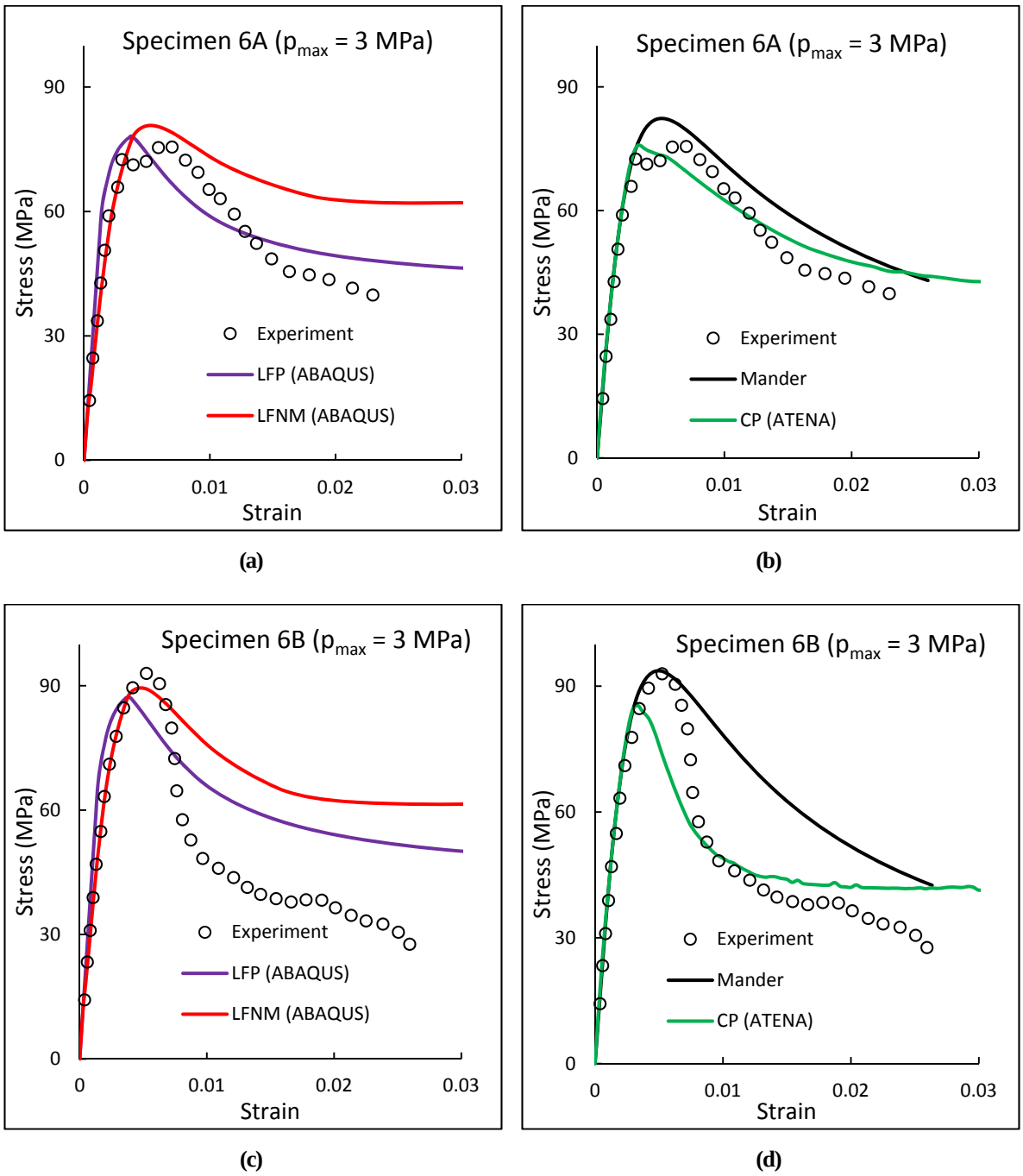

Fig. 23. Results of specimen with normal strength transverse steel
LFP: Lee-Fenves with Popovics model, LFNM: Lee-Fenves-Normalized Mander model, CP: Cervenka and Papanikolaou model

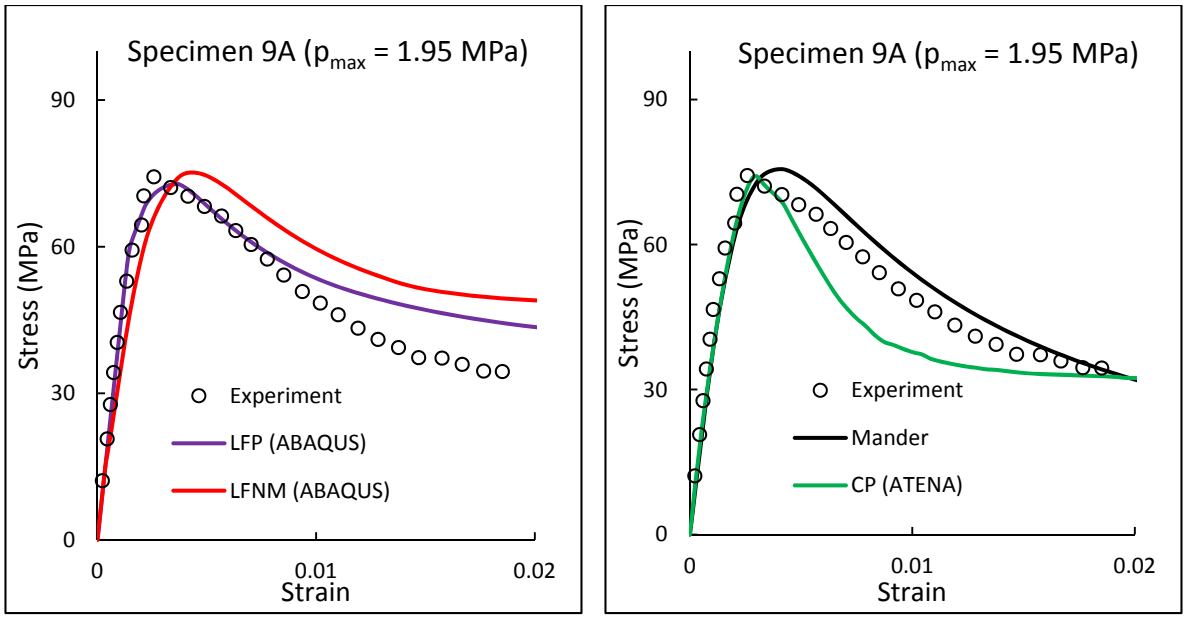

(e) **(f)**

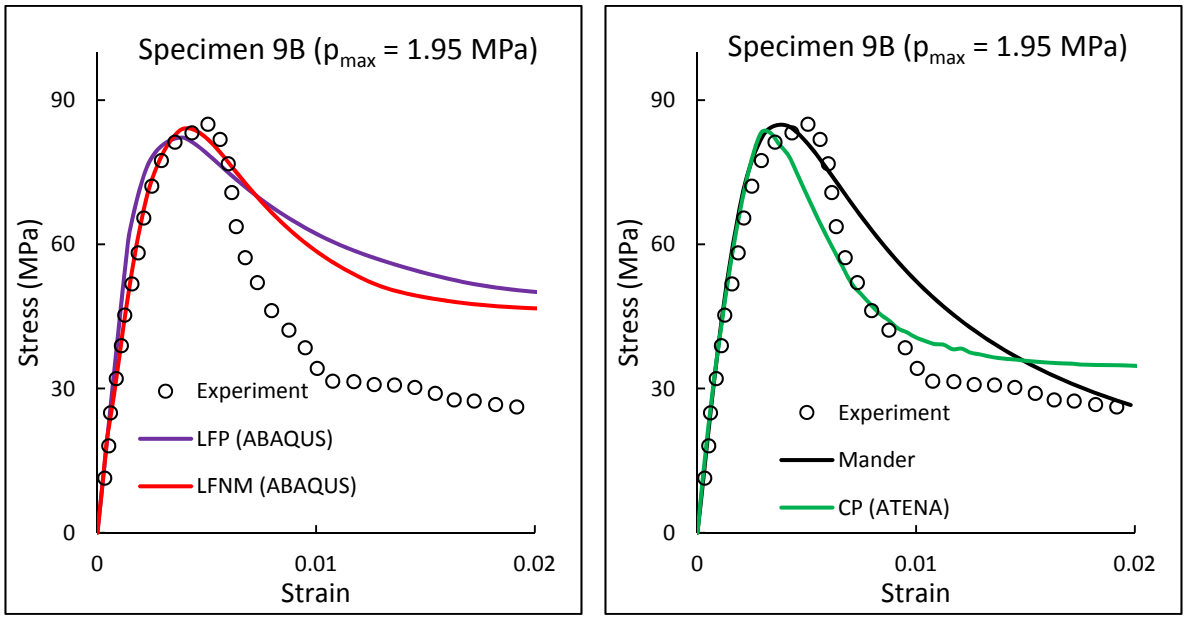

(g) **(h)**

Fig. 23 Continued. Results of specimen with normal strength transverse steel
LFP: Lee-Fenves with Popovics model, LFNM: Lee-Fenves-Normalized Mander model, CP: Cervenka and Papanikolaou model

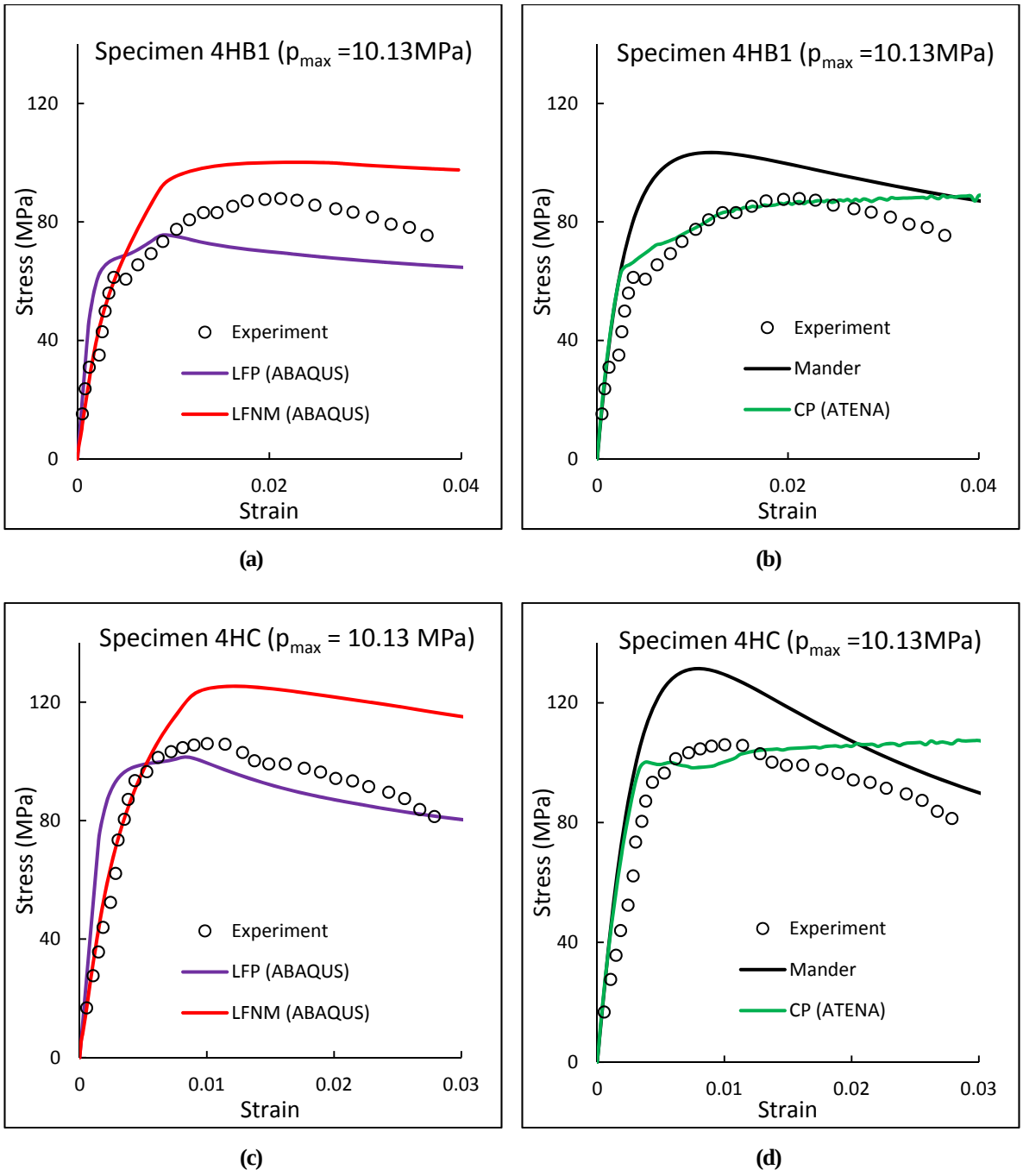

Fig. 24. Results of specimen with ultra-high strength transverse steel
LFP: Lee-Fenves with Popovics model, LFNM: Lee-Fenves-Normalized Mander model, CP: Cervenka and Papanikolaou model

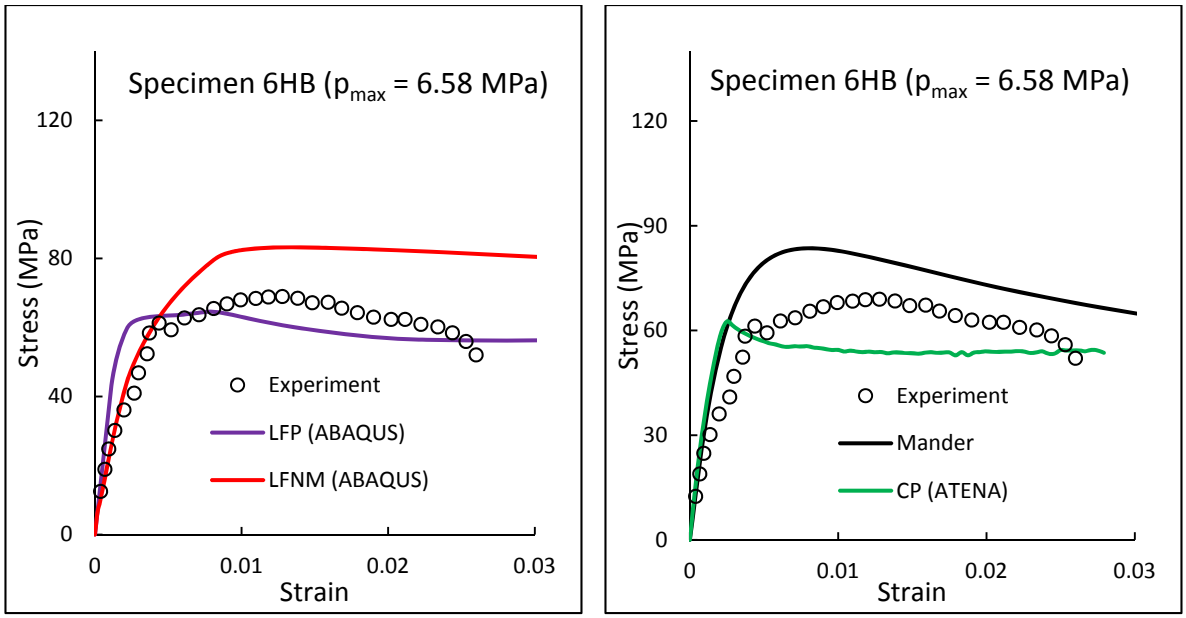

(e) **(f)**

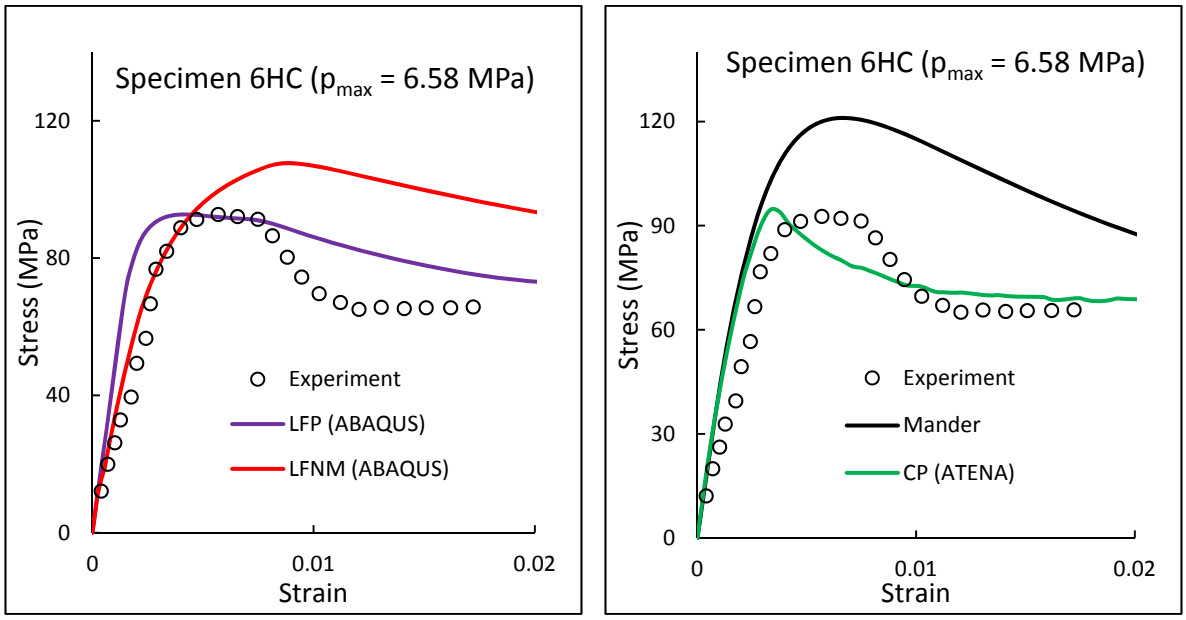

(g) **(h)**

Fig. 24 Continued. Results of specimen with ultra-high strength transverse steel
LFP: Lee-Fenves with Popovics model, LFNM: Lee-Fenves-Normalized Mander model, CP: Cervenka and Papanikolaou model

Comparison of the stress-strain responses of concrete at different locations in the cross section of RC column specimen '6A' is shown in Fig. 25. For this comparison, Lee and Fenves model [10] with Popovics model [1] is utilized. This comparison is made at the cross section equidistant from the transverse rebar which is the weakest cross section in RC column. In this comparison (Fig. 25a), 'location 1' indicates concrete on external surface which is not confined. 'Location 2' is the region at midway from the external surface to the core and 'Location 3' is the innermost region of concrete which have highest level of confinement. Stress-strain responses of concrete at all these locations are shown in Fig. 25b. Due to absence of confinement, ultimate stress at 'location 1' is same as unconfined strength of concrete which is 63 MPa. Whereas at the 'location 3', increased strength and ductility is observed. At the 'location 4' which is adjacent to longitudinal rebar, observed response are different than Mander model simulation. Lateral pressure prediction at this location is critical for prediction of buckling of the longitudinal rebars where lateral pressure on longitudinal rebars by concrete plays important role in buckling prediction. Interaction of longitudinal rebar with confining pressure from concrete is simulated by using 3D FE analysis.

For comparison purposes, simulation of stress-strain responses by Mander model [2] for given RC column (6A) is presented in Fig. 25b. This simulation indicates the uniaxial stress-strain response of the concrete. This uniaxial behavior of concrete constitutive model is considered in OPENSEES software. Due to lack of consideration of multiaxial effect of concrete, simulation of different confining pressure at different location (Fig. 25) is not possible by using uniaxial concrete models such as Mander model [2], Belarbi and Hsu [3], Chang and Mander [4], etc.

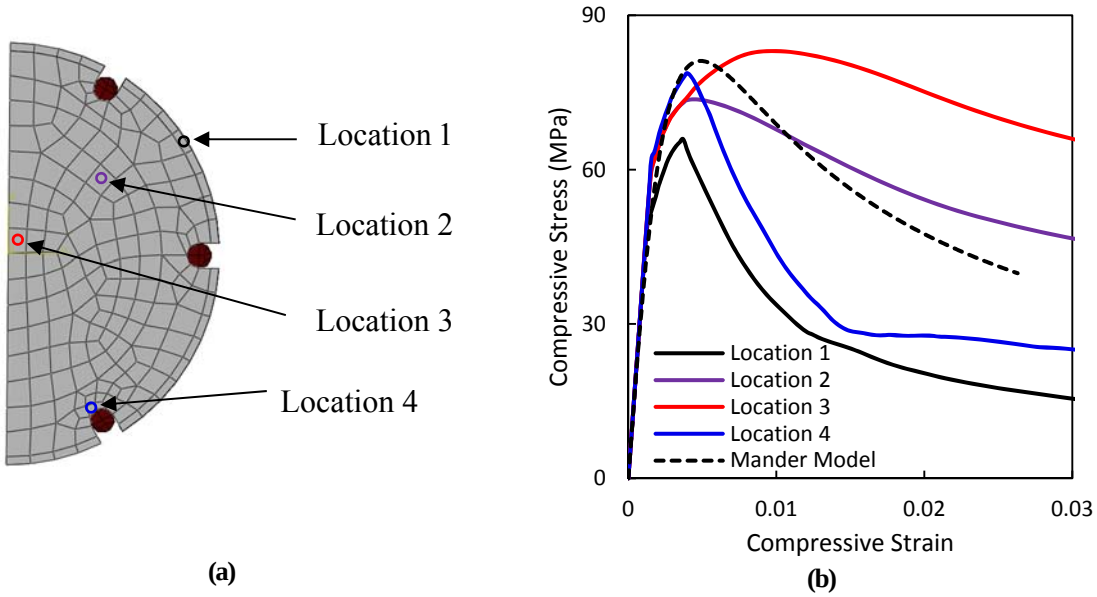

Fig. 25. (a) Location at which stress-strain responses are plotted (b) Stress-strain responses of different location in the RC column Comparison of stress-strain response of concrete at different locations

As mentioned earlier, in longitudinal rebar buckling mechanism, lateral pressure exerted by concrete on longitudinal rebar is an important factor. Uniaxial model fails to capture the effect of confining pressure on longitudinal rebars. Due to this reason, simulation of longitudinal rebar buckling is difficult by using uniaxial models. Along with this fact, uniaxial model don't consider multiaxial behavior of concrete, hence fails to simulate the interaction of concrete core, longitudinal rebar and transverse rebar. Failure mechanism observed in the experiment as shown in Fig. 26a, will not be possible to simulate by using uniaxial concrete constitutive model. This is one of the drawback of the uniaxial concrete constitutive models.

Demonstration of longitudinal rebar buckling obtained in the simulation is presented in Fig. 26. This longitudinal rebar buckling in the simulation is observed as per experimental observation. In the experiment, observed failure mechanism was fracture of the transverse rebar which was followed by buckling of the longitudinal rebar. Simulations suggested similar

mechanism which is shown in the Fig. 26c, where gray color represents the tensile stress and other color indicates compressive stress. This buckling is occurring across two spacing length of the transverse rebar. The necking of the transverse rebar explains the reason of buckling in the longitudinal rebar [20], [35]. This type of failure mechanism can't be simulated by using uniaxial analysis technique. Due to lack of physical modeling of rebars and lack of interaction of concrete and longitudinal rebar, simulation of failure mechanisms, such as, buckling of longitudinal rebar is not possible by using uniaxial analysis. On the other hand, 3D FE analysis using a multiaxial constitutive model of concrete would be able to simulate failure mechanism of RC member reasonably.Along with bar buckling, experiments demonstrated damage in the core concrete due to crushing of the concrete [20]. In simulation, concrete crushing was not modeled. Strength degradation was captured along with dilation of the concrete which can be observed in Fig. 26b.

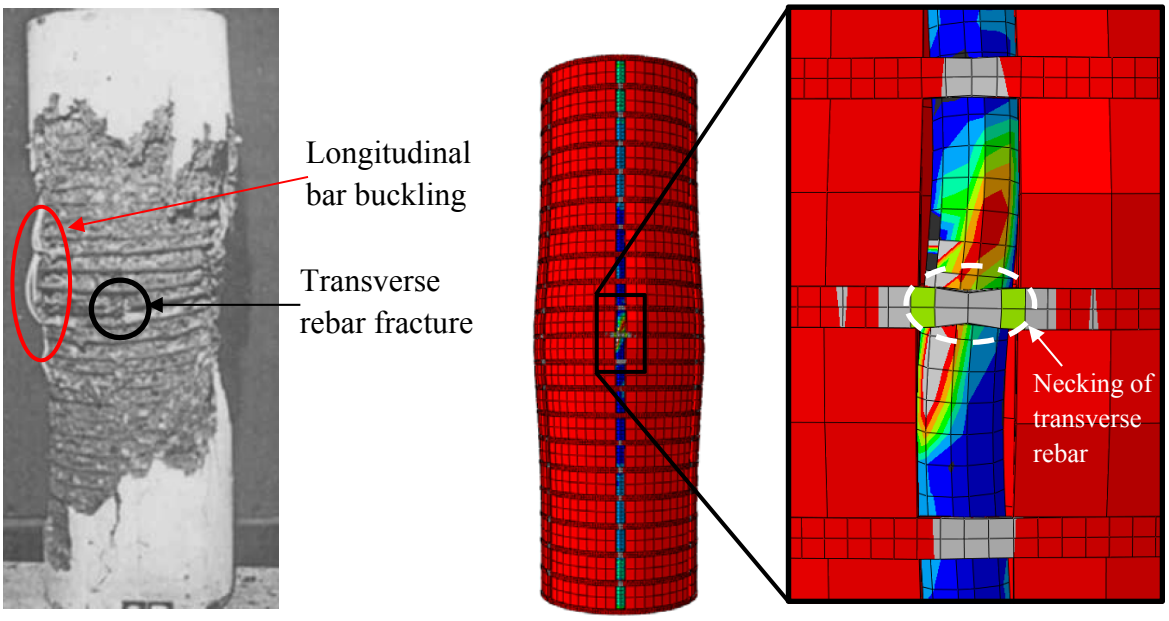

(a) Experimental observation **(b) Simulation** **(c) Bar buckling**

Fig. 26. Visual comparison of simulation with experimental observation

2.5 Summary

This chapter validated performance of available concrete constitutive models against the experimental responses of concrete cylinders with active confining pressure, concrete filled steel tubes (CFST), RC column subjected to monotonic compression. William and Warnke model [7] fails to predict the nonlinear stress-strain response hence it was not used for this study. Available smeared cracking model in ABAQUS lack the ability to consider multiaxial behavior of concrete due to which this model is not used for simulation purposes.

Lee and Fenves model [10] with Popovics model [1], under predict the strength of confined concrete at higher strains, when concrete is subjected to active confining pressure. In order to overcome this issue, normalized Mander model is introduced which can be used with Lee and Fenves model [10]. For active confining pressures, response simulations obtained by Lee and Fenves [10] with normalized Mander are better as compared to Lee and Fenves [10] with Popovics model [1].

These models are validated against passive confining pressure by simulating CFST. Response predictions by Lee and Fenves model with Popovics model are representative of experimental response. Mander model [2] is used for simulation of CFST where significant over prediction of response is observed. For RC column subject to compressive load, simulations by Lee and Fenves model [10] with Popovics model [1] are in well agreement with experimental response. Lee and Fenves model [10] with normalized Mander for normal strength transverse steel are reasonably well but over prediction of stress-strain response is observed in ultra-high strength transverse steel. Ultimate strength predictions for all columns under consideration are simulated well by Cervenka and Papanikolaou model [12]. Simulation

of stress-strain responses of columns by this model are representative of the experimental stress-strain responses.

This study confirmed the ability of multiaxial constitutive models to capture the response of RC column along with failure mechanism such as longitudinal rebar buckling occurring in RC column when subjected to monotonic compression load. Uniaxial concrete constitutive models such as Mander model [2] also can simulate the response of RC column but fails to predict the failure mechanism due to lack of consideration of multiaxial behavior of concrete. Hence, uniaxial constitutive models cannot be used to predict the failure mechanism of RC column.

2.6 References

[1] Popovics S., "A nuerical approach to the complete stress-strain curve of concrete," *Cement and concrete research, Volume 3,* pp. 583-599, 1973.

[2] Mander J. B., Priestley J. N. and Park R., "Theoretical Stress-Strain Model for Confined concrete," *Journal of Structural Engineering,* pp. 1804-1826, 1989.

[3] Belarbi A. and Hsu T. T., "Constitutive laws of concrete in tension and reinforcing bars stiffened by concrete," *Journal of American Concrete Institute,* vol. 91, pp. 465-474, 1994.

[4] Chang G. A. and Mander J. B., "Seismic energy based fatigue damage analysis of bridge columns: Part 1 - Evaulation of seismic capacity," NCEER-94-0006, University of Buffalo, New York, March, 1994.

[5] Le´geron F. and Paultre P., "Uniaxial Confinement Model for Normal- and High-Strength Concrete Columns," *J. Struct. Eng,* vol. 129, no. 2, pp. 241-252, 2003.

[6] D'Amato M., Braga F., Gigliotti R., Kunnath S. and Laterza M., "A numerical general-purpose confinement model for non-linear analysis of R/C members," *Computers and Structures,* vol. 102, no. 103, pp. 64-75, 2012.

[7] William K. J. and Warnke E. P., "Constitutive model for the triaxial behavior of concrete," *International Assiciation for Bridge and Structural Engineering,* vol. 19, pp. 1-30, 1975.

[8] Hsieh S. S., Ting E. C. and Chen W. F., "A plstic-fracture model for concrete," *Int. J. Solids structures,* vol. 18, no. 3, pp. 181-197, 1982.

[9] Lubliner J., Oliver J., Oller S. and Onate E., "A plastic-Damage Model for concrete," *Journal of solids structures,* pp. 299-326, 1989.

[10] Lee J. and Fenves G., "Plastic-Damage Model for cyclic Loading of Concrete structures," *Journal of engineering mechanics,* pp. 892-900, 1998.

[11] Nguyen G. D. and Korsunsky A. M., "Development of an approach to constitutive modeling of concrete: Isotropic damage coupled with plasticity," *International Journal of solids and structures,* vol. 45, no. 20, pp. 5483-5501, 2008.

[12] Cervenka J. and Papanikolaou V., "Three dimenxional combined fracture-plastic material model for concrete," *International Journal of Plasticity,* pp. 2192-2220, December, 2008.

[13] Moharrami M. and Koutromanos I., "Triaxial Constitutive Model for Concrete under Cyclic Loading," *Journal of Structural Engineering,* pp. 04016039-1 - 04016039-15, 2016.

[14] ANSYS, *Academic Research Help,* Release 2014, ANSYS INC..

[15] Sandler I. S., DiMaggio F. L. and Baladi G. Y., "A Generalized Cap Model for Geological Materials," *Journal of the Geotechnical Engineering Division,* vol. 102, no. 7, pp. 683-699, 1976.

[16] ABAQUS-SIMULIA, *ABAQUS Documentation, 6.14.*

[17] Červenka Consulting s.r.o., *ATENA Program Documentation, Theory,* 2013.

[18] Richart F. E., Brandtzaeg A. and Brown R. L., "A study of the failure of concrete under combined compressive stresses," *University of Illinois bulletin,* 20 November 1928.

[19] Schneider S. P., "Axially loaded concrete-filled steel tubes," *Journal of structural engineering,* pp. 1125-1138, October 1998.

[20] Bing L., Park R. and Tanaka H., "Stress-strain behavior of high-strength concrete confined by Ultra-high- and normal-strength transverse reinforcement," *ACI Structural Journal,* pp. 395-406, 2001.

[21] Mander J. B., Priestley J. N. and Park R., "Observed Stress-Strain Behavior of Confined Concrete," Journal of Structural Engineering, pp. 1827-1849, 1988.

[22] Kupfer H.and Hilsdorf H., "Behavior of Concrete Under Biaxial Stresses," ACI Journal, Vols. Title NO. 66-52, pp. 656-666, August, 1969.

[23] Chen W. F., Constitutive Equations for Engineering Materials, Volume 2, 1994.

[24] Drucker D. C. and Prager W., "Soil Mechanics and Plastic Analysis or Limit Design," *Quarterly of Applied Mathematics,* vol. 10, no. 2, pp. 157-165, 1952.

[25] Zhao J. and Sritharan S., "Modeling of strain penetration effects in fIber-based analysis of reinforced concrete strcutures," ACI Strut. J., vol. 104, no. 2, pp. 133-141, 2007.

[26] Babazadeh A., Burgueno R. and Silva P., "Use of 3D Finite-Element Models for Preducting Intermediate Damage Limit States in RC Bridge Columns," Journal of structural Engineering, pp. 04015012-1 to 04015012-11, 2015.

[27] Dodd L. L. and Restrepo-Posada J. I., "Model for Predicting Cyclic Behavior of Reinforcing Steel," vol. 121, no. 3, 1995.

[28] Chaboche J. L., "Time-Independent Constitutive Theories for Cyclic Plasticity," vol. 2, 1986.

[29] Armstrong P. J. and Frederick C. O., "A mathematical representation of the multiaxial baushinger effect," CEGB, Report No. RD/B/N 731, 1966.

[30] Johnson G. and Cook W., "Fracture characteristics of three metals subjected to various strains, strain rates, temperatures and pressures," Engineering Fracture Mechanics, vol. 21, no. 1, pp. 31-48, 1985.

[31] Ramberg W. and Osgood W. R., "Description of stress-strain curves by three parameters," National advisory committee for aeronautics, 902, Washington, 1943.

[32] Menegotto M. and Pinto P. E., "Method of analysis for cyclically loaded R.C. Plane Frames including changes in geometry and non-Elasitc behavior of elements under combined normal force and bending," vol. 13, 1973.

[33] Dhakal R. P. and Maekawa K., "Modeling for Postyield Buckling of Reinforcement," *Journal of Structural Engineering,* vol. 128, no. 9, pp. 1139-1147, 2002.

[34] Oller S., Onate E., Oliver J. and Lubliner J., "Finite element nonlinear analysis of concrete structures using a "Plastic damage model"," *Engineering Fracture Mechanics,* vol. 35, no. No. 1/2/3, pp. 219-231, 1990.

[35] Scott B. D., Park R. and Priestley M. J. N., "Stress-strain behavior of concrete confined by overlapping hoops at low and high strain rates," Journal of the American Concrete Institute, vol. 79, no. 2, pp. 13-27, 1982.

3 Concrete modeling for lateral loading on RC columns

In early chapter, concrete constitutive models are verified for response simulations of RC columns under compressive loading. Same concrete constitutive models are considered in this chapter for the validation of response simulation of RC columns under lateral loading. For this validation, lateral monotonic and simulated seismic loading are considered.

In ASCE 41, monotonic force-displacement responses are considered as envelope curve to predict the cyclic force-displacement responses. This consideration works only for standardized set of loading protocols such as '3-cycle' load history with increasing amplitude [1]. Normally earthquake ground motions are randomly distributed, hence standardized loading protocol is not representative of earthquake ground motion. Responses and accumulated damage in RC members are usually dependent on load history [2] due to which curve obtained from monotonic loading can't be used as 'backbone' for designing RC members for earthquake loading [1]. As accumulation of damage is different for different set of loading, failure mechanism occurred due to damage accumulation is dependent on load history. Because of this reason, cyclic lateral loading has to be simulated in order to determine the response of RC member for specific cyclic load.

For validation, three different RC column experiments are considered from the literature in this chapter. Two of the experiments considered the circular cross section of RC columns and one experiment on square cross section column. Details of these experiments are discussed in the following.

3.1 RC column experiments used for concrete constitutive model validation

3.1.1 Circular RC column

Experiment on reinforced concrete column conducted by Goodnight [1] under lateral loading is considered in this study for concrete constitutive model verification. In these experiments, circular columns were subjected to axial force and lateral load. Applied axial load was held constant throughout the experiment, while lateral load prescribed on the RC column was either monotonic or simulated seismic loading. One monotonic and one cyclic experiments are considered for constitutive material model validation as discussed below.

Column under consideration have diameter of 610 mm with L/D ratio as 4. Total number of longitudinal rebar used in the column are 16 with 19mm diameter (#6 bar) each and yield strength as 470 MPa. Diameter of transverse rebar is 9.5mm (#3 bar) at spacing of 50mm with yield strength of 510 MPa. Unconfined concrete strength and axial load ratio used for monotonic and cyclic load history experiments are shown in Table 1. These two experiments are considered in such a way that except strength of concrete and axial load ratio, all other parameter such as geometry of the columns is identical. Difference between concrete strength and axial load ratio is not significantly different due to which direct comparison of these experiments can be done.

Table 1. Experimental details for circular RC columns

Load history	Monotonic	Cyclic
Unconfined concrete strength	51 MPa (7.4 ksi)	47 MPa (6.81 ksi)
Axial load ratio (% of $P/f'_c A_g$)	5.1	5.5

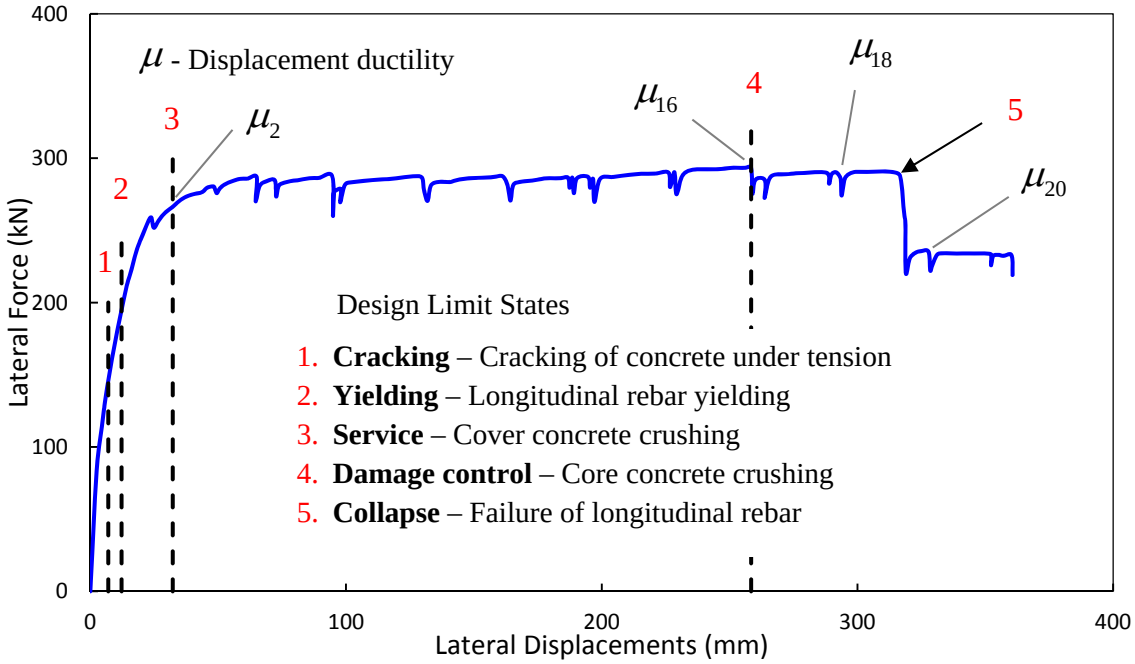

Fig. 1 Experimental response of circular RC column subjected to monotonic load (data from Goodnight [1])

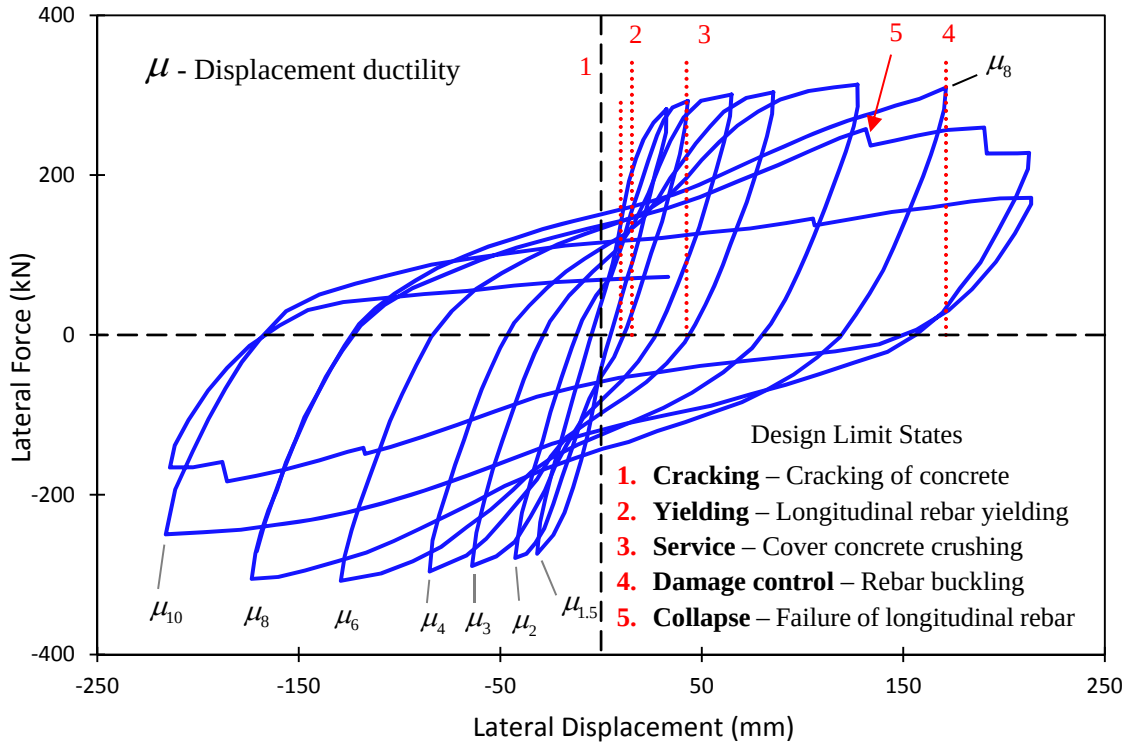

Fig. 2 Experimental response of circular RC column subjected to cyclic load (data from Goodnight [1])

In both experiments, detailed observation of the failure mechanism with accumulated damage is documented by Goodnight [1]. In Fig. 1, monotonic lateral response of RC column is presented, where along with limit states, displacement ductility attained by RC column is documented. In Fig. 2, hysteretic loops obtained under lateral simulated seismic loading on RC column are plotted. In this experiment, standard triple cyclic lateral load with increasing amplitude was applied on the top of the RC column. Detailed study on the failure mechanism of RC column along with limit states is presented by Goodnight [1], including the core concrete crushing, longitudinal rebar buckling and transverse rebar fracture (Fig. 2).

In the experiment under monotonic loading, displacement ductility achieved at damage control limit state of structure is 16 (Fig. 1). But under simulated seismic loading, damage control limit state is achieved at ductility level 8 (Fig. 2). Damage control limit state in monotonic load case was reached by core concrete crushing whereas in cyclic load case longitudinal rebar buckling was observed. Longitudinal rebar failure, which is considered as collapse limit state, was reached in cyclic load much earlier as compared to monotonic load experiment. This difference suggest that monotonic lateral loading envelope can’t be used for prediction of cyclic response of RC structure, primarily because RC structural response is dependent on the applied load history. In other words, accumulation of damage leading to failure of RC members under cyclic load is different than accumulation of damage under monotonic load.

3.1.2 Square RC column

Experiment conducted by Atalay [3] on square RC column is also considered for verification of concrete constitutive model. In these study, experiments were conducted with different spacing of transverse rebar, strength of concrete and yield stress of longitudinal rebar. One experiment is considered for validation of concrete constitutive model. The column considered has a width of 300mm and length 2L of 3350 mm. Unconfined strength of concrete is 29.4 MPa. Yield strengths of transverse rebar and longitudinal rebar are 392 and 429 MPa. Total number of longitudinal rebar are 4 (one at each corner) and transverse rebar have 50 mm spacing with clear cover of 32mm. Axial force (F) of 533.76 kN was applied on the top of column followed by cyclic load as shown in Fig. 3a. Observed response of this experiment is shown in Fig. 3b.

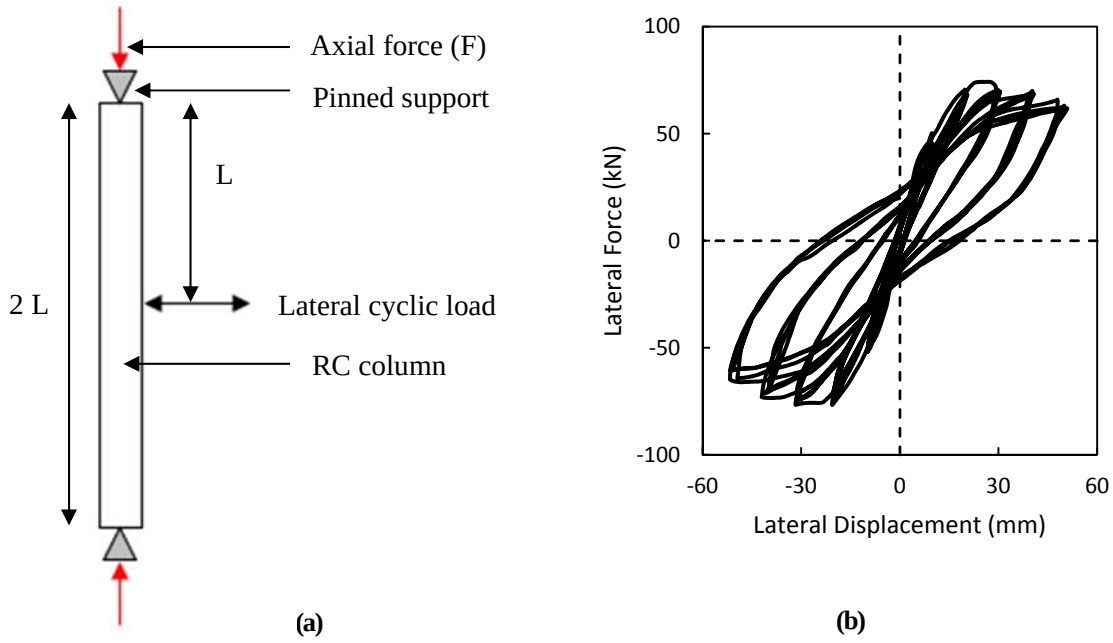

Fig. 3. (a) Geometry of square column tested by Atalay [3] and (b) Lateral force-displacement response of square RC column subjected to cyclic loading (data from Atalay [3])

3.2 Finite element modeling and response simulation of circular RC column specimens under monotonic loading

In this simulation, consideration of 3D elements for modeling of all longitudinal rebar and transverse rebar led to enormous number of nodes which lead to excessive computational time. In order to minimize time required for computation without sacrificing physical aspects of modeling, longitudinal rebar and transverse rebar were modeled as beam elements (B31) and concrete as 3D elements (C3D8R). This type of modeling technique with reinforcing steel modeled as beam elements was implemented by Babazadeh et al. [4] for prediction of intermediate damage limit states of RC column where large set of experimental data was compared against simulated limit states. In this study, intermediate damage limit states was successfully predicted by considering reinforcements as beam elements. Due to this reason, similar modeling approach is used for simulation of RC column. Perfect bond between concrete and steel reinforcements is assumed. Core concrete is meshed in such a way that height of the elements is equal to the spacing of the transverse rebar and two elements are modeled within adjacent longitudinal rebar as shown in Fig. 4. Cover concrete is neglected while modeling RC column.

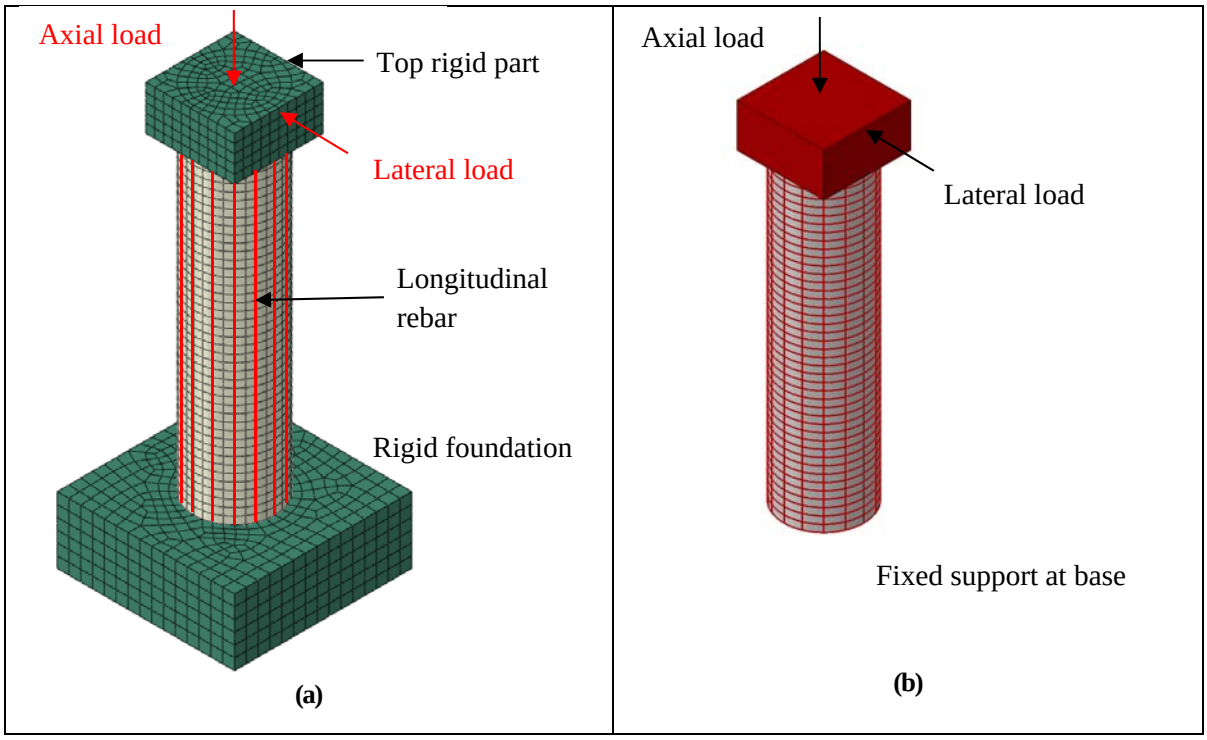

Fig. 4. Finite element mesh of the RC column, (a) with foundation (b) without foundation with fixed base

For material model of steel, multilinear isotropic hardening was used with von Mises plasticity. Lee and Fenves [5] with Popovics model [6] gave numerical convergence issues due to which response with this model for RC column under the lateral loading could not be obtained. Lee and Fenves model [5] with normalized Mander is used as concrete constitutive material. Simulation of the RC column with and without foundation is presented in Fig. 5.

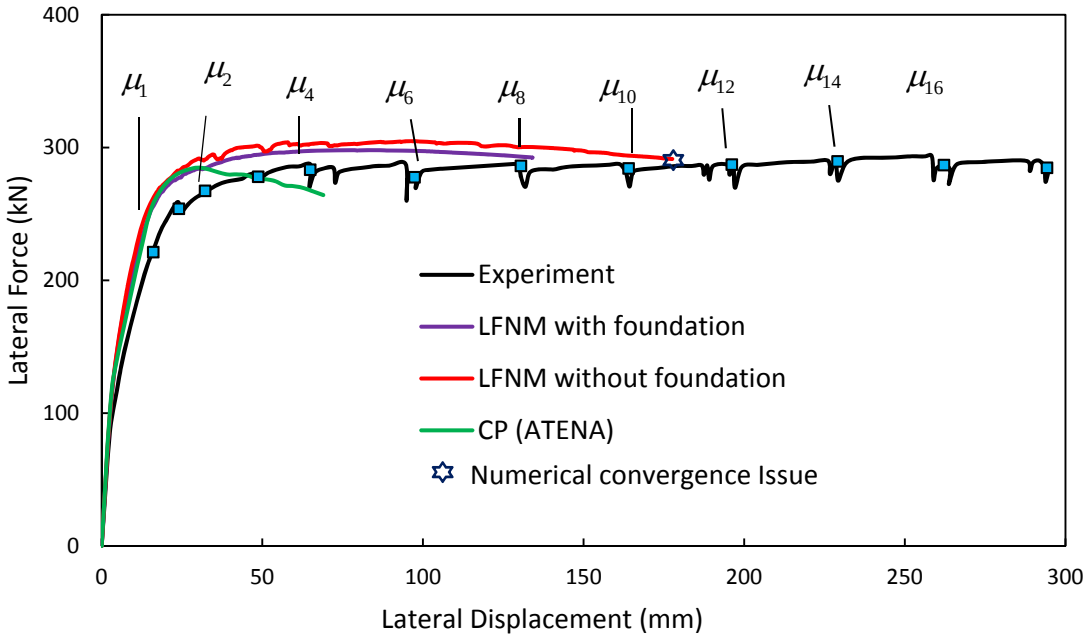

Fig. 5 Experimental and simulated responses of RC column under lateral loading by LFNM: Lee and Fenves model [5] with normalized Mander and CP: Cervenka and Papanikolaou [6]

In Fig. 5, RC column with foundation gives good estimation of ultimate force as well as force-displacement relationship but due to numerical convergence issues at the junction of foundation and RC column this analysis fails to simulate higher ductility response. RC column without foundation can simulate higher ductility level responses, but simulation over predicted strength as shown in Fig. 5. Cervenka and Papanikolaou model [6] yielded good prediction of maximum lateral force but overall response is not representative of the experimental observations. In addition, with this model extreme distortion is observed in concrete elements leads to instability and numerical convergence issues. From this simulation, it is concluded that only Lee and Fenves model [5] with normalized Mander can be used to simulate the response of the RC column.

3.3 Simulation of RC column response under simulated seismic loading

Two different experiments are considered as stated earlier. One experiment on circular column by Goodnight [1] and another experiment on square column by Atalay [3].

Cyclic load experiment by Goodnight [1] is simulated by using same geometric modeling and Lee and Fenves [5] with normalized Mander model for concrete material and bilinear kinematic hardening model for steel material. As discussed in earlier chapter, advanced constitutive material model for steel such as Chaboche Model [7] is available in ABAQUS, but this model is not supported by beam elements due to which bilinear kinematic hardening rule is used in cyclic loading simulation. Cyclic load up to ductility 3 was prescribed on RC column as shown in Fig. 6a and results obtained are plotted in Fig. 6b.

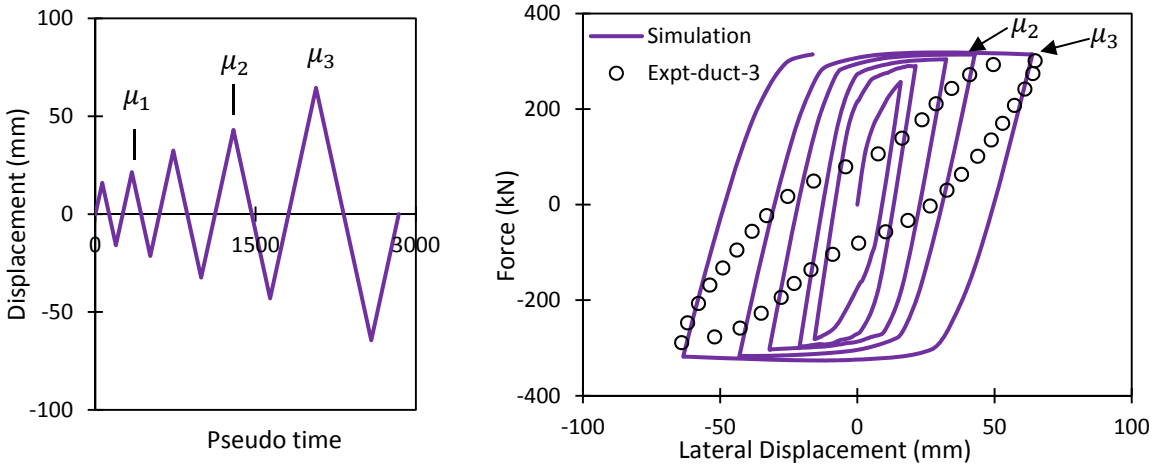

Fig. 6. (a) Applied cyclic load history (b) Comparison of simulation of cyclic load against experiment response at ductility level 3 (μ_3) (data from Goodnight [1])

Ultimate force predicted at ductility level 3 (μ_3) is in agreement with the experimental data but the shape of hysteretic curve is not representative of the experimental response due to lack of crack modeling in concrete. When higher level of ductility loading is prescribed such as ductility 4 and above with complete load history, convergence issues were observed. Hence,

for higher ductility levels, separate cycle at each ductility is prescribed on RC column and obtained simulation responses are presented in Fig. 7.

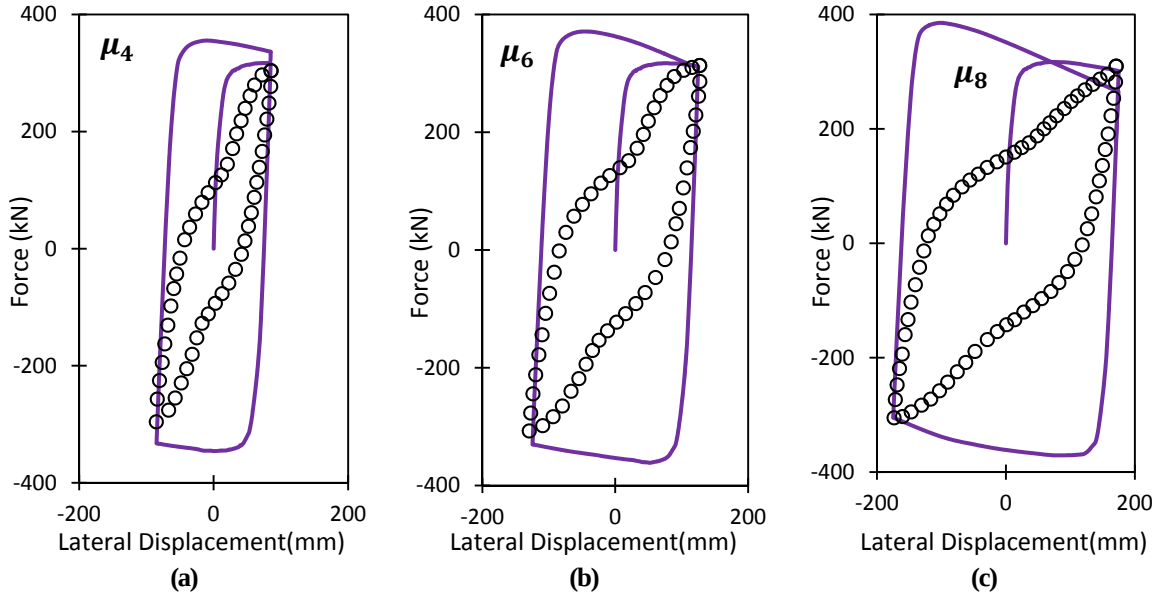

Fig. 7. Hysteresis loop simulation at ductility level μ, (a) 4,(b) 6, (c) 8 (data from Goodnight [1])

In Fig. 7, lateral force simulations at end of load cycles are in agreement with experimental force values, but shape of the hysteretic loops simulated is not representative of experimental hysteretic loops. One of the reasons behind the higher reloading stiffness is lack of consideration of crack in simulation as Lee and Fenves model [5] assumes concrete continuum for modeling of concrete. Hence, crack has to be modeled in order to predict the response of RC column accurately.

In Fig. 8, comparison of the strain in longitudinal rebar located in extreme compression and tension side of RC column is compared against experiment results for ductility levels of 4, 6 and 8. In these results, red line indicate longitudinal rebar in compression and black line indicate longitudinal rebar in tension under first positive peak of the loading. For first negative peak, stresses in these rebars are swapped due to change in direction of loading.

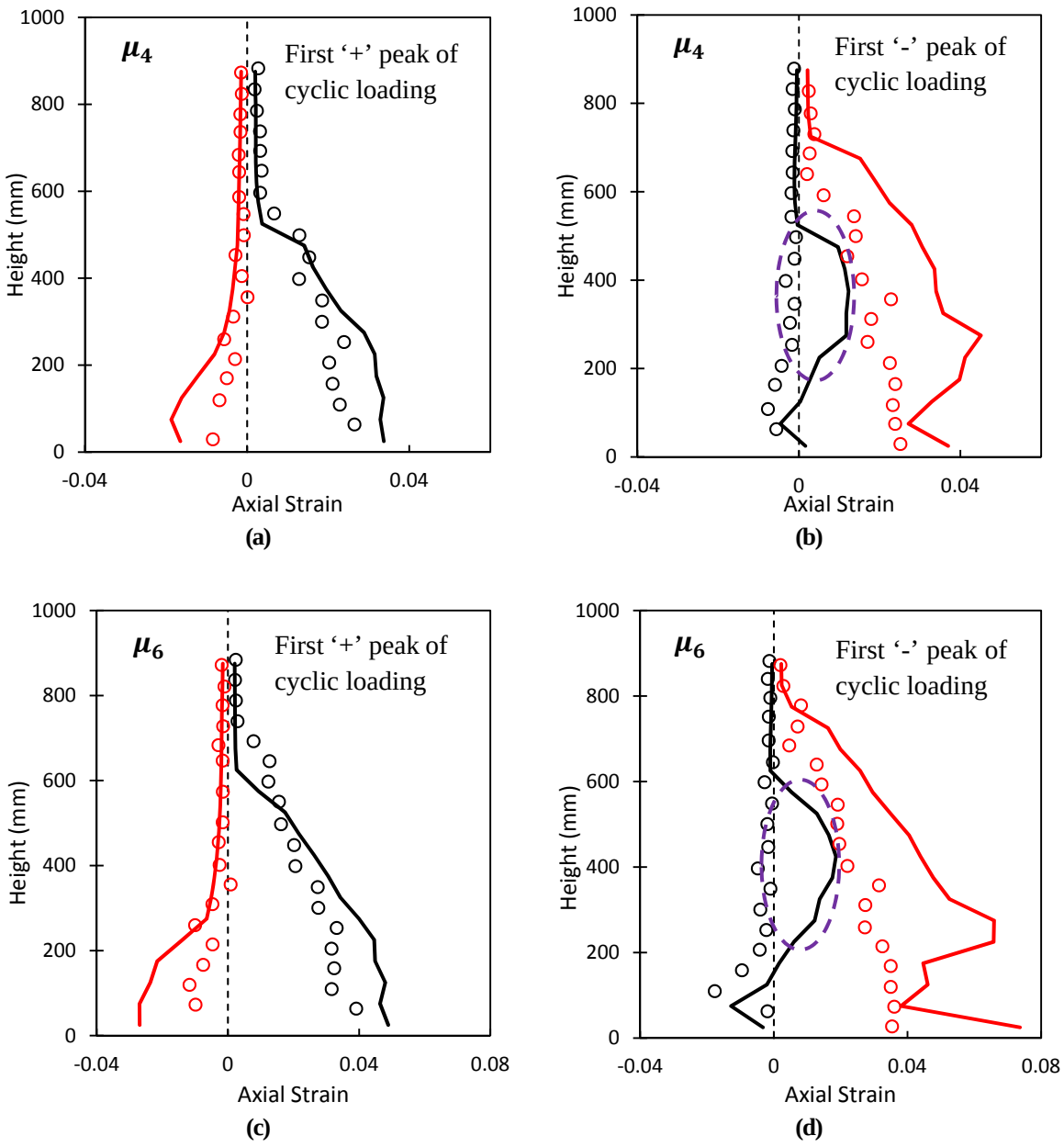

Fig. 8. Comparison of axial strain in longitudinal rebar obtained from simulations in solid line against experimental data in hollow circles

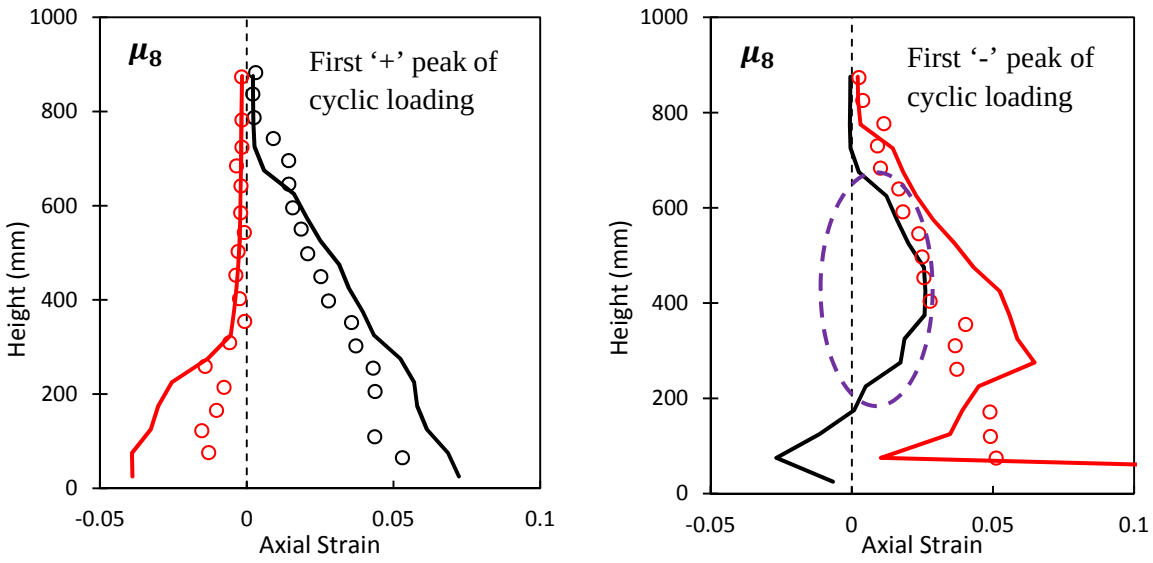

Fig. 8 Continued. Comparison of axial strain in longitudinal rebar obtained from simulations in solid line against experimental data in hollow circles

All the simulations of strains in longitudinal rebar are acceptable when compared against the experimental data for first positive peak of the loading in all ductility levels (Fig. 8 a, c, e). But for first negative peak of loading, residual tensile strain was observed in bar with compressive stress (black color curve) in all ductility levels which is indicated by violet color ellipse (Fig. 8b, d, f). The reason for this response is explained in the following.

Consider concrete cylinder as shown in Fig. 9a, where load is applied at top of the cylinder. In one cylinder no crack is considered whereas in the other, crack is considered at the middle with no aggregate interlock. The crack is assumed to be normal to the direction of the loading. Point A is at the center of cylinder in uncracked cylinder, and point B is just below the crack in cracked cylinder. Cyclic loading shown in Fig. 9b is such that displacement observed at the point A is as given in Fig. 9b. Under same loading cycle, the cracked cylinder will have displacement at point B as shown in Fig. 9c.

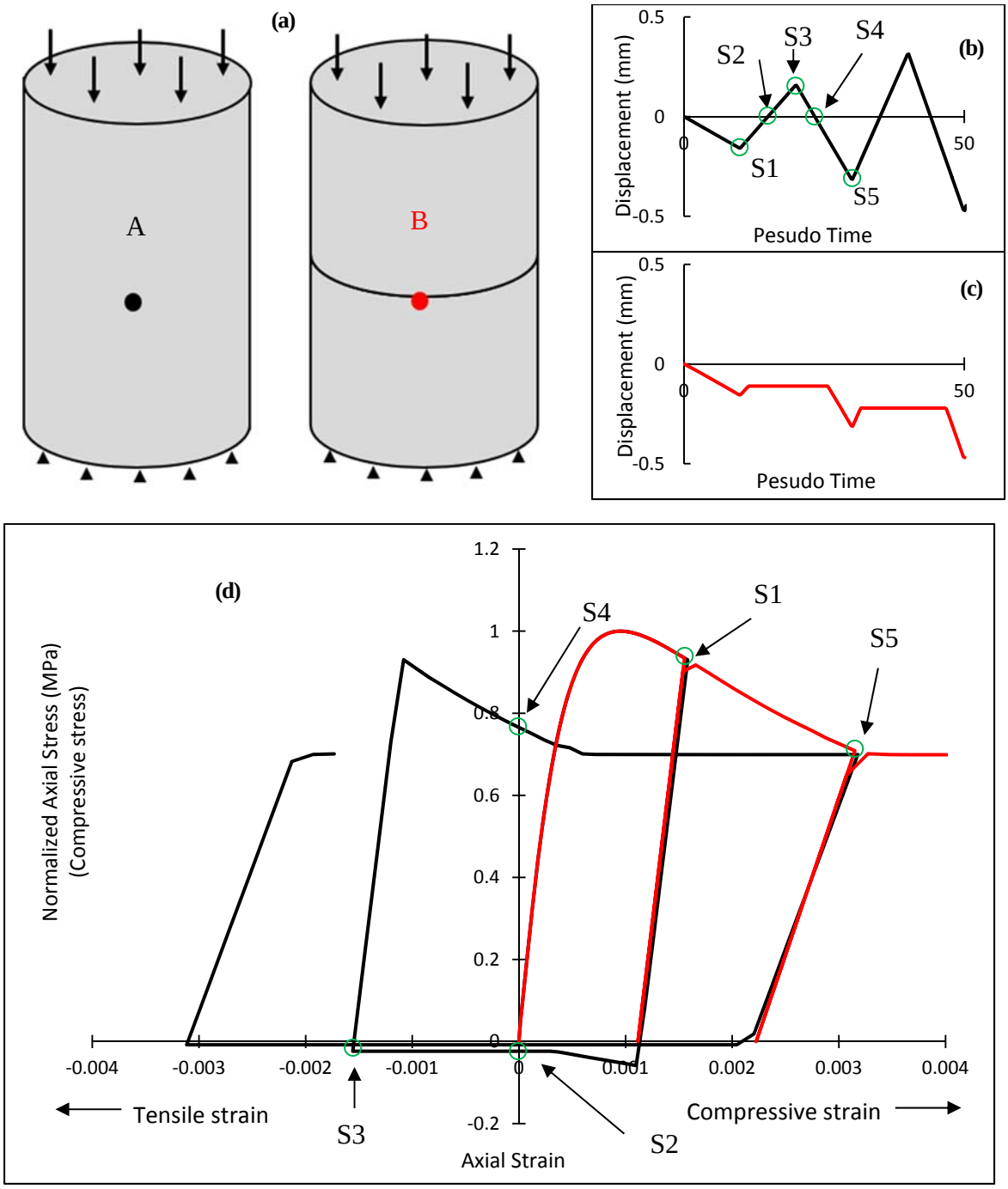

Fig. 9 Consideration of crack in concrete (a) Modeling details, (b) Observed loading in uncracked cylinder, (c) Observed loading in cracked cylinder, (d) Comparison of responses of cracked and uncracked concrete cylinders

In Fig. 9d, response of cylinders are presented where black curve indicates response of cylinder without crack and red curve indicates response of cracked cylinder. Now, consider

case where load is applied from S1 to S3. In this cycle, concrete is subjected to compression to tension and uncracked concrete cylinder undergoes large tensile strain. At point S2, strain in concrete is zero and stress state in cylinder is tensile stress. At point S3, cycle reaches peak tensile strain with tension stress. Now, when reloading is applied from S3 to S5, concrete stress shows sudden change from tension to compression. So from point S3 to S4, concrete cylinder have tensile strain but compressive stress in uncracked cylinder.

But in cracked cylinder, when loading is applied from S1 to S2, concrete cylinder does not undergo tensile strain due to presence of crack, rather tensile load leads to ‘opening of crack’ in the cylinder. In actual behavior, cracks are not smooth due to which there will be small tensile stresses and strains involved [5] but they are not as large as values suggested by simulation. Consequently cracked cylinder resembles the actual behavior of the concrete as opposed to the cylinder with no crack.

When simulation of reinforced concrete column is conducted for lateral cyclic loads without cracks, concrete under tension load undergoes tensile strain. As contact between steel and concrete was considered as perfect bond with no slip, longitudinal rebar undergoes same strain to maintain consistency. Due to this reason at the end of positive peak loading (Fig. 8b, d, f), there are residual tensile strains in longitudinal rebar which resembles to location S3 in Fig. 9d. When reloading is applied in opposite direction, these accumulated plastic strains undergo compression which gives tensile strain with compressive stress condition. This is the reason behind the tensile strain with compressive stress observed in Fig. 8b, d, f (violet ellipse). This study shows the significance of crack consideration for simulation of cyclic response of RC members.

Next, RC column was modeled by using Cervenka and Papanikolaou model [6] in ATENA, under cyclic load of ductility 1.5 which incorporated cracking in concrete numerically. Response obtained from the simulation are plotted in Fig. 10. For comparison purposes, simulation using the Lee and Fenves model [5] with normalized Mander is also plotted in Fig. 10. Lateral force prediction at the peak of the cycle by both models is in agreement with experimental force value. Response prediction of the Cervenka and Papanikolaou model [6] is promising as compared to the Lee and Fenves model. However, even at low ductility cycle, convergence issues were experienced due to distortion of cracked concrete elements in the plastic hinge region. Because of this convergence problem, Cervenka and Papanilolaou model [6] can't be used for the response simulation of RC column under lateral load cycle of large ductility.

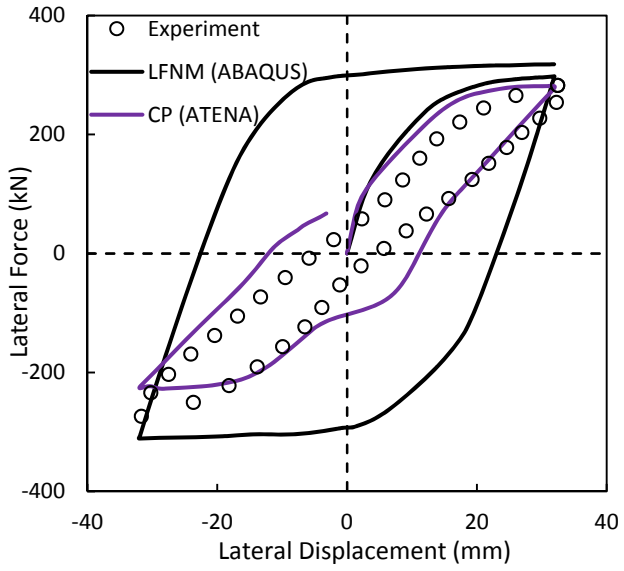

Fig. 10. Comparison of LFNM and CP (ATENA) against experimental response of cyclic load of displacement ductility 1.5 where LFNM: Lee and Fenves model [5] with normalized Mander and CP: Cervenka and Papanikolaou model [6]

As mentioned earlier, available smeared cracking in ABAQUS model don't consider confinement of concrete into modeling consideration due to which that model can't be used

for the response prediction of RC structure. Recent work from Moharrami and Koutromanos [8] proposed tri-axial constitutive model with smeared cracking to capture the cracking of concrete numerically. This study shows promising results for small ductility levels but as mentioned earlier, non-repairable damages such as core concrete crushing, transverse rebar failure and longitudinal rebar buckling is observed at higher ductility levels, this model has to be tested for large displacement ductility loading. Response prediction of smeared cracking model is not accurate when localized cracks are observed [8]. Also smeared cracking model for localized cracks may suffer stress locking effect and cause inaccurate results due to which discrete modeling of crack has to be coupled with continuum based model to represent the localized cracking [9].

Due to the convergence issues experienced with the smeared crack concrete modeling, discrete cracking approach was used to simulate the influence of concrete cracking on RC column cyclic response. One crack was modeled till half the depth of the RC column in ABAQUS and cyclic response was simulated by using Lee and Fenves model with normalized Mander. This consideration of half crack lead to numerical issues at the tip of the crack. Then crack was considered throughout the depth of the circular RC column and simulation is obtained as shown in Fig. 11. Location of crack is assumed in between two transverse rebars at the most bottom region of plastic hinge as shown in Fig. 11a. Contact elements are defined with in the crack with coefficient of friction to represent the concrete aggregate interlock in compression zone of RC column. This crack is allowed to open under tension load. Bond between concrete and steel reinforcements are considered as perfect bond with no slip. Rest of the modeling aspects are same as earlier and simulation is obtained and plotted in Fig. 11b.

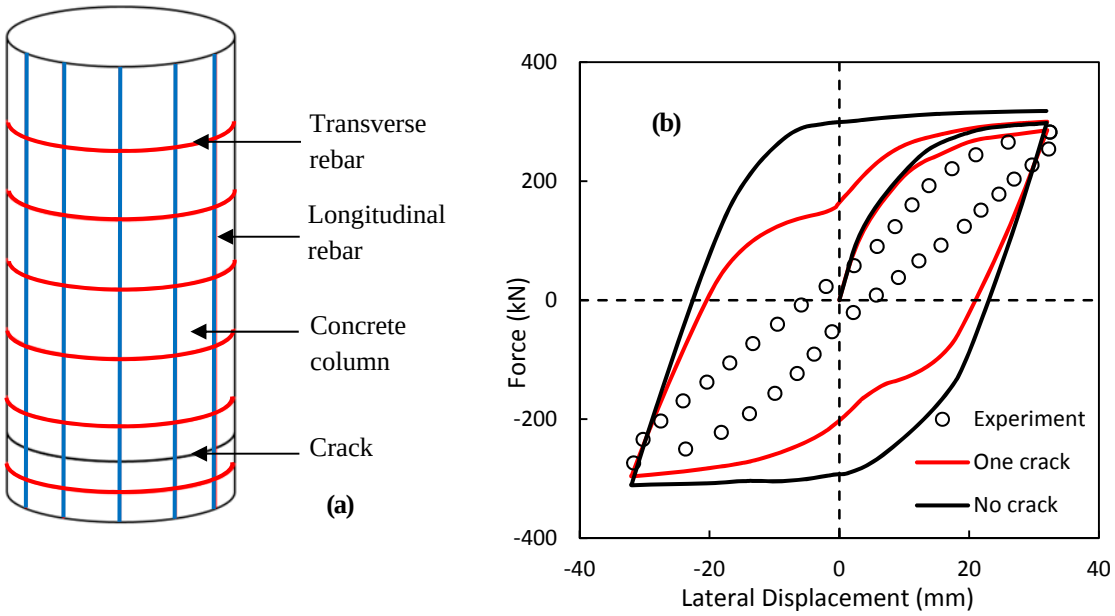

Fig. 11. (a) Modeling consideration of crack in RC column (b) Comparison of simulation with crack and without crack by using Lee and Fenves model with normalized Mander against experimental hysteretic response for ductility 1.5 (Expt. data from Goodnight [1])

Just consideration of one crack shown the significant difference of shape of the hysteretic loop which suggest the importance of crack consideration in simulation of RC column cyclic response. But one crack isn't sufficient to capture the experimental response, hence a simulation with several cracks is performed, but convergence problem due to mesh distortion and overclosure error of meshing in contact is experienced. Hence, similar analysis with the square column is performed.

For square columns, experiments conducted by Atalay [3] was simulated with same modeling consideration as the circular columns. All the reinforcements are modeled as beam elements. Cover concrete is neglected and meshing of core concrete and reinforcement is in such a way that nodes from steel and concrete elements coincide. Perfect contact between steel reinforcement and concrete is assumed, i.e. no slip. Multiple physical cracks are considered at

the locations equidistant from transverse rebars as shown in Fig. 12. Multiple cracks are modeled along the height of column.

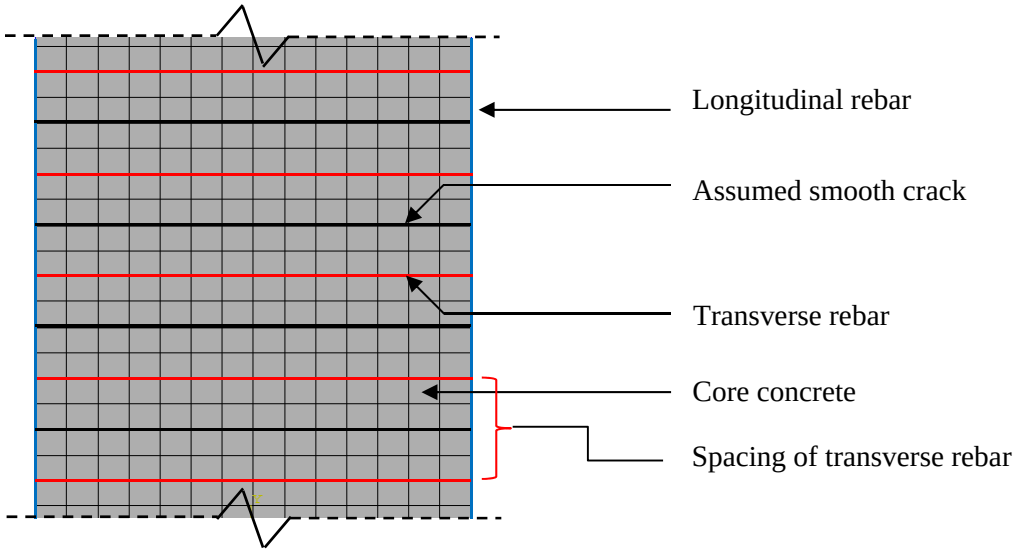

Fig. 12. Modeling cracks in square RC column

In each crack, contact element is defined with frictional coefficient and crack is allowed to open in tension. Coefficient of friction is assumed to simulate the aggregate interlock in compression zone. This contact between adjacent layers of concrete resembles the opening and closing mechanism of crack. These cracks are modeled along the entire depth of the column. Each concrete layer and steel reinforcements are perfectly bonded. This geometric model is subjected to one cycle loading and obtained results are plotted in Fig. 13 where comparison of hysteretic loops obtained from Lee and Fenves model [5] with normalized Mander with crack and without crack is presented. Effect of crack consideration can easily be observed. Response by cracked RC column simulation represents experimental loops much better than the response of RC column with no cracks. These results demonstrates the importance of including cracks into simulation of RC column subjected to lateral cyclic loading.

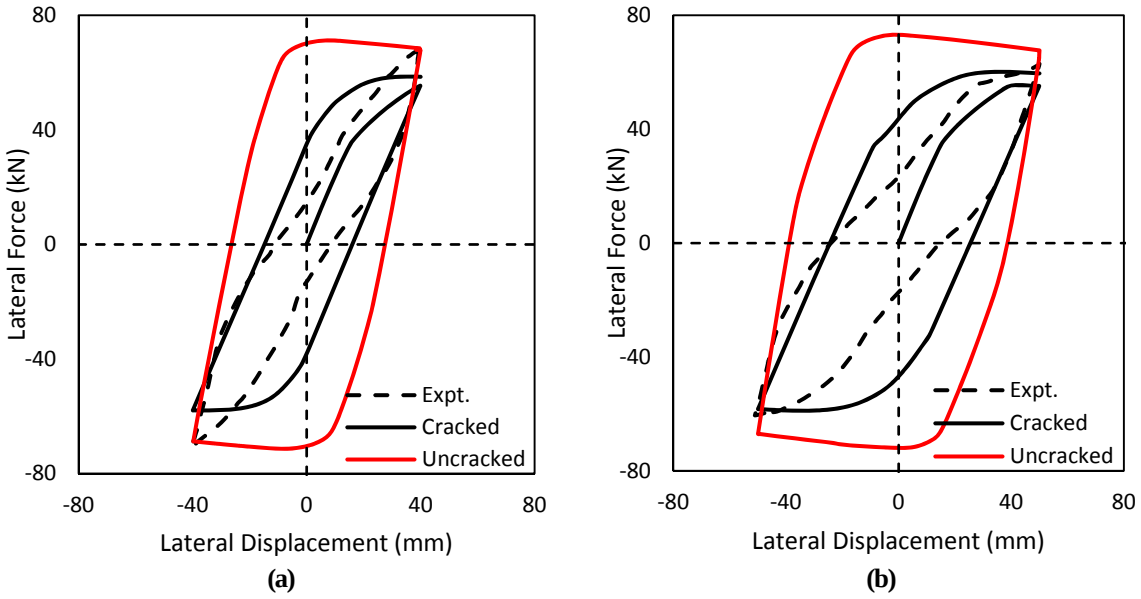

Fig. 13. Comparison of cracked and un-cracked RC column simulation (a) cycle of amplitude 40 mm (b) cycle of amplitude 50 mm, Red color solid line indicates simulation with no crack and black color solid line indicates simulation with cracking compared against experimental response in black dotted line

3.4 Summary

Available concrete constitutive models are validated for simulation of RC column under monotonic and cyclic lateral loading. Simulations by Cervenka and Papanikolaou model [6] presented numerical divergence at smaller ductility in lateral monotonic and cyclic loading hence this model cannot be used for response simulation and failure mechanism of RC columns. When Lee and Fenves model [5] is used for simulation of RC column under monotonic lateral loading, lateral force-displacement response prediction is in well agreement with experimental response till ductility 10 but for higher ductility, convergence issues were observed. For lateral cyclic loading, force prediction at the end of the ductility cycles are well simulated along with strains in longitudinal rebar at the end of first peak of loading. But shapes of simulated hysteretic responses are different as that of shapes of experimental hysteretic loops due to lack of crack modeling. Here, one point is noted that even without crack

simulation, strain prediction in longitudinal rebar at the end of first peaks are in well agreement with experimental values of strains in longitudinal rebar (Fig. 8a, c, e).

In order to overcome issue of lack of crack consideration in modeling, physical cracks are simulated in the modeling of RC column. Introduction of physical crack improved the lateral force-displacement response of RC column. This study states the importance of the physical crack consideration in simulation of RC column subjected to lateral cyclic loading. Consideration of physical crack modeling works well for low ductility range of loading but for higher ductility loading, it yields numerical divergence. Hence, further study of the concrete constitutive models with contact element for simulation of higher ductility loading in RC column is required.

3.5 References

[1] Deierlein, Gregory G., Reinhorn, Andrei M., and Willford, Michael R. (2010). “Nonlinear structural analysis for seismic design,” NEHRP Seismic Design Technical Brief No. 4, produced by the NEHRP Consultants Joint Venture, a partnership of the Applied Technology Council and the Consortium of Universities for Research in Earthquake Engineering, for the National Institute of Standards and Technology, Gaithersburg, MD, NIST GCR 10-917-5.

[2] Goodnight J., *The effects of Load History and Design Varialbes on Performance Limit States of Circular Bridge Columns,* 2015.

[3] Atalay M. B.and Penzien J., "The seismic behavior of critical regions of Reinforced Concrete Components as influenced by moment, shear and axial force," Earthquake Engineering Research Center, Univeristy of California Berkeley, California, December, 1975.

[4] Babazadeh A., Burgueno R. and Silva P., "Use of 3D Finite-Element Models for Predicting Intermediate Damage Limit States in RC Bridge Columns," *Journal of structural Engineering*, pp. 04015012-1 to 04015012-11, 2015.

[5] Lee J. and Fenves G., "Plastic-Damage Model for cyclic Loading of Concrete structures," *Journal of engineering mechanics*, pp. 892-900, 1998.

[6] Popovics s., "A nuerical approach to the complete stress-strain curve of concrete," *Cement and concrete research, Volume 3*, pp. 583-599, 1973.

[7] Cervenka J. and Papanikolaou V., "Three dimenxional combined fracture-plastic material model for concrete," *International Journal of Plasticity*, pp. 2192-2220, December, 2008.

[8] Chaboche J. L., "Time-Independent Constitutive Theories for Cyclic Plasticity," vol. 2, 1986.

[9] M. Moharrami and I. Koutromanos, "Triaxial Constitutive Model for Concrete under Cyclic Loading," *Journal of Structural Engineering*, pp. 04016039-1 - 04016039-15, 2016.

[10] Koutromanos I. and Shing P. B., "Cohesive Crack Model to Simulate Cyclic Response of Concrete and Masonry Structures," *ACI Structural Journal*, vol. 109, no. 3, pp. 349-358, May-June 2012.

4 Conclusion

When a RC structure is subjected to earthquake loading, various degree of damages are experienced. Accumulation of this damage may leads to failure of structures. As response of RC structure is depended on the characteristics of the load history [1], damage prediction of RC structure is a challenging task. For design, various types of damages are defined as limit states. Robust analysis technique is needed to predict the limit states for determination of performance and required repair [2]. After repair and retrofit, analysis of repaired member has to be performed to anticipate seismic performance. Present simplified analysis, such as, fiber modeling techniques lack the capability to predict limit states of RC member and failure mechanism especially longitudinal rebar buckling [3]. Due to this reason, 3D finite element analysis technique can be used for the prediction of RC responses, damage accumulation and limit states.

Available multiaxial concrete constitutive models in finite element analysis software, such as ANSYS, ABAQUS and ATENA, are studied for concrete cylinder and RC specimen. In chapter 2, concrete constitutive models are validated against experimental data for monotonic axial compressive loading. This chapter presented simulation of responses of concrete cylinder under active confining pressure and passive confining pressure. For active confining pressure, Lee and Fenves model [4] along with Popovics model [5] gives good estimation of confined strength of concrete but stress predictions at higher level of strain is under predicted. In order to overcome this issue, a concept of normalized Mander model was developed and used with Lee and Fenves model [4] to improve, prediction of stresses at higher

level of strain. Both of these models are evaluated in simulation responses of concrete filled steel tubes and reinforced concrete columns under monotonic compressive loading.

It is demonstrated that Lee and Fenves [4] and Cervenka and Papanikolau [6] concrete constitutive models gives good simulation of the compressive loading responses of monotonic axial compressive loading for concrete filled steel tubes and RC column. It is observed that Lee and Fenves model [4] with normalized Mander over predicts the response for high confining pressure. For the RC column responses with Mander model [7] predictions for low confining pressures is in well agreement with experimental responses but for high confining pressure over prediction is observed. Failure mechanism of the RC column under monotonic axial load such as longitudinal rebar buckling is predicted in the simulation. This is one of the advantage of using 3D FE analysis techniques using which detailed responses of the longitudinal rebar can be simulated. Buckling of longitudinal rebar can be simulated in pseudo way by adjusting constitutive material model as shown by Dhakal and Maekawa model [8]. But this technique fails to capture interaction between longitudinal rebar and concrete which is critical in simulation of longitudinal rebar buckling. Due to this reason, uniaxial model can capture the response of overall structure but simulation of local damages and failure mechanism is difficult which is essential for seismic performance evaluation, repairs and retrofits of structures for enhancing seismic resilience.

In chapter 3, concrete constitutive models are verified against experimental responses of RC columns subjected to lateral loading. Lee and Fenves model [4] with Popovics model [5] yielded numerical divergence in early stage of loading, due to which this model was not considered for RC column simulations. Lee and Fenves model [4] with normalized Mander can simulate the monotonic response of RC column till displacement ductility 10, but beyond

this ductility, numerical divergence was observed. Cervenka and Papanikolaou model [6] fails to simulate higher ductility also due to convergence issues indicated by concrete constitutive model.

These concrete constitutive models were then used to simulate the cyclic responses of RC columns. Hysteretic loops obtained from the simulation have different shapes compared to experimental hysteretic loops. Lack of crack consideration into simulation caused prediction of higher reloading stiffness which led to different shape of hysteretic loops. As shown in chapter 2, smeared cracking model available in ABAQUS don't consider confining effect into account due to which smeared cracking model was not used for the RC column simulations. Recently, a new smeared cracking concrete constitutive model is developed by Moharrami and Koutromanos [9] to simulate RC column responses under seismic loading. This model have shown successful simulation of cyclic response of RC member but for smaller displacement ductility loadings cycles only. Damage control limit states such as core concrete crushing, longitudinal rebar buckling happens at higher ductility loadings, this model is not sufficient for damage simulation. Numerical divergence by concrete smeared cracking model due to stress locking and thereby incorrect predictions has been demonstrated [10], [9]. Due to these reasons, physical crack is modeled in RC column with Lee and Fenves model [4] with normalized Mander model. This crack was defined with contact elements to consider effect of aggregate interlock in concrete under compression zone. Simulation by this consideration are promising for smaller displacement ductility.

For steel constitutive model, as mentioned in chapter 2, Chaboche model [11] have better capability to capture the cyclic response of steel including accumulative plastic strains which is essential in prediction of rebar buckling. As this model is advanced enough to capture

the mechanism of longitudinal rebar buckling, further study on concrete constitutive modeling is required to capture the cyclic response of RC column.

Existing uniaxial models available in the literature for concrete such as Mander model [7], Chang and Mander [12] and recently published model from Andriotis et al. [13] considers confining effect of concrete, cracking of concrete along with crack opening-closing mechanism, numerically. These models demonstrated good prediction of hysteretic curves of force-displacement responses of RC columns. Available uniaxial steel models such as Dodd and Restrepo-Posada [14] with modification by Dhakal and Maekawa [8] can simulate effect of buckling of longitudinal rebar on prediction of force-displacement response of RC member. But these models lack the ability to consider multiaxial stresses of RC members [9]. Hence detailed aspects of RC columns such as interaction between dilation of concrete core and longitudinal rebar which is essential in prediction of longitudinal rebar buckling, is not considered in uniaxial analysis [15]. As discussed in the Introduction chapter, longitudinal rebar buckling is damage control limit state which dependents on the load history [1] and the accumulated tensile strains in longitudinal rebars [3]. Exceeding the limit states under seismic loading dictates replacement of structure, due to which simulation of rebar buckling in RC structures is critical. Due to these limitations, uniaxial concrete model can't be used for simulation of buckling of longitudinal rebars [15]. Hence, 3D FE analysis technique is required for simulation of failure mechanisms, such as, longitudinal rebar buckling.

This study demonstrate that available multiaxial concrete constitutive models are unable to simulate the lateral monotonic and cyclic response of RC columns. Incorporating a physical cracks improves, the simulation of RC column response, but even this modeling technique yields numerical divergence for simulation of more than one cycle. Hence,

development of new concrete constitutive model is required in 3D analysis technique which can simulate physical crack in RC column along with cyclic response.

4.1 Reference

[1] Goodnight J., *The effects of Load History and Design Varialbes on Performance Limit States of Circular Bridge Columns,* 2015.

[2] Deierlein, Gregory G., Reinhorn, Andrei M., and Willford, Michael R. (2010). “Nonlinear structural analysis for seismic design,” NEHRP Seismic Design Technical Brief No. 4, produced by the NEHRP Consultants Joint Venture, a partnership of the Applied Technology Council and the Consortium of Universities for Research in Earthquake Engineering, for the National Institute of Standards and Technology, Gaithersburg, MD, NIST GCR 10-917-5.

[3] Feng Y., Kowalsky M. J. and Nau J. M., "Finite-Element Method to predict reinforcing bar buckling in RC structres," *ASCE,* 2014.

[4] Lee J.and Fenves G., "Plastic-Damage Model for cyclic Loading of Concrete structures," *Journal of engineering mechanics,* pp. 892-900, 1998.

[5] Popovics S., "A nuerical approach to the complete stress-strain curve of concrete," *Cement and concrete research, Volume 3,* pp. 583-599, 1973.

[6] Cervenka J. and Papanikolaou V., "Three dimenxional combined fracture-plastic material model for concrete," *International Journal of Plasticity,* pp. 2192-2220, December, 2008.

[7] Mander J. B., Priestley J. N. and Park R., "Theoretical Stress-Strain Model for Confined concrete," *Journal of Structural Engineering,* pp. 1804-1826, 1989.

[8] Dhakal R. P. and Maekawa K., "Modeling for Postyield Buckling of Reinforcement," *Journal of Structural Engineering,* vol. 128, no. 9, pp. 1139-1147, 2002.

[9] Moharrami M. and Koutromanos I., "Triaxial Constitutive Model for Concrete under Cyclic Loading," *Journal of Structural Engineering,* pp. 04016039-1 - 04016039-15, 2016.

[10] Koutromanos I. and Shing P. B., "Cohesive Crack Model to Simulate Cyclic Response of," *ACI Structural Journal,* vol. 109, no. 3, pp. 349-358, May-June 2012.

[11] Chaboche J. L., "Time-Independent Constitutive Theories for Cyclic Plasticity," vol. 2, 1986.

[12] Chang G. A. and Mander J. B., "Seismic energy based fatigue damage analysis of bridge columns: Part 1 - Evaulation of seismic capacity," NCEER-94-0006, University of Buffalo, New York, March, 1994.

[13] Andriotis C., Gkimousis I. and Koumousis V., "Modeling Reinforced Concrete Structures Using Smooth Plasticity and Damage Models," *Journal of Structural Engineering,* vol. 142, no. (2):04015105, pp. 1-11, 2015.

[14] Dodd L. L. and Restrepo-Posada J. I., "Model for Predicting Cyclic Behavior of Reinforcing Steel," vol. 121, no. 3, 1995.

[15] Feng Y., "Numerical Simulation and Analysis of Circular Reinforced Concrete Bridge Columns for," North Carolina State University, Raleigh, North Carolina, 2013.